OPEN ACCESS

Nomenclature of the perovskite supergroup: A hierarchical system of classification based on crystal structure and composition

ROGER H. MITCHELL[1,*], MARK D. WELCH[2] AND ANTON R. CHAKHMOURADIAN[3]

[1] Department of Geology, Lakehead University, Thunder Bay, Ontario P7B 5E1, Canada,
[2] Department of Earth Sciences, The Natural History Museum, Cromwell Road, London SW7 5BD, UK
[3] Department of Geological Sciences, University of Manitoba, Winnipeg, Manitoba R3T 2N2, Canada

ABSTRACT

On the basis of extensive studies of synthetic perovskite-structured compounds it is possible to derive a hierarchy of hettotype structures which are derivatives of the arisotypic cubic perovskite structure (ABX_3), exemplified by $SrTiO_3$ (tausonite) or $KMgF_3$ (parascandolaite) by: (1) tilting and distortion of the BX_6 octahedra; (2) ordering of A- and B-site cations; (3) formation of A-, B- or X-site vacancies. This hierarchical scheme can be applied to some naturally-occurring oxides, fluorides, hydroxides, chlorides, arsenides, intermetallic compounds and silicates which adopt such derivative crystal structures. Application of this hierarchical scheme to naturally-occurring minerals results in the recognition of a perovskite supergroup which is divided into stoichiometric and non-stoichiometric perovskite groups, with both groups further divided into single ABX_3 or double $A_2BB'X_6$ perovskites. Subgroups, and potential subgroups, of stoichiometric perovskites include: (1) silicate single perovskites of the bridgmanite subgroup; (2) oxide single perovskites of the perovskite subgroup (tausonite, perovskite, loparite, lueshite, isolueshite, lakargiite, megawite); (3) oxide single perovskites of the macedonite subgroup which exhibit second order Jahn-Teller distortions (macedonite, barioperovskite); (4) fluoride single perovskites of the neighborite subgroup (neighborite, parascandolaite); (5) chloride single perovskites of the chlorocalcite subgroup; (6) B-site cation ordered double fluoride perovskites of the cryolite subgroup (cryolite, elpasolite, simmonsite); (7) B-site cation ordered oxide double perovskites of the vapnikite subgroup [vapnikite, (?) latrappite]. Non-stoichiometric perovskites include: (1) A-site vacant double hydroxides, or hydroxide perovskites, belonging to the söhngeite, schoenfliesite and stottite subgroups; (2) Anion-deficient perovskites of the brownmillerite subgroup (srebrodolskite, shulamitite); (3) A-site vacant quadruple perovskites (skutterudite subgroup); (4) B-site vacant single perovskites of the oskarssonite subgroup [oskarssonite]; (5) B-site vacant inverse single perovskites of the cohenite and auricupride subgroups; (6) B-site vacant double perovskites of the diaboleite subgroup; (7) anion-deficient partly-inverse B-site quadruple perovskites of the hematophanite subgroup.

KEYWORDS: perovskite, group theory, ordered perovskites, hydroxide perovskites, crystal structure, hierarchial classification.

Introduction

SINCE the last revision to the nomenclature of the perovskite group of minerals by Nickel and McAdam (1963) several new members of this structural group have been approved by the Commission on New Minerals, Nomenclature and Classification (CNMNC) of the International Mineralogical Association (IMA). These include the silicate perovskite, bridgmanite [$(Mg,Fe)SiO_3$], which is now considered to be the dominant mineral of the silicate mantle of the Earth.

*E-mail: rmitchel@lakeheadu.ca

(Tschauner *et al.*, 2014). The recognition of Mg and Ca-based silicate perovskites, although these are stable only at high pressures, has stimulated an extraordinary interest in the stability and phase transformations of silicate perovskites (Liu, 1976; Hirose, 2014) and their fluoride analogues, such as the $NaMgF_3$–$KMgF_3$ solid solution series (Zhao *et al.*, 1994; Chakhmouradian *et al.*, 2001). Contemporaneously, interest in perovskite as a petrogenetic indicator mineral resulted in numerous studies (see summary by Mitchell, 2002) of the paragenesis, composition and crystallography of minerals with the perovskite structure occurring in a wide variety of igneous and metamorphic rocks. Perovskite-group minerals have also gained import-ance in isotopic (Woodhead *et al.*, 2009; Zurevinski *et al.*, 2011) and geochronological (Smith *et al.*, 1989; Wu *et al.*, 2010) studies as it was recognized that their Sr and Nd isotopic compositions are sensitive indicators of the mantle sources of kimberlites, lamproites and melilitites. Perovskite-structured compounds of diverse composition are important constituents of slags produced by the aluminothermic reduction of pyrochlore (Mitchell and Mariano, 2016) and SYNROC-type nuclear waste forms (Ringwood, 1985; Lumpkin, 2014).

Simultaneously with renewed interest in naturally-occurring perovskites, studies of perovskites by the materials science and solid state chemistry communities have resulted in thousands of publications on the structure and properties of synthetic perovskites and related compounds. This work is driven by the actual, and potential, industrial uses of materials with the perovskite structure in applications ranging from ferroelectric ceramics through superconductivity and giant magnetoresistance devices to photovoltaic cells (Gallaso, 1990; Bruce *et al.*, 2010; see also Table 1 of Chakhmouradian and Woodward, 2014). Much of this work was driven by the observation that the perovskite structure is extremely 'flexible' with regard to cationic and anionic replacements and tolerance to ionic defects. Unlike many other structural types, every element of the periodic table, including the noble gases (Shcheka and Keppler, 2012; Britvin *et al.*, 2015; 2016), can be found in some variant of perovskite-structured compounds.

Of particular relevance to the mineralogical community were investigations of the *P-T-X*-driven distortions of the aristotypic cubic lattices of single (ABX_3) and ordered or double ($A_2BB' X_6$) perovskites. The application of group theory (Howard and Stokes, 1998, 2002, 2004, 2005; Stokes *et al.*, 2002) resulted in the establishment of

a hierarchy of space groups of perovskites with distorted crystal structures, termed hettotypes. Most perovskite supergroup minerals do not adopt the cubic space groups $Pm\overline{3}m$ or $Fm\overline{3}m$ and thus are considered as hettotypes of reduced symmetry.

Synthetic perovskites can be classified according to a hierarchy of structural types (Fig. 1) ranging from simple ABX_3 compounds and ordered variants through cation- and anion-deficient varieties to layered complex derivatives (Mitchell, 2002). This classification is in principle applicable to naturally-occurring perovskite supergroup minerals and can be used to explain why particular space groups are adopted and to predict the structural and compositional variants of perovskites that might be expected to occur in nature. Note that many of the more complex non-stoichiometric or layered derivatives of the ABX_3 aristotype structure, such as high temperature superconducting compounds, depart too far in topology to be considered as members of the perovskite supergroup as defined in this work.

Aristotype perovskite

The 'ideal' perovskite structure (Goldschmidt, 1926) from which the structures of all other compounds having the perovskite structure are derived is illustrated in Fig. 2. Ideal, or single, perovskites, where 'single' refers to the number of symmetrically non-equivalent *A* and *B* sites, have the general formula ABX_3, where the *A*-site cations are larger than the *B*-site cations and similar in size to the *X*-site anions. To a first approximation the structure consists of a cubic close-packed array of *X* anions with one quarter of these replaced by *A*-site cations in an ordered manner. The *A*-site cations are surrounded by 12 anions in twelve-fold cubo-octahedral coordination, and the *B*-cations are surrounded by 6 anions in octahedral coordination. The *X* anions are coordinated by two *B*-site cations and four *A*-site cations (Goldschmidt, 1926). Perovskites having the ideal structure adopt the cubic space group $Pm\overline{3}m$ ($P4/m\overline{3}2/m$; #221). The compound $SrTiO_3$ is commonly regarded as the archetypal cubic perovskite, although $KMgF_3$ is a better alternative as, unlike $SrTiO_3$, it remains cubic from 3.6 K to its melting point, and its structure is not affected by pressure up to 50 GPa (Mitchell *et al.*, 2006; Aguado *et al.*, 2008). Many naturally-occurring oxide and fluoride perovskites probably crystallized initially as cubic or tetragonal perovs-kites, and adopted their room temperature structure
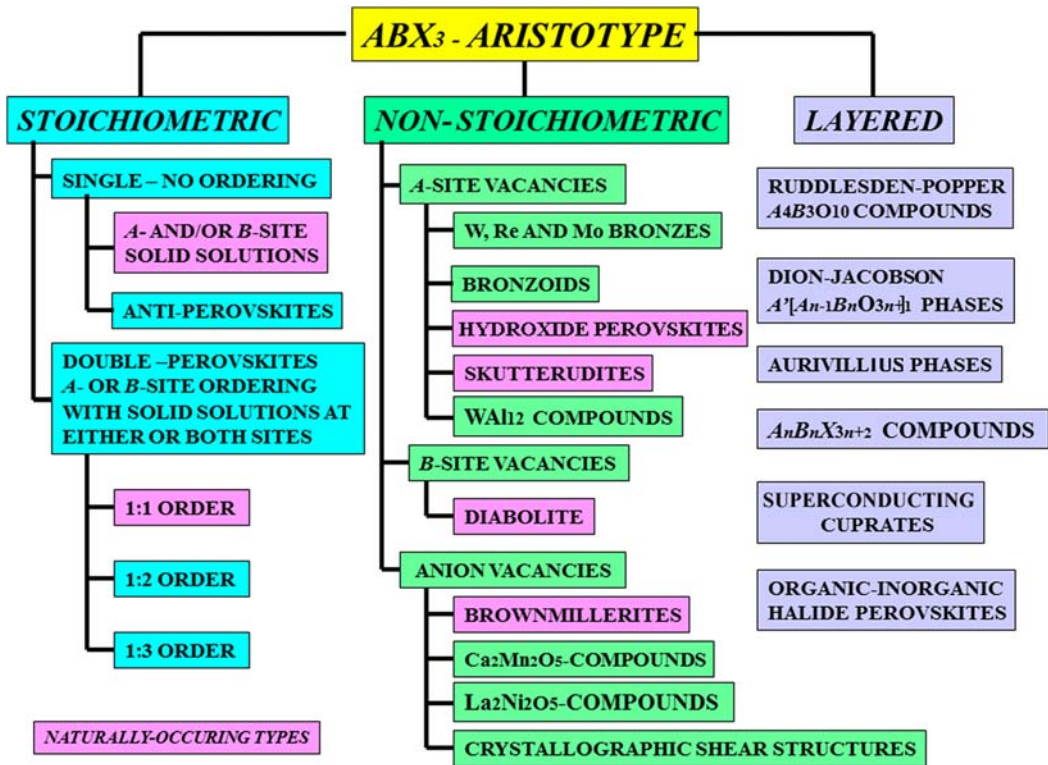
FIG. 1. Hierarchical classification of synthetic compounds with the perovskite structure and its derivatives.
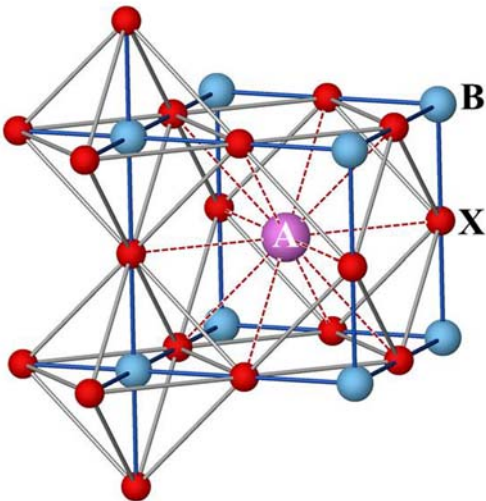

FIG. 2. The ideal ABX_3 perovskite structure showing the octahedral and icosahedral (12-fold) coordination of the B- and A-site cations, respectively.

as a consequence of distortion of these structures during cooling. Other perovskite-group minerals, including $CaTiO_3$ perovskite, typically crystallize at temperatures below the temperature required for phase transitions to a higher symmetry (e.g. located at >1100°C for synthetic $CaTiO_3$; Redfern, 1996; Carpenter et al., 2006). It is essentially unknown what the effect of composition is on the phase transition temperatures of complex naturally-occurring perovskite-group minerals. For example, the cubic-to-tetragonal transition can be reduced by several hundred degrees with the substitution of 25% Ca for Sr in synthetic $CaTiO_3$ (Carpenter et al., 2006). Hu et al. (1992) used transmission electron microscopy to examine several perovskite-group minerals, including cumulus loparite from igneous rocks, and found no evidence for transformation twinning in any of the samples investigated as many twins appear to be growth twins. Note that hydroxide perovskites, such as dzhalindite or stottite, which form in supergene environments are unlikely to have undergone phase transitions in
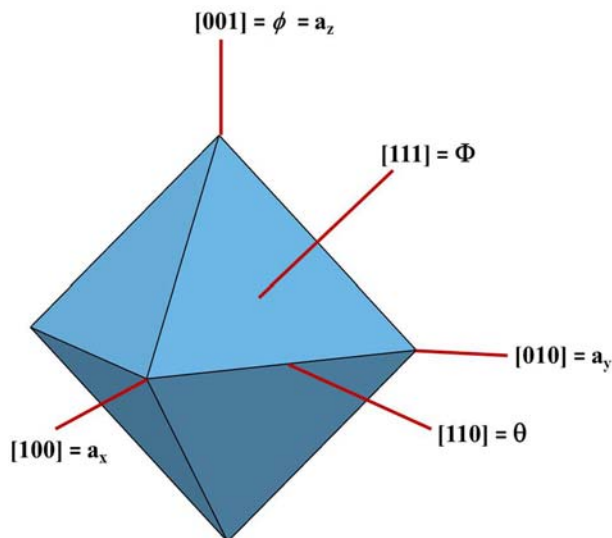
413

FIG. 3. Directions of rotation of the BX_6 octahedron relative to the pseudocubic cell axes. Glazer (1972) tilt axes are shown as a_x, a_y and a_z. Also shown is the commonly used notation (Zhao *et al.*, 1994) for describing the magnitude of the tilts about the pseudocubic $[110]_p$, $[001]_p$ and $[111]_p$ axes as the rotation angles θ, φ and Φ. Note that the θ angle is the resultant of the Glazer a_x and a_y tilts.

nature, although these have been observed in some experimental studies (see below).

Distorted ABX_3 perovskites

The majority of simple synthetic and natural perovskites are distorted derivatives of the aristotypic perovskite structure resulting from: (1) tilting (i.e. rotation) of rigid BX_6 polyhedra; (2) first order Jahn-Teller distortion of BX_6 octahedra; (3) second order Jahn-Teller effects affecting the *A*- and *B*-cation polyhedra, and reflecting the mixing of molecular orbitals and/or lone-pair effects. Tilting of the BX_6 polyhedra is the commonest type of distortion found in naturally-occurring perovskites, although the other modes can be found in barioperovskite, macedonite and diaboleite.

BX$_6$ octahedron tilting

Octahedron tilting occurs when the size of the *A* cation is too small for the 12-fold site within the BX_6 polyhedral framework: e.g. Ca^{2+} in the synthetic $(Sr,Ca)TiO_3$ solid solution series (Yamanaka *et al.*, 2002). To accommodate such cations, the octahedra tilt about the three axes of the pseudocubic precursor cubic cell (*x*, *y* and *z*), so as

to achieve the lowest energy mode for the crystal. In most tilting models it is assumed that the BX_6 octahedra are rigid, but not necessarily ideal, and the rotation does not disrupt their corner-sharing connectivity. Tilting results in changes in the *A–X* bond lengths so that they are no longer equal. This changes the *A*-site coordination, with concomitant reduction in symmetry from space group $Pm\bar{3}m$ to that of a hettotype. Coordination of the *A*-site cation as determined from bond valence analysis of the first coordination sphere can range from 12 to 8, depending upon the style and magnitude of the octahedron tilt. Many naturally-occurring ABX_3 perovskite-group minerals, including $CaTiO_3$ (perovskite *sensu stricto*), adopt the orthorhombic *Pbnm* $GdFeO_3$ structure type with the *A*-site cations in 8-fold coordination.

Distorted perovskites are commonly described using the nomenclature devised by Glazer (1972). In this scheme BX_6 octahedron rotations are described in terms of three orthogonal Cartesian axes coincident with the three axes of the aristotype cubic unit cell (Fig. 3). In the general case of unequal rotation angles about the *x*, *y* and *z* axes, the rotation scheme is denoted as *a*, *b* and *c* degrees, with sense of the rotations (i.e. clockwise or anticlockwise) in successive layers of octahedra perpendicular to a specific rotation axis given as
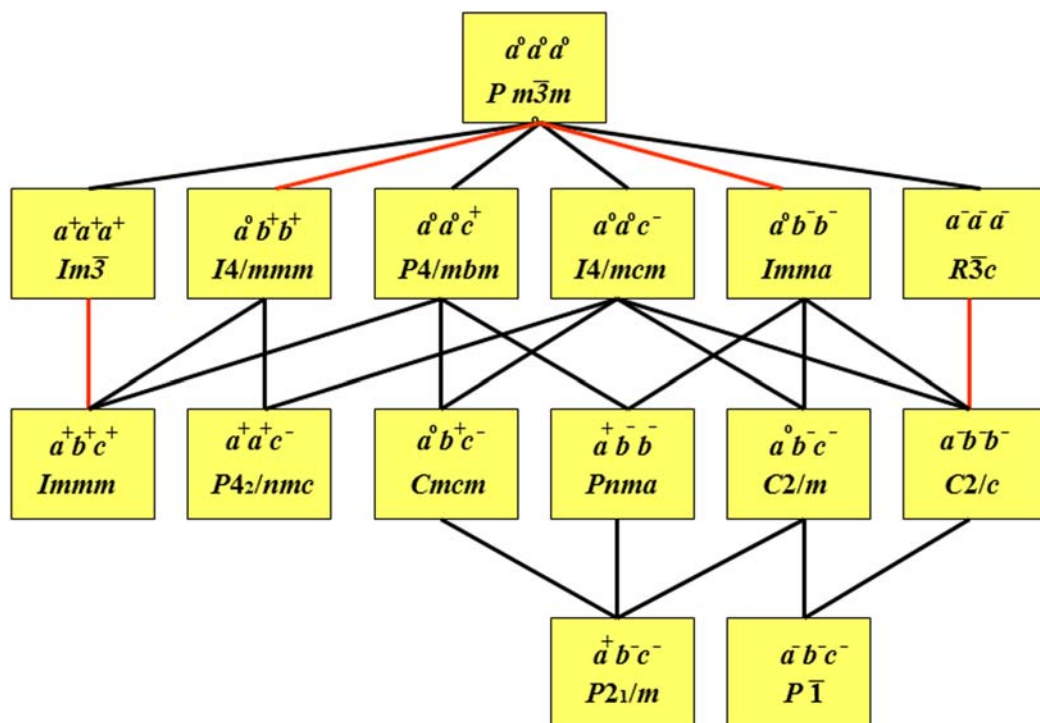
Fig. 4. Group–subgroup relations associated with particular tilt systems for ABX_3 single perovskites as evaluated by Howard and Stokes (1998, 2002) using group theoretical methods. Space group $Pm\bar{3}m$ is the aristotype from which all hettotypes are derived. Red and black lines indicate possible first and second order phase transitions, respectively.

superscripts. A positive superscript indicates tilt of octahedra in successive layers in the same direction (i.e. an in-phase tilt), whereas a negative superscript indicates rotation of consecutive octahedra along a specific rotation axis in the opposite sense (i.e. an anti-phase tilt). Thus, the symbol $a^+b^+c^+$ indicates three unequal angles of rotation about x, y and z with consecutive octahedra along the same axis (i.e. x, y or z) rotating in the same sense. For equal angles of rotation the notation would become $a^+a^+a^+$. A zero superscript is used for no rotations about a specific axis, e.g. the cubic aristotype lacking any octahedron tilting has the tilt symbol $a^0b^0c^0$ and space group $Pm\bar{3}m$.

Glazer (1972) used crystallographic principles to evaluate all possible combinations of tilting for single ABX_3 perovskites and identified 23 tilt systems corresponding to particular space groups. Howard and Stokes (1998) using group theory, confirmed Glazer's (1972) analysis, but reduced the number of tilt systems to 15, as some of Glazer's tilt systems were combinations of one or more of the basic fifteen. Such combinations and their

associated space groups are possible in principle but have not been observed in real crystals. Certain tilting patterns, e.g. those combining in-phase rotations about x and/or y with an antiphase rotation about z, cannot maintain the connectivity of rigid octahedra and hence require polyhedral distortions (Woodward, 1997). Figure 4 illustrates the space-group relationships associated with particular tilt systems for ABX_3 perovskites and identifies possible first and second order phase transitions from the cubic aristotype. These relationships are directly applicable to the P-T-X space-group transitions possible for natural perovskite-group minerals.

Similar analyses of octahedron tilting have been subsequently provided for 1:1, 1:2, and 1:3 B-cation ordered perovskites by: Woodward (1997); Howard et al. (2003); Lufaso and Woodward (2004); Howard and Stokes (2004); and Lufaso et al. (2006). The tilt schemes and the hierarchy of phase transitions (Fig. 5) for 1:1 ordered (or double) perovskites are given by Howard et al. (2003) and are applicable

directly to fluoride-based ordered perovskite-group minerals such as simmonsite and cryolite (see below).

Perovskite nomenclature

Perovskite-supergroup minerals as defined here are those minerals whose structures consist of three-dimensional networks of corner-sharing octahedra and which adopt the aristotypic ABX_3 perovskite structure or those of its derivatives. The octahedra can be tilted and/or distorted without destroying the connectivity. Cations at the B-site can be distributed randomly and termed single perovskites or ordered and termed double perovskites. The A-site can be filled or vacant, in the latter case forming A-site deficient single or double perovskites such as the hydroxide perovskites. The B-site can be partially, or entirely, vacant as in the minerals **diaboleite** or **oskarssonite**, respectively.

Naturally-occurring perovskite supergroup minerals occur as oxides, fluorides, chlorides, hydroxides, arsenides, antimonides, intermetallic compounds and silicates. Many of these have the ABX_3 perovskite structure and exhibit significant solid solution, coupled with the compositionally-driven space group changes which occur between potential ideal end-member compositions.

Perovskite supergroup minerals can be also described as 'homeotypic' in that they have the same essential topology but not necessarily the same space group.

Tables 1–3 together with Figs 6 and 7, present a hierarchical classification of the currently named members of the perovskite supergroup together with their room temperature space group as determined from diffraction studies of natural crystals or by analogy with synthetic analogues. This classification has been approved by the IMA-CNMNC (Hålenius *et al.*, 2016). The etymology of members of the supergroup is given in the Appendix to this paper (deposited with the Principal Editor of *Mineralogical Magazine* and available from http://www.minersoc.org/pages/e_journals/dep_mat_mm.html).

Two major groups are recognized in the perovskite supergroup: stoichiometric and non-stoichiometric groups. The former have ABX_3 or $A_2BB'X_6$ stoichiometry, and the latter include hydroxide- and arsenide-based minerals, which are also known as defect perovskites, characterized by A- and/or B-site vacancies together with the anion-deficient minerals of the brownmillerite and hematophanite subgroups. Note that many 'non-stoichiometric' perovskites have well-defined fixed ratios of A- or B-site cations or X anions but are considered here as non-stoichiometric relative to

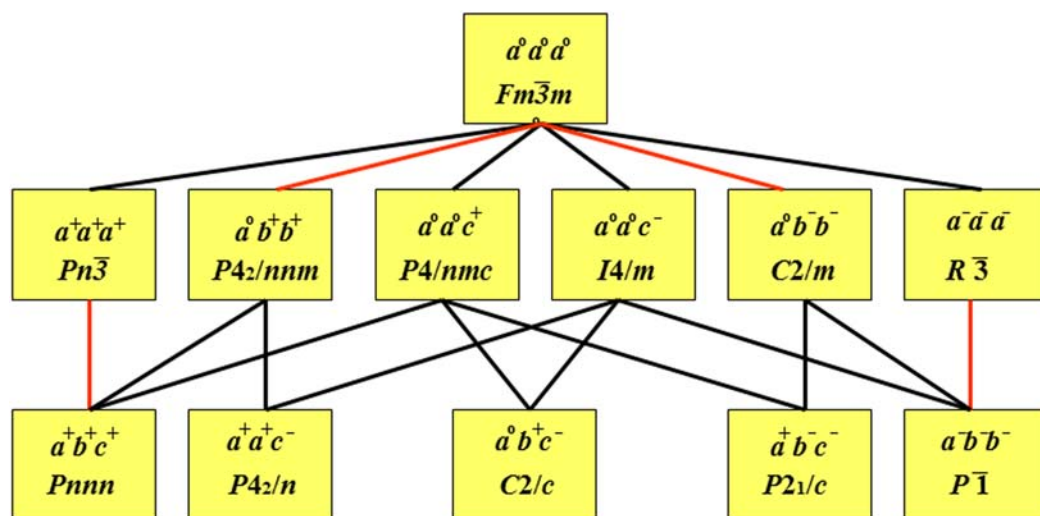
Fig. 5. Group–subgroup relations associated with particular tilt systems for 1:1 B-site ordered, or double perovskites, perovskites as evaluated by Howard *et al.* (2003) using group theoretical methods. Space group $Fm\bar{3}m$ is the aristotype from which all hettotypes are derived. Red and black lines indicate possible first and second order phase transitions, respectively.

TABLE 1. Classification of stoichiometric perovskites ABX_3 and $A_2BB'X_6$.

Group/subgroup	Composition	Ideal	Sp. gp.	Tilt
Single perovskites ABX$_3$				
Bridgmanite subgroup				
Bridgmanite	$(Mg,Fe)SiO_3$	$MgSiO_3$	*Pbnm*	$a^-a^-c^+$
Unnamed	?	$CaSiO_3$	?	
Perovskite subgroup				
Barioperovskite	$BaTiO_3$	$BaTiO_3$	*Amm*2*	$a^oa^oa^o$
Isolueshite	$(Na,La,Ce)(Nb,Ti)O_3$	$(Na,La)NbO_3$	*Pm$\bar{3}$m*	$a^oa^oa^o$
Lakargiite	$(Ca)(Zr,Sn,Ti)O_3$	$CaZrO_3$	*Pbnm*	$a^-a^-c^+$
Loparite	$(Na,REE,Ca,Sr,Th)(Ti,Nb)O_3$	$(Na,REE)Ti_2O_6$	*Pbnm*	$a^-a^-c^+$
Lueshite	$(Na,REE,Ca)(Nb,Ti)O_3$	$NaNbO_3$	*Pmmn*	
Macedonite	$(Pb,Bi)TiO_3$	$PbTiO_3$	*P4mm**(?)	$a^oa^oa^o$
Megawite	$(Ca)(Sn,Zr,Ti)O_3$	$CaSnO_3$	*Pbnm*	$a^-a^-c^+$
Perovskite	$(Ca,REE,Na)(Ti,Nb)O_3$	$CaTiO_3$	*Pbnm*	$a^-a^-c^+$
Tausonite	$(Sr,Ca,REE,Na)(Ti,Nb)O_3$	SrTiO3	*Pm$\bar{3}$m*	$a^oa^oa^o$
Neighborite subgroup				
Neighborite	$(Na,K)MgF_3$	$NaMgF_3$	*Pbnm*	$a^-a^-c^+$
Parascandolaite	$KMgF_3$	$KMgF_3$	*Pm$\bar{3}$m*	$a^oa^oa^o$
Chlorocalcite subgroup				
Chlorocalcite	$KCaCl_3$	$KCaCl_3$	*Pbnm*	$a^-a^-c^+$
Double perovskites A$_2$BB$'$ X$_6$				
Elpasolite subgroup				
Elpasolite	K_2NaAlF_6	K_2NaAlF_6	*Fm$\bar{3}$m*	$a^oa^oa^o$
Cryolite	Na_2NaAlF_6	Na_2NaAlF_6	*P2$_1$/n*	$a^-a^-c^+$
Simmonsite	Na_2LiAlF_6	Na_2LiAlF_6	*P2$_1$/n*	$a^-a^-c^+$
Vapnikite subgroup				
Vapnikite	Ca_2CaUO_6	Ca_2CaUO_6	*P2$_1$/n*	$a^-a^-c^+$
Latrappite (?)	$(Ca,Na)(Nb,Fe^{3+},Ti)O_3$	$Ca_2NbFe^{3+}O_6$	*P2$_1$/n*	$a^-a^-c^+$
Double antiperovskites B$_2$XX$'$A$_6$				
Sulphohalite subgroup				
Sulphohalite	$Na_6FCl(SO_4)_2$	$Na_6FCl(SO_4)_2$	*Fm$\bar{3}$m*	$a^oa^oa^o$

* Octahedra in space groups *Amm*2 and *P*4*mm* are not tilted and the reduction in symmetry from *Pm$\bar{3}$m* results from second order Jahn-Teller distortion.

Composition = compositional range of the mineral. Ideal = ideal composition of the end-member molecule. Sp.gp. = space group. Tilt = Glazer (1972) tilt scheme. *REE* = rare-earth element.

ABX_3 or $A_2BB'X_6$ perovskites. Within these groups following the dominant-constituent or dominant valency rules we recognize several compositional and structural subgroups depending on diverse combinations of the dominant *A*- or *B*-site cation or *X* anion. Together these constitute the perovskite supergroup.

We do not intend to use the modifying prefix 'keno' (from the Ancient Greek κενόζ = empty), as introduced by Atencio *et al.* (2010) for the *A*-site deficient minerals of the pyrochlore supergroup, as we consider this to be redundant for all *A*-site deficient perovskite structures. Moreover, the terms *A*-site deficiency, *A*-site vacancy, and defect perovskite are entrenched in the materials science and solid-state chemistry literature and thus have precedence; especially with regard to keyword search terms and potential interactions of mineralogists with those communities.

Although many compounds termed hexagonal perovskites have been synthesized (Mitchell, 2002) only a few are found in nature (Krivovichev, 2008). The structures of the majority of these are hexagonal antiperovskite polytypes characterized by combinations of face- and corner-sharing of octahedra rather than corner-sharing alone (Krivovichev, 2008). For this reason we do not consider such minerals as: 2*H*-nacaphite;

417

TABLE 2 Classification of non-stoichiometric perovskites.

	Composition	Ideal	Sp. gp.	Tilt
***A*-site vacant hydroxide perovskites**				
Single hydroxide perovskites				
Söhngeite subgroup				
Dzhalindite	$(In,Fe)(OH)_6$	$In(OH)_3$	$Im\bar{3}$	$a^+a^+a^+$
Söhngeite	$(Ga,Al,Fe)(OH)_3 \cdot xH_2O$	$Ga(OH)_3$	$P4_2/nmc$ or $P4_2/n$	$a^+a^+c^-$
Bernalite	$(Fe_{0.93}Si_{0.06}Zn_{0.01})[(OH)_{2.95}O_{0.04}]$	$Fe(OH)_3$	$Pmmn$	$a^+b^+c^-$
Double hydroxyperovskites				
Schoenfliesite subgroup				
Schoenfliesite[#]	$(Mg_{0.94}Mn_{0.13})_{1.07}Sn_{0.97}(OH)_6$	$MgSn(OH)_6$	$Pn\bar{3}$	$a^+a^+a^+$
Burtite	$(Ca_{0.98}Mg_{0.02})Sn(OH)_6 \cdot 0.39H_2O$	$CaSn(OH)_6$	$Pn\bar{3}$	$a^+a^+a^+$
Jeanbandyite	$Fe_x^{3+}Fe_{(1-x)}^{2+}Sn(OH)_{(6-x)}O_x(1 \geq x \geq 0.5)$	$Fe^{3+}Sn(OH)_5O$	$Pn\bar{3}$	$a^+a^+a^+$
Mushistonite	$(Cu_{0.48}Zn_{0.39}Fe_{0.17})_{1.04}Sn(OH)_{5.95}$	$CuSn(OH)_6$	$Pn\bar{3}$	$a^+a^+a^+$
Natanite[#]	$(Fe_{0.46}Zn_{0.36}Cu_{0.28})Sn(OH)_{6.09}$	$FeSn(OH)_6$	$Pn\bar{3}$	$a^+a^+a^+$
Vismirnovite	$(Zn_{0.89}Fe_{0.08}Cu_{0.1})Sn(OH)_{6.04}$	$ZnSn(OH)_6$	$Pn\bar{3}$	$a^+a^+a^+$
Wickmanite[#]	$(Mn_{095}Mg_{0.03}Ca_{0.2})Sn(OH)_6$	$MnSn(OH)_6$	$Pn\bar{3}$	$a^+a^+a^+$
Stottite subgroup				
Stottite	$(Fe_{1.15}^{2+}Mg_{0.03}Mn_{0.03}Ca_{0.01})_{1.22}Ge_{0.95}(OH)_6$	$FeGe(OH)_6$	$P4_2/n$	$a^+a^+c^-$
Mopungite	$NaSb(OH)_6$	$NaSb(OH)_6$	$P4_2/n$	$a^+a^+c^-$
Tetrawickmanite	$[(Mn_{0.94}Fe_{0.05}Ca_{0.01})(Sn_{0.98}Si_{0.11}Al_{0.010}(OH)_6$	$MnSn(OH)_6$	$P4_2/n$	$a^+a^+c^-$

[#] Extensive solid solution exists between natanite, schoenfliesite and wickmanite from Pitkäranta (Nefedov *et al.*, 1977). Composition = compositional range of the mineral. Ideal = ideal composition of the end-member molecule. Sp. gp. = space group. Tilt = Glazer (1972) tilt scheme.

5*H*-galeite; 7*H*-schairerite; 9*R*-kogarkoite; and 9*R*-hatrurite, as members of the perovskite supergroup. Only **sulphohalite**, $Na_6FCl(SO_4)_2$, an ordered double antiperovskite which adopts a cubic ($Fm\bar{3}m$) anti-elpasolite 3*C* polytype structure, is considered here as a member of the perovskite supergroup, as corner-sharing of the FNa_6 and $ClNa_6$ octahedra is maintained. The minerals palmierite, a derivative of the 9*R* hexagonal perovskite structure type (Mitchell, 2002), and orthorhombic *Pnma* javoreite ($KFeCl_3$; Kodera *et al.*, 2016) contain only face-sharing octahedra and thus are not a members of the perovskite supergroup.

Recently, McDonald *et al.* (2013) have noted that peatite-(Y) and ramikite-(Y), both complex Na-Li ± Zr phosphate carbonate minerals, can be described as cluster compounds based on simpler unit cells, and which are cation-deficient perovskite-related structures. Similar cluster compounds, such as $Cs_3Zr_6Br_{15}C$, are known as synthetic phases (Qi and Corbett, 1995) suggesting that there could exist a large number of perovskite-related cluster phases and minerals. In this work peatite-(Y) and ramikite-(Y) are not considered as members of the perovskite supergroup as their

structures are far-removed from those of other members.

Stoichiometric perovskite group – single *ABX*₃ perovskites

Silicate single perovskites – bridgmanite subgroup

The presence of silicates having the perovskite structure in the Earth's mantle has long been postulated on the basis of experimental petrological studies of pyrolite and lherzolite at high pressures and temperatures (Ringwood, 1991; Jackson and Rigden, 1998; Hirose, 2014) together with circumstantial evidence based on the character of decompressed silicate inclusions in diamonds (Stachel *et al.*, 2000). Recently, sub-micrometre crystals with the composition of $(Mg,Fe)SiO_3$ occurring in a four-phase mixture in shock-induced veins in the Tenham (L6) chondritic meteorite, were found by full profile refinement of X-ray diffraction (XRD) data to adopt space group *Pbnm*. This material with the perovskite structure was named bridgmanite by Tschauner *et al.* (2014). By analogy it is now

TABLE 3. Classification of A- and B-site vacant, and anion deficient perovskites.

PEROVSKITE SUPERGROUP

	Composition	Ideal	Sp. gp.	Tilt
A-site vacant skutterudites				
Skutterudite subgroup				
Skutterudite	$(Co,Fe,Ni)As_{2-3}$	$CoAs_3$	$Im\bar{3}$	$a^+a^+a^+$
Kieftite	$(Co,Ni,Fe,Cu)(Sb,Cl)_3$	$CoSb_3$	$Im\bar{3}$	$a^+a^+a^+$
Nickelskutterudite	$NiAs_{2-3}$	$NiAs_3$	$Im\bar{3}$	$a^+a^+a^+$
Ferroskutterudite	$(Fe,Co)As_3$	$FeAs_3$	$Im\bar{3}$	$a^+a^+a^+$
B-site vacant perovskites				
Single perovskites				
Oskarssonite subgroup				
Oskarssonite	$Al(F_{2.62}(OH)_{0.49})$	AlF_3	$R\bar{3}c$	$a^-a^-c^-$
Single antiperovskites				
Cohenite subgroup				
Cohenite	$C(Fe,Ni,Co)_3$	CFe_3	Pm	$a^-a^-c^+$
Auricupride subgroup				
Auricupride	$(Au,Pd)Cu_3$	$AuCu_3$	$Pm\bar{3}m$	$a^oa^oa^o$
Atokite	$Sn(Pd,Pt)_3$	$SnPd_3$	$Fm\bar{3}m$	$a^oa^oa^o$
Awaruite	$Fe(Ni,Co)_3$	$FeNi_3$	$Pm\bar{3}m$	$a^oa^oa^o$
Chengdeite	$(Fe,Ni,Co,Cu)(Ir,Pt)$	$FeIr_3$	$Pm\bar{3}m$	$a^oa^oa^o$
Isoferroplatinum	$(Fe,Cu,Ni)Pt_3$	$FePt_3$	$Pm\bar{3}m$	$a^oa^oa^o$
Rustenburgite	$Sn(Pt,Pd)_3$	$SnPt_3$	$Fm\bar{3}m$	$a^oa^oa^o$
Yixunite	$InPt_3$	$InPt_3$	$Pm\bar{3}m$	$a^oa^oa^o$
Zvyagintsevite	$(Pb,Bi)(Pd,Pt)_3$	$PbPt_3$	$Pm\bar{3}m$	$a^oa^oa^o$
Double Perovskite				
Diaboleite	$[Pb_2Cu(OH)_4Cl_2]$	$[Pb_2Cu(OH)_4Cl_2]$	$P4mm$	$a^oa^oa^o$
Anion deficient perovskites				
Brownmillerite subgroup				
Brownmillerite	$Ca_2Fe^{3+}AlO_5$	$Ca_2Fe^{3+}AlO_5$	$Ibm2$	-
Srebrodolskite	$Ca_2(Fe,Mg,Mn)_2O_5$	$Ca_2Fe_2^{2+}O_5$	$Pcmn$	-
Shulamitite	$(Ca,Sr,REE)(Ti,Zr,Nb)(Fe^{3+},Mn,Mg)(Al,Fe^{3+},Si)O_8$	$Ca_3TiFe^{3+}AlO_8$	$Pmma$	-
Hematophanite subgroup				
Hematophanite	$Pb_4(Fe_3^{3+},\square)(Cl,OH)O_8$		$P4/mmm$	-

Composition = compositional range of the mineral. Ideal = ideal composition of the end-member molecule. Sp. gp. = space group. Tilt = Glazer (1972) tilt scheme.
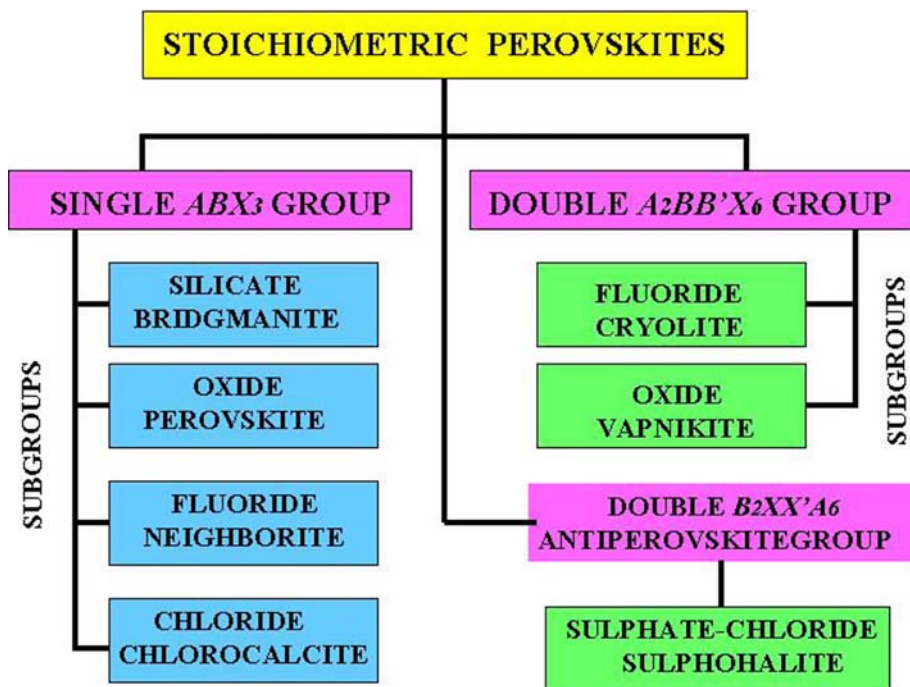
419

FIG. 6. Hierarchical classification of the stoichiometric perovskite supergroup minerals.
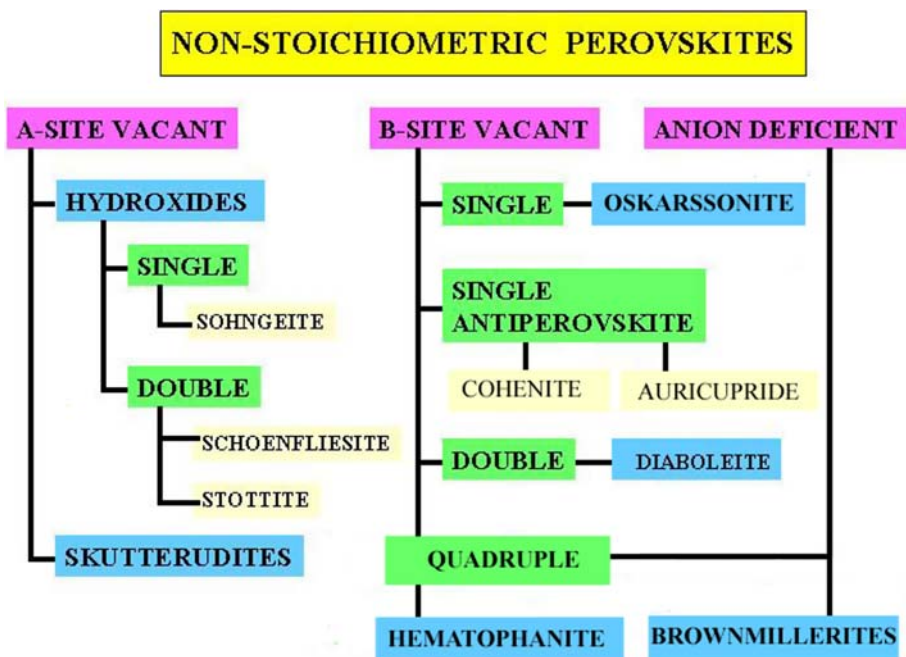

FIG. 7. Hierarchical classification of the non-stoichiometric perovskite supergroup minerals.

assumed that *Pbnm* bridgmanite is the most abundant mineral in the Earth and the dominant mineral in the lower mantle, i.e. from below ~700 km depth to near the core-mantle boundary where it probably transforms to a *Cmcm* $CaIrO_3$-type structure, commonly referred to as 'post-perovskite' by the geophysical community. This phase is stable above 120 GPa at 2500 K (Murakami *et al*., 2004; Oganov and Ono, 2004; Tsuchiya *et al*., 2004). These conditions correspond to a depth of ~2600 km and the location of the D″ seismic discontinuity at the base of the lower mantle. The 'post-perovskite' $CaIrO_3$-type phase has a pseudo-two-dimensional layer structure (Sugahara *et al*., 2008) and is not a member of the perovskite supergroup.

Experimental studies of the phase relationships of $CaSiO_3$ at high pressures (Gasparik *et al*., 1994) coupled with observations on decompressed calcium silicate inclusions in diamonds (Stachel *et al*., 2000; Kaminsky *et al*., 2001), clearly indicate that bridgmanite must be accompanied by $CaSiO_3$ with the perovskite structure in the lower mantle. The symmetry of this phase, initially identified as cubic (Liu and Ringwood, 1975), has been debated by Akber-Knutson *et al*. (2002), Caracas and Wentzcovitch, (2005); and Fang and Ahuja (2006). *In situ* experimental diffraction data relevant to resolution of this question are limited. As yet, quenched examples of this phase have not been found and the mineral remains unnamed.

Oxide single perovskites – perovskite subgroup

Members of this group (Table 1; Fig. 6) are characterized by oxygen as the dominant anion. Many of these ABO_3 perovskites are titanates which typically exhibit extensive solid solution between potential end-member compositions, as diverse cations can occupy the *A* and *B* sites. These minerals are the commonest members of the perovskite supergroup in the Earth's crustal environment (Mitchell, 2002), and as calcium-aluminum-rich (CAI) inclusions in chondritic meteorites. The latter are considered to represent remnants of the earliest accretionary material in the Solar System (McPherson *et al*., 2005).

Tausonite (SrTiO₃)

Tausonite was described initially from the Little Murun potassic alkaline complex, Sakha (Russia) by Vorob'yev *et al*. (1984). Most tausonite from
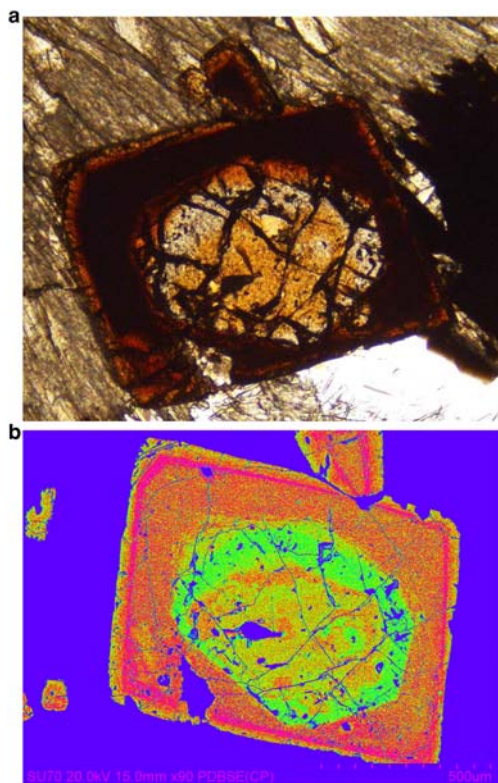
FIG. 8. Tausonite-strontian loparite from the Little Murun complex, Yakutia, Russia. Tausonite occurs in the core of this strongly-zoned crystal. (*a*) Plane polarized light optical image; (*b*) false coloured back-scattered electron image. See Mitchell and Vladykin (1993) for compositional data.

Little Murun is complexly zoned (Fig. 8) and contains significant amounts of Na and rare-earth elements (*REE*), representing a solid solution towards loparite (Vorob'yev *et al*., 1984; Mitchell and Vladykin, 1993). The material studied by Vorob'yev *et al*. (1984) represents an average composition in the tausonite–loparite series (~85 mol.% $SrTiO_3$), and thus is not that of pure $SrTiO_3$. In addition, silicate inclusions, represented by 2.2–5.0 wt.% SiO_2, were present in the material analysed by Vorob'yev *et al*. (1984). Calcium-bearing tausonite (2.1–2.5 wt.% CaO; 92–93 mol.% $SrTiO_3$) has been described from the P2-West lamproite, Wajrakurur (India) by Gurmeet Kaur and Mitchell (2013), where it occurs with baryte, pectolite and hydrogarnet as pseudomorphs after an unidentified primary phase. Tausonite with a composition close to that of pure $SrTiO_3$ (98 mol.%)
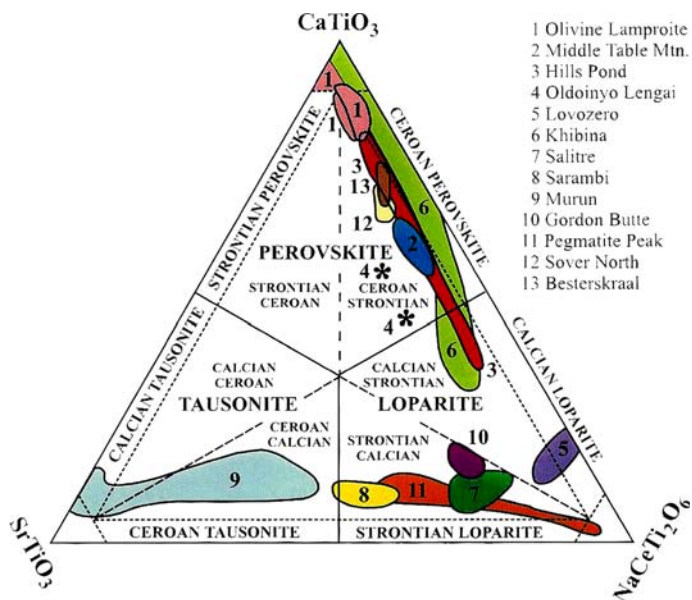
FIG. 9. Compositional variation (mol.%) of perovskite-group minerals from potassic and agpaitic syenites, rheomorphic fenites, lamproites and orangeites depicted in the ternary system $SrTiO_3$–$NaCeTi_2O_6$–$CaTiO_3$ (tausonite–loparite–perovskite) (after Mitchell, 2002). Note subdivisions of the compositional fields are used for the complete description of diverse compositions of these perovskite-supergroup minerals (Mitchell and Valdykin, 1993; Mitchell, 2002).

has also been found in Sr-rich metamorphic rocks of the Itoigawa-Ohmi District (Japan) by Miyajima *et al.* (2002). Tausonite with elevated levels of CaO (5–9 wt.%) and Na_2O (1.9–2.6 wt.%) has been described from several types of feldspathic hornfels xenoliths entrained in foyaite in the Khibiny alkaline complex (Kola Peninsula, Russia) by Yakovenchuk *et al.* (2005)

The crystal structures of tausonites from all of the above occurrences have not been determined. However, Vorob'yev *et al.* (1984) noted that as the powder XRD pattern ($a = 3.9048$ Å) of the holotype tausonite from Little Murun was similar to that of synthetic $SrTiO_3$ ($a = 3.9050$ Å; Hutton and Nelmes, 1981), it was assumed, by analogy, that the mineral must adopt space group $Pm\bar{3}m$. Synthetic compounds forming solid solutions in the binary system $SrTiO_3$–$NaNdTi_2O_6$ with >90 wt.% $SrTiO_3$ have cubic $Pm\bar{3}m$ structures (Ranjan *et al.* 2006; Mitchell and Tavener, unpublished data). Thus, although single-crystal determination of the structure of naturally-occurring pure tausonite has not been undertaken, it can be assumed reasonably that the end-member adopts space group $Pm\bar{3}m$. Stronitum-bearing perovskites exhibiting significant solid solution towards loparite most probably

have tetragonal structures (Ranjan *et al.*, 2006; Mitchell *et al.*, 2000*a*) thus the strontian loparite described by Haggerty and Mariano (1983) as 'cubic Sr-tausonite' (*sic*), probably has an *I*4/*mcm* structure (see below).

We recommend that **tausonite** be retained as the name for perovskite-supergroup minerals with the

FIG. 10. Perovskite crystals from the type locality, Akhmatovskaya Kop, in the Kusinskii Massif, Urals (Russia). Photo credit: A. A. Evseev, Fersman Museum, Moscow.
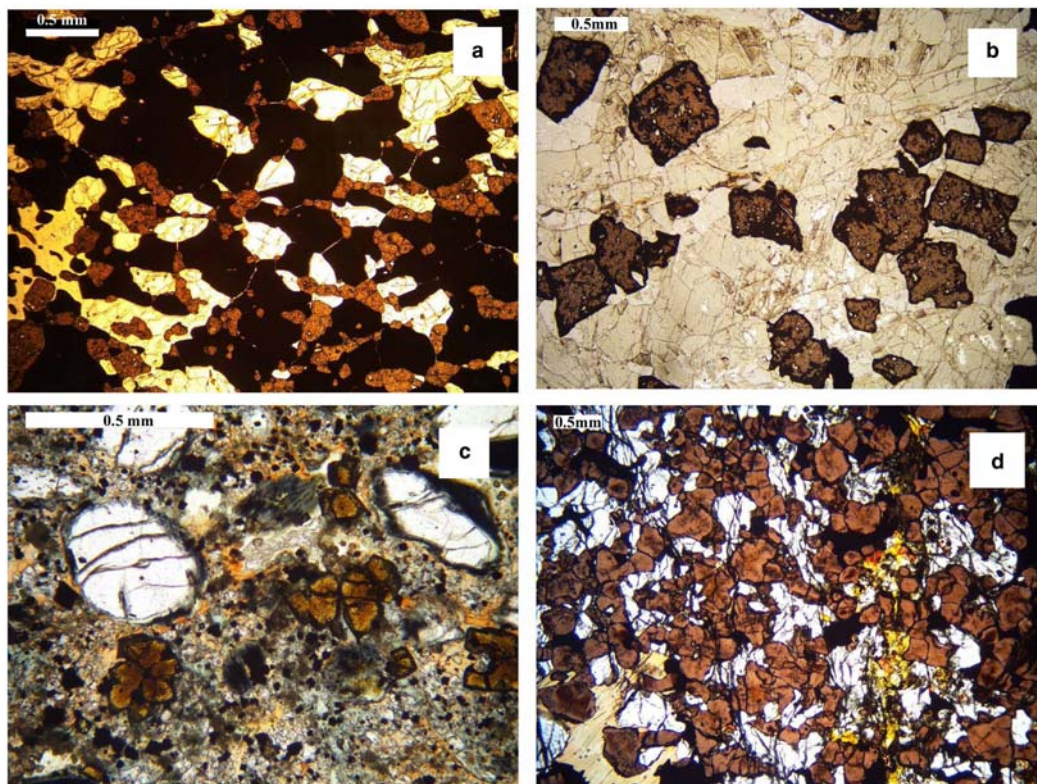
422

FIG. 11. Plane polarized light images of perovskite in: (*a*) afrikandite, Afrikanda complex, Kola (Russia); (*b*) uncomphagrite, Iron Hill, Colorado (USA); (*c*) kimberlite, Pipe 200, Lesotho; (*d*) perovskite pyroxenite, Tapira complex (Brazil).

general formula $(Sr,Ca,REE,Na)(Ti,Nb)O_3$ and no *A*- or *B*-site cation ordering, whose compositions (following the IMA dominant constituent/valency rules) are such that: (1) divalent cations predominate in the *A*-site with Sr as the dominant constituent; tetravalent cations predominate in the *B*-site with Ti as the dominant constituent. Compositions fall within the tausonite field in the ternary compositional (mol.%) system $SrTiO_3$–$CaTiO_3$ (Fig. 9).

Following IMA nomenclature protocols (Nickel and Grice, 1998; Hatert *et al*., 2013) 'impurity-stabilized' derivatives of tausonite, whose structures are topologically similar to, but depart from that of the cubic end-member, cannot be defined as distinct mineral species. We recommend that their relationship to tausonite be reflected in the root name, rather than an entirely new name to reduce the proliferation of mineral names that has plagued other mineral groups. Thus, the name of the tetragonal Na-*REE*-rich members of the

tausonite–loparite series should indicate the true symmetry by means of a hyphenated suffix i.e. tausonite-*I4*/*mcm*. Although these minerals, following the recommendations of Nickel and Grice (1998), could be referred to as 'tausonite-Q', we consider this symbolism not to be informative, or useful, especially if the true symmetry has been determined.

Perovskite (CaTiO₃)

Perovskite (*sensu stricto*), was initially described by Rose (1839) in calc-silicate contact metamorphic rocks in the Ural Mountains, Russia (Fig. 10). Perovskite is a characteristic minor-to-accessory mineral in a wide variety of undersaturated alkaline rocks ranging from kimberlite through melilitolites to carbonatites (Fig. 11). Investigations of the crystal structure have been hampered by the ubiquitous twinning, and initially the mineral was considered to be: orthorhombic (Bowman, 1908);

423

cubic (Barth, 1925); monoclinic $P2_1/m$ (Náray-Szabó, 1943); orthorhombic or monoclinic (Megaw, 1946). Kay and Bailey (1957) recognized that the powder XRD patterns of synthetic and natural $CaTiO_3$ were identical and suggested by analogy that the mineral adopts the orthorhombic space group *Pcmn*; a non-standard setting of space group *Pnma* (#62).

The determination of the room-temperature crystal structure of natural near end-member $CaTiO_3$ perovskite by single-crystal methods was not undertaken until that of Beran *et al.* (1996) on twin-poor crystals from the Benitoite Gem mine (San Benito, California), followed by that of Arakcheeva *et al.*,(1997) using material from near the type locality (Akhmatovskaya Kop) in the Kusinskii Massif, Urals (Russia). These studies demonstrated conclusively that $CaTiO_3$ perovskite adopts the space group #62, with the structural data reported in the *Pnma* setting. However, the structure is now commonly described in terms of the *Pbnm* setting (Fig. 12; Glazer tilt system $a^-a^-c^+$), and considered to represent the $GdFeO_3$ structure type following the work of Geller (1956) and Sasaki *et al.* (1987).

We recommend that **perovskite** be retained as the name for a mineral in the perovskite supergroup with the general formula $(Ca,REE,Na)(Ti,Nb)O_3$ and no *A*- or *B*-site cation ordering, whose compositions are such that: (1) divalent cations predominate in the *A* site with Ca as the dominant constituent; (2) tetravalent cations predominate in the *B* site with Ti as the dominant constituent. Perovskite compositions fall within the perovskite field in the ternary compositional (mol.%) systems $NaNbO_3$–$NaREETi_2O_6$–$CaTiO_3$ (Fig. 13) and $SrTiO_3$–$NaREETi_2O_6$–$CaTiO_3$ (Fig. 9).

Loparite $(Na,REE,Sr,Ca)(Ti,Nb)_2O_6$

Loparite was the second oxide perovskite-structured mineral to be recognized and was described briefly from nepheline syenite of the Lovozero peralkaline complex (Kola Peninsula, Russia) as 'Mineral no.1' by Ramsay and Hackman (1894). Subsequently, the mineral was misinterpreted as being perovskite by Ramsay (1897). The first complete description of loparite as a member of the perovskite group was by Kuznetsov (1925) using material from a nepheline syenite pegmatite in the adjacent Khibiny alkaline complex (Fig. 14). The mineral is typically complexly-twinned both macroscopically and at the resolution of the transmission electron microscope (Hu *et al.*,
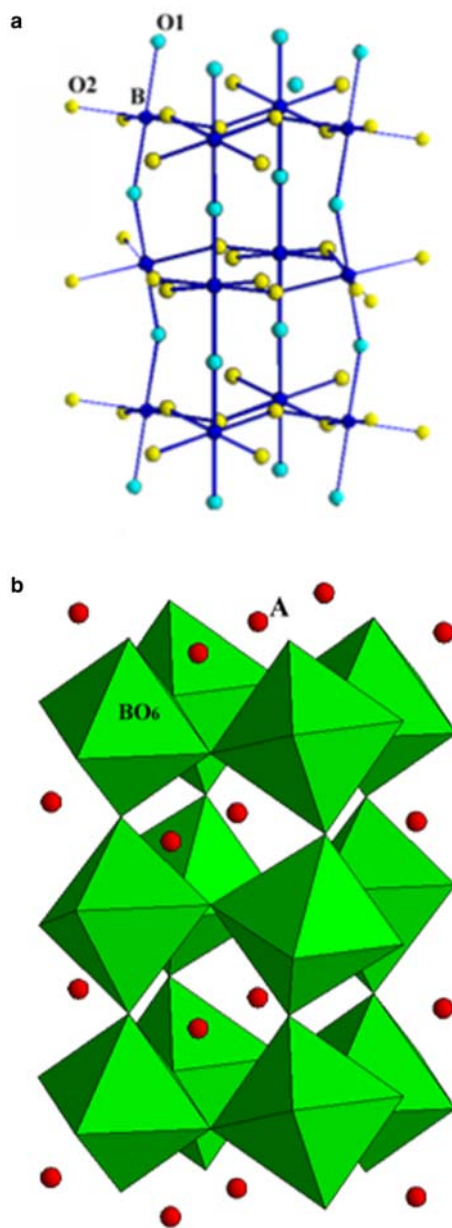
FIG. 12. Structure of $CaTiO_3$ and other ABX_3 stoichiometric oxide, silicate and fluoride perovskites adopting the $GdFeO_3$ structure with space group *Pbnm*. (*a*) Coordination of the BO_6 octahedra; (*b*) polyhedral model showing the location of the *A*-site cations relative to the BO_6 octahedra.

1992). Loparite is, incorrectly, described in most glossaries of mineralogy as possessing cubic or pseudocubic symmetry. Loparite occurs principally

Fig. 13. Compositional variation (mol.%) of perovskite-group minerals from: (1) kimberlites; (2) alkaline ultramafic rocks and carbonatites; (3) Khibina nepheline syenites and ijolites; (4) Lovozero nepheline syenites and urtites; (5) Burpala albitites and aegirinites; (6) Lueshe carbonatite, depicted in the ternary system 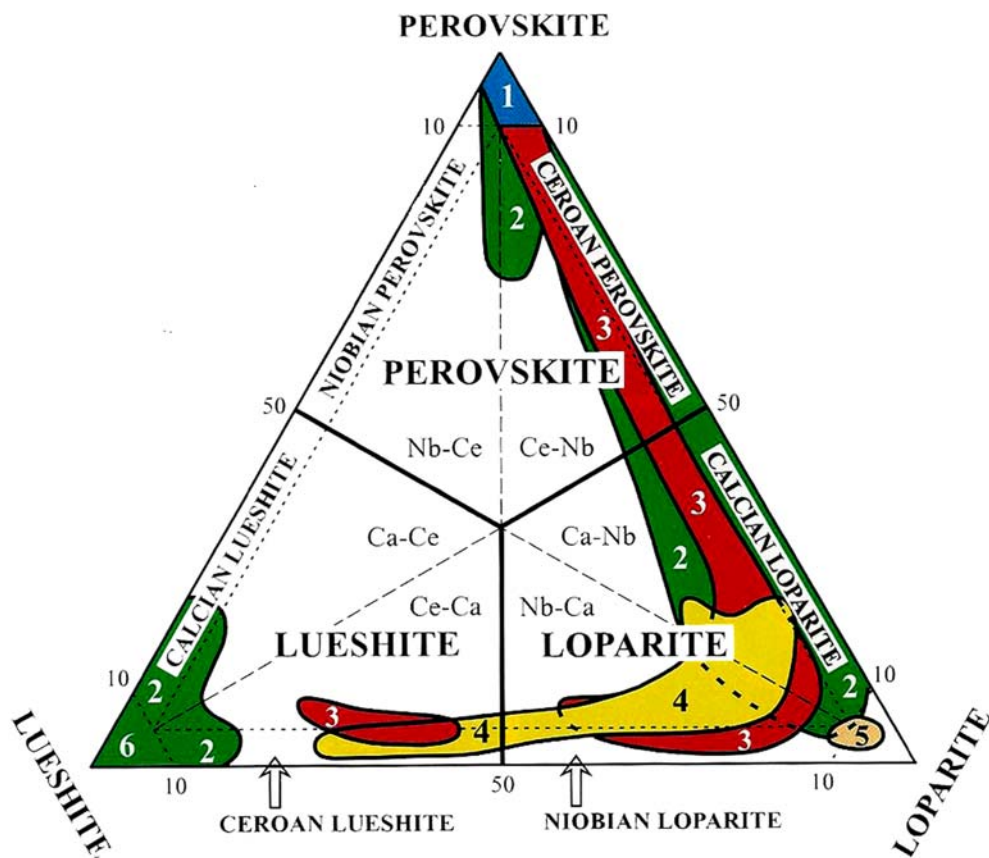$NaNbO_3–NaCeTi_2O_6–CaTiO_3$ (lueshite–loparite–perovskite) (after Mitchell, 2002). Note subdivisions of the compositional fields are used for the complete description of diverse compositions of these perovskite-supergroup minerals (Mitchell and Valdykin, 1993; Mitchell, 2002).

in peralkaline nepheline syenites and carbonatites (Mitchell, 2002)

Importantly, none of the loparite samples analysed show the predominance of *REE* among the large cations present (Mitchell and Chakhmouradian, 1996, 1998; Chakhmouradian and Mitchell, 1997, 2002). As a consequence of the presence of Nb (±Ta) in this mineral, which requires the incorporation of monovalent cations for charge compensation, Na is invariably the predominant *A*-site cation in loparite, including material from the type locality (Chakhmouradian and Mitchell, 1997), and in samples investigated by X-ray diffraction from three different localities by Mitchell *et al*. (2000*b*). Given the disordered distribution of cations in the structure of this

mineral (see below), the use of Levinson modifiers [e.g. loparite-(Ce)] to indicate the dominant *REE* species is clearly unwarranted. The ubiquitous presence of Nb, which can be assigned to the $NaNbO_3$ end-member, in natural loparite explains the predominance of Na over *REE* in its composition. The only exception is metamict loparite which has been affected to variable degrees by cation leaching. This primarily affects Na and produces a Na-deficient phase (or phases) of uncertain status, referred to in the literature as 'metaloparite' (Chakhmouradian *et al*., 1999).

Loparite (*sensu lato*) exhibits a very wide range in composition and is typically a quaternary solid solution. The space group adopted by any particular example is determined by whether the solid
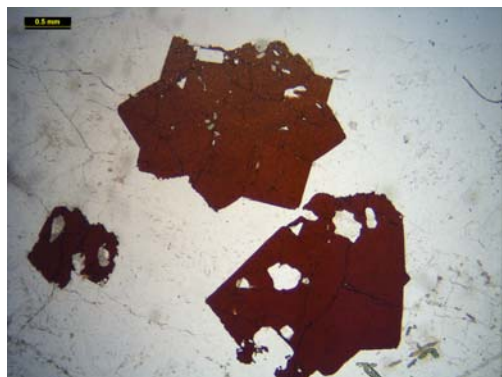
425

FIG. 14. Plane polarized light image of twinned loparite crystals from the type locality, the Khibiny peralkaline complex, Kola (Russia).

solution present is towards lueshite ($NaNbO_3$), tausonite ($SrTiO_3$) or perovskite ($CaTiO_3$). Very few single-crystal determinations of the structure of loparite have been undertaken, although the structures of synthetic analogues have been well-characterized by Rietveld methods. Mitchell *et al.* (2000*b*) determined the structures of three compositionally-distinct crystals by single-crystal methods and showed that depending on composition, loparite can adopt space groups *Pbnm* (#62) or *I4/mcm* (#140).

Stronium-poor niobian calcian loparite (mol.%: 3.4–3.5 $SrTiO_3$; 9.0–9.3 $CaTiO_3$; 24.0–25.4 $NaNbO_3$; 57.0–61.4 $Na_{0.5}REE_{0.5}TiO_3$: Mitchell *et al.*, 2000*b*) similar in composition to the holotype material from Khibiny has a similar structure to *Pbnm* $CaTiO_3$, but with a smaller octahedron tilt angle resulting from the presence of the significant amounts of the large, relative to Ca, *A*-site disordered cations. This loparite is close to being metrically tetragonal as $a > b$, suggesting that a slight increase in Na or Sr content would result in adoption of the *I4/mcm* space group. Studies of synthetic $NaREETi_2O_6$ compounds containing individual *REE* (Shan *et al.*, 1998; Sun *et al.*, 1997; Chakhmouradian *et al.*, 1999) have shown that, with the exception of $NaLaTi_2O_6$, all adopt the *Pbnm* $GdFeO_3$ structure. Depending upon the synthesis method $NaLaTi_2O_6$ can be rhombohedral $R\bar{3}c$ (Mitchell *et al.*, 2000*a*), tetragonal *I4/mcm* (Feng *et al.*, 2016) or orthorhombic *Pbnm* (Sun *et al.*, 1997). Mitchell and Liferovich (2005) determined that light-*REE*-rich synthetic perovskites in the system $Na_{0.75}REE_{0.25}Ti_{0.5}Nb_{0.5}O_3$, apart from the La compound, adopt space group *Pbnm*. Chakhmouradian *et al.* (1999) considered that

loparite from the Burpala complex (*c.* 81 mol.% $NaREETi_2O_6$) probably adopts the same structure, as determined by Rietveld methods, as the synthetic *Pbnm* compound $NaCeTi_2O_6$. Thus, given that the *REE* content of the majority of analysed loparite is dominated by Ce it is considered that the structures of synthetic *Pbnm* $NaCeTi_2O_6$ and Khibiny loparite as determined by single-crystal methods (Mitchell *et al.*, 2000*b*) best reflects that of the natural material approaching the end-member composition.

Mitchell *et al.* (2000*b*) have determined by single-crystal methods that both calcian niobian loparite (mol.%: 4.3–4.8 $SrTiO_3$; 12.6–13.9 $CaTiO_3$; 10.7–15.7 $NaNbO_3$; 60.6–69.4 $Na_{0.5}REE_{0.5}TiO_3$) and strontian calcian loparite (mol.%: 7.2–8.2 $CaTiO_3$; 5.2–5.8 $NaNbO_3$; 27.1–32.0 $SrTiO_3$; 48.7–52.1 $Na_{0.5}REE_{0.5}TiO_3$) adopt the space group *I4/mcm* as a consequence of compositionally-driven space group changes in the quaternary solid solution series loparite–lueshite–tausonite–perovskite (Mitchell *et al.*, 2000*b*). Thus, in common with tausonite (see above), without both structural and compositional data it is not possible to describe completely any particular loparite. Accordingly, we consider it is possible to recognize both *Pbnm* and *I4/mcm* varieties of loparite *sensu lato*.

We recommend that **loparite** be retained as the name for the mineral in the perovskite subgroup with the general formula (Na,*REE*,Ca,Sr,Th)(Ti,Nb)O_3 and no *A*- or *B*-site cation ordering, whose compositions are such that: (1) monovalent cations predominate in the *A*-site with Na as the dominant constituent; (2) tetravalent cations predominate in the *B*-site with Ti as the dominant constituent. Compositions fall within the loparite field in the ternary systems (mol.%) $SrTiO_3$–$NaREETi_2O_6$–$CaTiO_3$ (Fig. 9) or $NaNbO_3$–$NaREETi_2O_6$–$CaTiO_3$ (Fig 13). Specific structural varieties can be named as loparite-*Pbnm* or loparite-*I4/mcm*, etc. if their crystal structures have been determined by either Rietveld or single-crystal methods.

For the reasons discussed above, the Levinson modifier, loparite-(Ce), as previously used in descriptions of loparite should be discontinued. The hypothetical end-member loparite (*sensu stricto*) can be defined as *Pbnm* $NaREETi_2O_6$ for the purposes of calculation of end-member molecules from the compositions of natural loparite (*sensu lato*), where *REE* is the sum of the rare-earth elements present (atoms per formula unit, apfu) combined with an equivalent amount of Na (apfu). Any remaining Na is assigned with Nb to lueshite as $NaNbO_3$.

426

Lueshite (Na,REE)(Nb,Ti)O$_3$

Lueshite (Fig. 15) was originally described by Safianikoff (1959) from the Lueshe carbonatite complex (North Kivu, Democratic Republic of the Congo). Simultaneously, Danø and Sørenson (1959) described a mineral of similar composition in agpaitic nepheline syenite from the Ilímaussaq complex (Greenland). This mineral was provisionally termed 'igdloite'. Because this mineral was inadequately characterized with respect to its composition and properties, the name was abandoned in favour of lueshite in the revision of perovskite-group nomenclature by Nickel and McAdam (1963).

Safianikoff (1959) noted that the powder XRD pattern of lueshite was 'similar' to that of synthetic NaNbO$_3$ studied by Vousden (1953), who claimed that the room temperature space group was orthorhombic $P22_12$ (#17). Safianikoff (1959) did not determine the actual crystal structure of lueshite and merely assumed this was identical to that determined by Vousden and reported the structure in the conventional setting $P222_1$. This space group has been assigned to lueshite in some glossaries of mineral names (Blackburn and Dennen, 1997). Other glossaries (Anthony *et al*., 1997) following the determination of the crystal structure of synthetic NaNbO$_3$ by Sakowski-Cowley *et al*. (1969) and Hewat (1974) consider by analogy that lueshite adopts space group $Pbma$ (#57; a nonstandard setting of $Pbcm$). Note that the many crystal structures of synthetic NaNbO$_3$ remain under active discussion (Johnson *et al*., 2010; Peel *et al*., 2012; Cheon *et al*., 2015)

No determinations of the actual structure of lueshite were undertaken until those of Mitchell *et al*. (2002; 2014) who showed that the XRD powder patterns of lueshite were not compatible with synthetic NaNbO$_3$ and that the mineral probably adopts the space group $Pbnm$ (#62). Single-crystal X-ray determinations of the structure of lueshite from several localities by Mitchell *et al*. (2014) indicated that the mineral might adopt the space group $Pbnm$. However, conventional and time-of-flight powder neutron diffraction methods of structure determination were inconclusive, but indicated that lueshite at room temperature might consist of intergrown pinned metastable domains with orthorhombic (?$Pbnm$ + $Cmcm$) and/or monoclinic (?$P2_1/n$) structures. Such structural changes are analogous to those observed for NaTaO$_3$ during cooling which shows phase coexistence of $Pbnm$ + $Cmcm$ structures at room temperature (Knight and Kennedy, 2015). Arulesan *et al*. (2016*a*,*b*) have demonstrated, using K- and CaTiO$_3$-doped
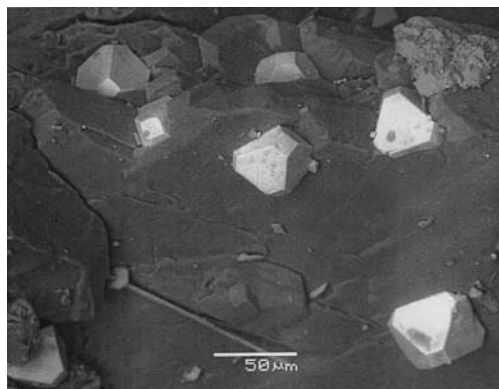

FIG. 15. Scanning electron micrograph of euhedral crystals of lueshite perched on aegirine from the St. Amable sill, Varennes Québec.

NaTaO$_3$, that the phase coexistence is not a function of hysteresis on cooling but is related to compositional heterogeneities or defects stabilizing the $Cmcm$ phase. These data could explain why lueshite does not exhibit the same crystal structure as pure NaNbO$_3$. However, recently, we have re-assessed the room-temperature structure of lueshite using time-of-flight high-resolution neutron diffraction data and concluded that a phase coexistence model is not appropriate (Mitchell, Kennedy and Knight, unpublished data). Instead we have determined that lueshite at room temperature adopts the space group $Pmmn$ [a = 7.8032(4) Å; b = 7.8193 (4) Å; c = 15.6156(9) Å], analogous to that of phase S of synthetic NaNbO$_3$ at 480–510°C (Peel *et al*., 2012) with a $2a_p \times 2a_p \times 4a_p$ superlattice This structure cannot be described using the original Glazer tilt scheme as there are compound octahedron tilts along the c axis. Peel *et al*. (2012) describe the structure as resulting from combinations of zero (0), in-phase (C) and anti-phase tilts (A) along the c axis, with the compound tilt scheme being $a^+b^+c^*$ where c^*, represents a compound tilt system composed of three distinct contributions; ACAC, CCCC; A0C0.

We recommend that **lueshite** be retained as the name for perovskite-group minerals with the general formula (Na,*REE*,Ca)(Nb,Ti)O$_3$ and no *A*- or *B*-site cation ordering, whose compositions are such that: (1) monovalent cations predominate in the *A*-site with Na as the dominant constituent; (2) pentavalent cations predominate in the *B*-site with Nb as the dominant constituent. Compositions fall within the lueshite field in the ternary compositional system (mol.%) NaNbO$_3$–Na*REE*Ti$_2$O$_6$–CaTiO$_3$ (Fig. 13).
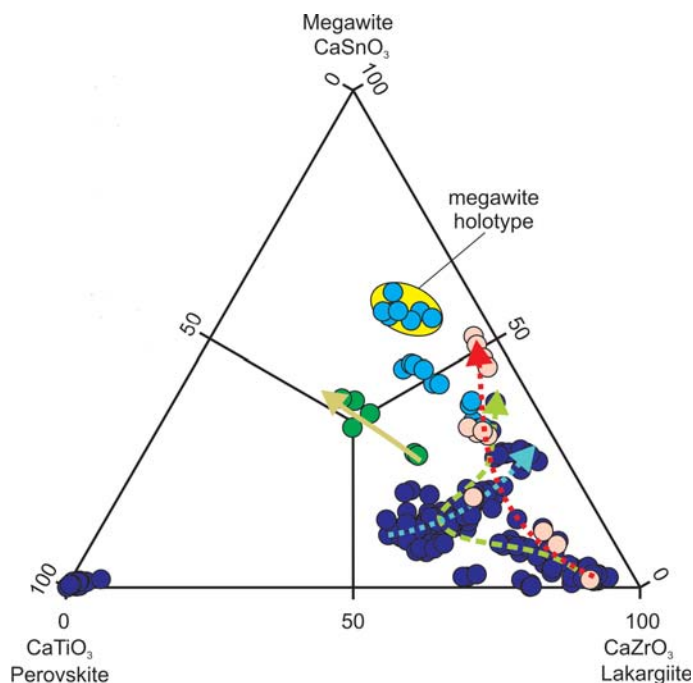
Fig. 16. Composition variation (mol.%) of megawite and lakargiite expressed in the ternary system $CaTiO_3$–$CaZrO_3$–$CaSnO_3$ (perovskite–lakargiite–megawite). Arrows indicate direction of composition change (after Galuskin *et al.*, 2011)

Recently, Menesez Filho *et al.* (2015) have described a polymorph of $NaNbO_3$ with a trigonal structure from the Jacupiranga carbonatite complex (Brazil). The mineral, named pauloabibite, adopts an ilmenite-type structure and is thus not a member of the perovskite supergroup.

Isolueshite (Na,La,Ce,Ca,Sr)(Nb,Ti,Ta)O₃

Isolueshite is found only in a hydrothermally-altered pegmatite vein in urtite-ijolite at the Khibiny alkaline complex (Chakhmouradian *et al.*, 1997). Isolueshite exhibits discontinuous compositional zoning with the La/Ce ratio, Nb, Th, Sr and Ca contents decreasing from the cores of cubo-dodecahedral crystals to their margin. The mineral in terms of its composition, but not structure, can be regarded as *REE*-rich (La-dominant) lueshite, and is approximately an intermediate member of the solid solution series between $NaNbO_3$ and $NaREETi_2O_6$. Isolueshite is not an end-member $NaNbO_3$ composition and is considered by Chakhmouradian *et al.* (1997) not to be a dimorph of lueshite, although the mineral is listed simply as $NaNbO_3$ in the current IMA list of mineral names. Krivovichev *et al.* (2000)

have shown by single-crystal diffraction methods that the mineral is cubic $Pm\bar{3}m$ and, unlike other cubic perovskites, is characterized by a disordered arrangement of the oxygen atoms in the 12 *h* site. The *A*-site is cation deficient (0.05–0.07 apfu) and the presence of hydroxyl groups (0.1 apfu) replacing oxygen was confirmed by infrared spectrometry.

The status of isolueshite as a distinct mineral species rather than a higher-symmetry variety of lueshite is perhaps ambiguous. However, isolueshite is topologically distinct from lueshite in that the oxygen atoms are disordered (Krivovichev *et al.*, 2000), thus justifying a different root name (Nickel and Grice, 1998). Applying the dominant constituent rule, Na and Nb are the dominant cations in the *A*- and *B*-sites with *REE* occurring as subordinate *A*-site constituents. As **isolueshite** is an IMA approved mineral name we recommend retention of this name.

Lakargiite (CaZrO₃)

Lakargiite occurs in high-temperature skarns in calc-silicate rocks found as xenoliths in ignimbrites of the Upper-Chegem volcanic structure, North

Caucasus (Galuskin *et al.*, 2008). Lakargiite is a member of the ternary solid solution series $CaZrO_3$–$CaTiO_3$–$CaSnO_3$. The maximum content of the $CaZrO_3$ component reaches 93 mol.%, whereas the minimum content is *c.* 50 mol.% (Fig. 16), with the remainder consisting of $CaTiO_3$, $CaSnO_3$, and in some examples, minor $Ca_2(Fe^{3+}Nb)O_6$. Galuskin *et al.* (2008) were unable to obtain structural data using single-crystal methods because of the complex twinning of all crystals examined. However, powder X-ray diffraction patterns could be refined by Rietveld methods in space group *Pbnm* in accord with the space group of synthetic $CaZrO_3$ (Koopmans *et al.*, 1983). Note that all end-members of the ternary system $CaZrO_3$–$CaTiO_3$–$CaSnO_3$ (Fig. 15) are *Pbnm* $GdFeO_3$-structured compounds, thus it is reasonable to assume that all samples of lagarkiite are orthorhombic *Pbnm* minerals. Lakargiite has also been found as sub-micrometre crystals in a carbonaceous chondritic meteorite (Ma, 2011).

We recommend that **lakargiite** be retained as the name for perovskite-group minerals with the general formula $(Ca)(Zr,Sn,Ti)O_3$ and no *A*- or *B*-site cation ordering, whose compositions are such that: (1) divalent cations predominate in the *A*-site with Ca as the dominant constituent; (2) tetravalent cations predominate in the *B*-site with Zr as the dominant constituent. Compositions fall within the lakargiite field in the ternary compositional (mol.%) system $CaZrO_3$–$CaTiO_3$–$CaSnO_3$ (Fig. 16).

Megawite ($CaSnO_3$)

Megawite occurs in high-temperature skarns in calc-silicate rocks found as xenoliths in ignimbrites of the Upper-Chegem volcanic structure, North Caucasus (Galuskin *et al.*, 2011). The mineral occurs in the same paragenetic association as lakargiite (see above) and is also a member of the ternary system $CaZrO_3$–$CaTiO_3$–$CaSnO_3$. The $CaSnO_3$ content of the holotype reaches 61 mol.%, and the mineral represents the limit of the compositional evolutionary trend of Sn-rich lakargiite (Fig. 16).

All megawite crystals so far found have been too small (<15 μm) for investigation by single-crystal diffraction methods and the structure was determined from electron back-scattered diffraction patterns. These data were compatible with structural data obtained for synthetic $Ca(Sn_{1-x}Zr_x)O_3$ perovskites (Tarrida *et al.*, 2009) and indicated that the mineral adopts the orthorhombic space group *Pbnm.*

We recommend that **megawite** be retained as the name for perovskite-group minerals with the general formula $(Ca)(Sn,Zr,Ti)O_3$ and no *A*- or *B*-site cation ordering, whose compositions are such that: (1) divalent cations predominate in the *A*-site with Ca as the dominant constituent; (2) tetravalent cations predominate in the *B*-site with Sn as the dominant constituent. Compositions fall within the lakargiite field in the ternary compositional (mol.%) system $CaZrO_3$–$CaTiO_3$–$CaSnO_3$ (Fig. 16).

Oxide single perovskites with second order Jahn-Teller distortions

Second order Jahn-Teller distortions result from weak covalent bonding and/or lone-pair effects. Compounds having the perovskite structure exhibiting this style of distortion are characterized by displacements of the *A*- and *B*-site cations from the centres of coordination polyhedra with (e.g. $PbHfO_3$) or without (e.g. $PbTiO_3$) octahedron tilting. Megaw (1968, 1973) noted that three styles of Jahn-Teller distortion are possible for perovskite BX_6 polyhedra: (I) along the tetrad axis resulting in a tetragonal unit cell; (II) along a diad giving an orthorhombic unit cell; (III) along a triad giving a rhombohedral unit cell. Macedonite and barioperovskite are examples of types I and II distortion, respectively (see below).

Macedonite ($PbTiO_3$)

Macedonite was initially described from Crni Kamen (or Kara Kamen), near Prilep, south-central Republic of Macedonia (Radusinović and Markov, 1971). The holotype mineral consisted of small (<0.2 mm) crystals in amazonite quartz syenite veins emplaced in pyroxene amphibole schist. Subsequently, macedonite was found as small inclusions (<50 μm) within hematite and ganomalite from Mn-rich skarns at Långban and Jakobsberg, Värmland (Sweden) by Burke and Kieft (1971) and Dunn *et al.* (1985). Macedonite from Crni Kamen is the only natural perovskite mineral known to contain significant amounts of Bi_2O_3 (2.2 wt.%). The crystal structure has not been determined by single crystal or Rietveld methods, but is considered on the basis of the powder X-ray diffraction pattern to be isomorphous with synthetic tetragonal *P4mm* $PbTiO_3$ (Nelmes and Kuhs, 1985) and $BaTiO_3$ (Buttner and Maslen, 1992).

Macedonite, if analogous in structure to *P4 mm* $PbTiO_3$, is the only known example of a perovskite-group mineral whose structure is determined by

type I second order Jahn-Teller effects from the aristotype. For synthetic $P4mm$ $PbTiO_3$, the Ti atoms are displaced 0.32 Å along the c axis of the TiO_6 polyhedra with the Pb cations displaced in the same sense, but with a different magnitude (0.48 Å), resulting in the adoption of tetragonal symmetry.

We recommend that **macedonite** be retained as the name for naturally-occurring $PbTiO_3$ whose compositions are such that: (1) divalent cations predominate in the A-site with Pb as the dominant constituent; (2) tetravalent cations predominate in the B-site with Ti as the dominant constituent.

Barioperovskite ($BaTiO_3$)

Barioperovskite occurs as micro-to-nanocrystals in a host of amorphous material within hollow tubular inclusions in benitoite at the Benitoite Gem mine, California (Ma and Rossman, 2008). Although Ma and Rossman (2008) report the presence of 0.89 wt.% SiO_2, this is considered to result from excitation of the host matrix. The crystals found were too small for single-crystal X-ray diffraction studies and the structure was determined from electron back-scattered diffraction patterns as compared to those of synthetic $BaTiO_3$. These patterns gave a best fit with the orthorhombic $Amm2$ structure, which is stable between 183 and 278 K. This orthorhombic polymorph of $BaTiO_3$ is an example of a type II second order Jahn-Teller distortion. Note that synthetic $BaTiO_3$ also adopts a $P4mm$ structure between 278 and 393 K (Kwei *et al*., 1993) and that the material examined by Ma and Rossman (2008) could have inverted from this tetragonal precursor. Note also that structural studies of $BaTiO_3$ are hampered by the development of metastable monoclinic and rhombohedral domains in tetragonal and orthorhombic crystals (Cao *et al*., 2009; Tsuda *et al*., 2013). The only other report of a natural occurrence of $BaTiO_3$, in the matrix of the Allende meteorite (Tanaka and Okumura, 1977), was not confirmed by Ma and Rossman (2008).

We recommend that **barioperovskite** be retained as the name for naturally-occurring $BaTiO_3$ where the compositions are such that: (1) divalent cations predominate in the A-site with Ba as the dominant constituent; (2) tetravalent cations predominate in the B-site with Ti as the dominant constituent.

Fluoride single perovskites – neighborite subgroup

The fluoride single perovskites ABF_3 (Table 1; Fig. 6) are the fluoride analogues of the oxide single perovskites. The structures of minerals in this group can be described by the octahedron tilting schemes used for ABO_3 perovskites.

Neighborite (Na,K)(Mg,Ba)F_3

Neighborite, $NaMgF_3$, was initially described by Chao *et al*. (1961) from a dolomitic shale of the Eocene Green River Formation, South Ouray, Uintah County, Utah, USA. Subsequently, neighborite has been found in a variety of parageneses ranging from biotite albitite through alkaline granites to calcite carbonatites (see Mitchell, 2002). In all of these examples the mineral is essentially pure $NaMgF_3$. Only, the neighborite occurring in the natrocarbonatite lavas erupted by the volcano Oldoinyo Lengai (Tanzania) differs in containing 15.5–16.8 wt.% K and 8.0–15.2 wt.% Ba, thus exhibiting solid solution towards $KMgF_3$ and $KBaF_3$ (Mitchell, 1997).

Chao *et al*. (1961) were unable to determine the crystal structure of neighborite, and on the basis of the similarity of the powder XRD pattern with that of $CaTiO_3$, following Kay and Bailey (1957), assigned it to space group $Pcmn$. As the mineral is effectively pure $NaMgF_3$, and in keeping with the space group settings used for other members of the supergroup, neighborite is best described in the orthorhombic $Pbnm$ setting (Zhao, 1998; Chakhmouradian *et al*., 2001).

We recommend that **neighborite** be retained as the name for naturally-occurring (Na,K)(Mg,Ba) F_3, whose compositions are such that: (1) monovalent cations predominate in the A-site with Na as the dominant constituent; (2) divalent cations predominate in the B-site with Mg as the dominant constituent.

Parascandolaite ($KMgF_3$)

Parascandolaite, $KMgF_3$, occurs as a volcanic sublimate in a fumarole developed on scoria produced by the 1944 eruption of Vesuvius (Demartin *et al*., 2014). Previously, a mineral with the probable composition of $KMgF_3$ had been reported in sublimates from Nyiragongo volcano (Democratic Republic of Congo) by Herman *et al*. (1960), although this was not recognised as a novel mineral species. Parascandolaite, has also been found as nano-inclusions in diamonds from Juina by Kaminsky *et al*. (2016).

Parascandolaite is pure $KMgF_3$, and single-crystal X-ray diffraction studies show conclusively that it adopts the cubic space group $Pm\bar{3}m$, in

430

common with the synthetic analogue (Zhao, 1998; Chakhmouradian *et al.*, 2001).

The material from Oldoinyo Lengai shows that neighborite and parascanodolaite undoubtedly form a continuous solid solution series in agreement with studies of the synthetic system NaMgF$_3$–KMgF$_3$ (Zhao, 1998; Chakhmouradian *et al.*, 2001). Note that intermediate members (35–55 mol.% KMgF$_3$) of this solid solution adopt the tetragonal space group *P4/mbm* (#127; Glazer tilt $a^\circ a^\circ c^+$). Thus, potassian neighborite and sodian parascanodolaite are probably tetragonal minerals. These fluoroperovskites provide a good illustration of how the room temperature structure of single *ABX$_3$* perovskites change as a consequence of compositional changes not involving any variations in intensive parameters.

We recommend that **parascandolaite** be retained as the name for naturally-occurring (K,Na)(Mg,Ba)F$_3$, whose compositions are such that: (1) monovalent cations predominate in the *A*-site with K as the dominant constituent; (2) divalent cations predominate in the *B*-site with Mg as the dominant constituent

Chloride single perovskite – chlorocalcite subgroup

Chlorocalcite, KCaCl$_3$, was recognized in 1872 as a sublimate in fumaroles from Vesuvius volcano (Palache *et al.*, 1951). No single-crystal X-ray diffraction studies of the mineral have apparently been undertaken although synthetic KCaCl$_3$ adopts the space group *Pbnm* (Midorikawa *et al.*,1979).

Stoichiometric double perovskites *A$_2$BB′X$_6$*

Ordered members of the perovskite supergroup (Table 1; Fig. 6) are derivatives of the aristotype *Pm$\bar{3}$m* structure formed when either or both of the *A*- and *B*-site cations are replaced by a combination of other cations located at a specific crystallographic site. If these cations are ordered at only one site the compounds are termed double perovskites, whereas if ordering occurs at both sites they are referred to as complex or quadruple perovskites.

The commonest of the *B*-site ordered perovskites have the general formula *A$_2$BB′X$_6$*, where *B* and *B′* are different cations in octahedral coordination situated in crystallographically-distinct sites. The *A*-site ordered double perovskites *AA′BX$_6$* and quadruple perovskites *AA′BB′X$_6$* have not yet been found as minerals but are well-known as synthetic phases. Skutterudites can be considered

as non-stoichiometric *A*-site vacant quadruple perovskites □□*BB′X$_6$*. The quadruple perovskite KCa(NaXe)O$_6$ with Na$^+$ and Xe^{8+} ordered on *B* and *B′* sites synthesized by Britvin *et al.* (2015) is possibly important with respect to terrestrial noble gas geochemistry. Britvin *et al.* (2015) have suggested that the observed depletion in Xe in the Earth's atmosphere could result from trapping of Xe in lower mantle perovskites.

Compounds with equal proportions of *B* and *B′* cations are termed 1:1 *B*-site ordered perovskites. In these, the *B* cations are ordered along (111)$_p$ planes (Fig. 17). Ideally, they exhibit long range order with no mixing of the cations over the two available crystallographic sites. However, site mixing is well-known in synthetic double perovskites and can be quantified by X-ray diffraction by calculation of a long range order parameter (Sleight, 1963; Mitchell, 2002). Such *B*-site mixing is present in vapnikite (see below). If the *B*O$_6$ and *B′*O$_6$ octahedra are not tilted, the compounds adopt the space group *Fm$\bar{3}$m* (#225) with a 2a_p (~8 Å) unit cell. With octahedron tilting, eleven space groups (Fig. 5) of reduced symmetry are possible (Howard *et al.*, 2003). The majority of natural minerals are fluorides of monovalent and trivalent cations with 1:1 *B*-site ordering (i.e. $A_2^+B^+B^{3+}F_6$), although a hydroxy-chloride (diaboleite) and an oxide (vapnikite) have also been recognized.

Double fluoride perovskites – cryolite subgroup

Cryolite (Na$_2$NaAlF$_6$)

Cryolite is the commonest mineral of the double fluoride perovskite subgroup. Cryolite was discovered during the latter part of the eighteenth century in pegmatites associated with F-rich albitized riebeckite granites at Ivigtut, West Greenland. The first description by Abilgaard (1799) predates that of CaTiO$_3$-perovskite by Rose (1839), making cryolite the earliest perovskite-supergroup mineral to be recognized. Cryolite occurs in a very wide range of parageneses (see Mitchell, 2002 for a summary).

Initial optical studies (Krenner, 1883; Böggild, 1912) indicating that cryolite adopts monoclinic symmetry were confirmed by Náray-Szabó and Sasvári (1938), who determined the space group to be monoclinic *P2$_1$/n* (#14: an unconventional setting of *P2$_1$/c*). Subsequently, the crystal structure has been confirmed and refined using single-crystal (Hawthorne and Ferguson, 1975) and Rietveld (Ross *et al.*, 2003) methods. Thus, cryolite is a 1:1 *B*-site ordered fluoride perovskite characterized by
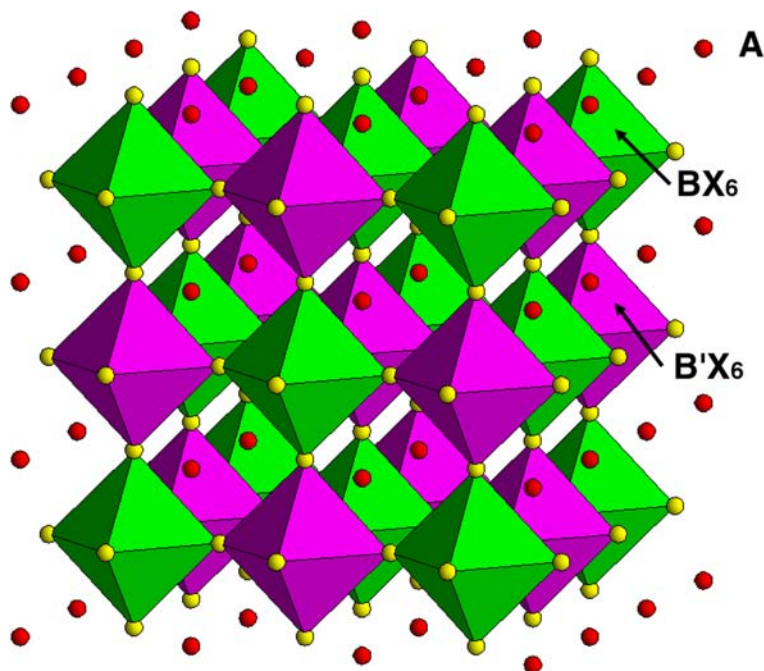
F<small>IG</small>. 17. Ideal 1:1 *B*-site ordering in $Fm\bar{3}m$ $A_2BB'X_6$ double perovskites illustrated by ordering of the BX_6 (green) and $B'X_6$ (purple) octahedra on rock-salt sublattices.

tilting of the NaF_6 and AlF_6 octahedra about three axes ($a^+b^-b^-$). The mineral is typically complexly twinned, possibly as a consequence of inversion from the high temperature $Fm\bar{3}m$ structure, via a first-order phase transition to a monoclinic $C2/m$ (#12; $a^\circ b^-b^-$) intermediate structure, with the transition from the latter to the room temperature monoclinic $P2_1/n$ structure being a second-order phase transition (Howard *et al*., 2003). Solid solution between cryolite and elpasolite has not been reported.

Elpasolite (K₂NaAlF₆)

Elpasolite, was described initially from quartz riebeckite microcline pegmatites of the Mount Rosa area of the St.Peter's Dome district, El Paso County, Colorado (Cross and Hillebrand, 1885). Subsequently, the mineral has been found in a wide variety of parageneses [see Mitchell (2002) for a summary].

Frondel (1948) on the basis of a powder XRD pattern of the holotype material concluded that elpasolite adopts the space group $Fm\bar{3}m$. Subsequently, Sabelli (1987), using single-crystal diffraction confirmed this hypothesis and

determined that the mineral is a 1:1 *B*-site ordered perovskite. The NaF_6 and AlF_6 octahedra are neither tilted nor distorted. The presence of the large K^+ cations in the 12-fold coordinated *A*-site prevents tilting of the BF_6 octahedra.

Simmonsite (Na₂LiAlF₆)

Simmonsite was described initially from the Zapot pegmatite amazonite-topaz-zinnwaldite pegmatite, Hawthorne, New Mexico (Foord *et al*., 1999). Here the mineral occurs in a late-stage breccia pipe with cryolite, cryolithionite and elpasolite. Simmonsite has been reported, but not described, from the cryolite-bearing Katuginskoye peralkaline granite (Seltman *et al*., 2010), Transbaikalia, Eastern Siberia.

Foord *et al*. (2009) were unable to determine the crystal structure because of the ubiquitous twinning, although suggesting the mineral was monoclinic. Ross *et al*. (2003) have shown that synthetic Na_2LiAlF_6, in common with cryolite, adopts space group $P2_1/n$ and concluded that the natural material must adopt this space group.

In summary, we recommend retention of the mineral names **elpasolite**, **cryolite** and **simmonsite** and classify them as members of the cryolite

subgroup of 1:1 ordered double fluoride perovskites.

Oxide double perovskites – vapnikite subgroup

Vapnikite (Ca_2CaUO_6)

Although 1:1 B-site ordered double perovskites are one of the commonest structural types of synthetic perovskite (Mitchell, 2002), the only *bona fide* naturally-occurring example is vapnikite (Galuskin *et al.*, 2014). Other minerals with this structure recognised in the future would be members of a potential vapnikite (or latrappite see below) subgroup. Vapnikite occurs as small (<10 μm) crystals in larnite-bearing pyrometasomatic rocks of the Hatrurim Formation at Jabel Harmun, Israel. Single-crystal structure determination showed that the mineral adopts the monoclinic space group $P2_1/n$ (#14), as a consequence of ordering and tilting of the CaO_6 and UO_6 octahedra. The mineral is the natural analogue of β-$Ca_2CaU^{6+}O_6$, a member of a large group of synthetic U-bearing double perovskites (Knyzazev *et al.*, 2011). Numerous compounds with Te^{6+} instead of U^{6+}, including the Te-analogue of vapnikite have also been synthesized (Christy *et al.*, 2016). Vapnikite differs from the synthetic compound in having a larger degree of Ca and U disorder at the octahedral sites and minor incorporation of U^{6+} at the A site coupled with splitting of the O3 site. The structural formula for vapnikite proposed by Galuskin *et al.* (2014) is $[(Ca_{1.96}U_{0.04})(Ca_{0.92}U_{0.08})(U_{0.83}Ca_{0.17})$ $(O1_2O2_2O3_{1.85}O3A_{0.15})]$. Vapnikite does not exhibit any solid solution with any other elements but is hydrated (1.3–3.4 wt.% H_2O) at the margins of the crystals. We recommend retention of the name **vapinkite** and recognise a vapnikite subgroup, into which other oxide double perovskites could be placed upon their recognition.

Nb- and Fe-rich perovskites – The status of latrappite

The nomenclature of niobium- and iron-rich perovskites has not yet been satisfactorily resolved. In the older literature niobium-rich perovskite was termed 'knopite', 'nioboloparite' or 'dysanalyte'. Nickel and McAdam (1963) recommended that both knopite and dysanalyte be abandoned as these minerals are merely Nb-bearing perovskites and members of the loparite–perovskite solid solution series. However, 'dysanalyte' from the Kaiserstuhl and Oka carbonatite complexes contains

significant amounts of Fe^{3+} and in this respect is not similar to other Nb-bearing perovskites (Mitchell *et al.*, 1998). Following Bonshtedt-Kupletskaya (1946), Tikhnenkov and Kazakova (1957) recognized that $Ca_2Fe^{3+}NbO_6$ could be a significant, though not dominant component of 'dysanalyte'. This component was not given a specific name. Regardless of Nickel and McAdam's (1963) recommendations the term 'dysanalyte' remains in use as a varietal name for Nb-Fe-rich perovskites. The name nioboloparite was discredited by Mitchell *et al.* (1996) as this mineral was shown to be niobian calcian loparite and/or niobian loparite.

The name 'latrappite' was introduced by Nickel (1964) on the grounds that unlike $CaTiO_3$ perovskite, the Nb content was greater than the Ti content, although the significant Fe^{3+} content was not considered. It is important to note that the material investigated by Nickel (1964) and Nickel and McAdam (1963) is not a potential end-member composition, and is actually a complex quaternary solid solution involving the components $Ca_2Nb_2O_7$, $Ca_2Fe^{3+}NbO_6$, $CaTiO_3$ and $NaNbO_3$ (Fig. 18). The dominant components of this solid solution are $Ca_2Nb_2O_7$ and $Ca_2Fe^{3+}NbO_6$. The latter component was termed 'latrappite' by Mitchell *et al.* (1998) and Mitchell (2002), following Tikhnenkov and Kazakova (1957).

In this work, Na-poor, very Ca-Nb-Fe-rich perovskites are considered as unlikely to be a simple solid solution given that one of the three synthetic polymorphs of $Ca_2Nb_2O_7$ (Scheunemann and Müller-Buschbaum, 1974: Ishizawa *et al.*, 1980; Lewandowski, *et al.*, 1992; Levin and Bendersky, 1999) is an orthorhombic $Pbn2_1$ layered perovskite (Scheunemann and Müller-Buschbaum, 1974; Levin and Bendersky, 1999) belonging to the $A_nB_nX_{3n+2}$ structural group. The orthorhombic, and monoclinic $Ca_2Nb_2O_7$ compounds, are different in topology from 'true' perovskites in that the B-X-B links are broken and slabs of perovskite-like units are mutually displaced (see below). Note that if the $Ca_2Nb_2O_7$ component of Nb-rich perovskite is considered to have the same structural topology as ABX_3 perovskite it would be required to have A- and B-site vacancies i.e $(Ca_{1.714}\square_{0.286})(Nb_{1.714}\square_{0.286})O_3$.

Synthetic $Ca_2Fe^{3+}NbO_6$ is a 1:1 B-site ordered double perovskite which adopts the monoclinic space group $P2_1/n$ (tilt scheme $a^-a^-c^+$; Chakhmouradian and Mitchell, 1998; Barnes *et al.*, 2009). In addition, synthetic $Ca_2Fe^{3+}NbO_6$ has also been shown by Chakhmouradian and
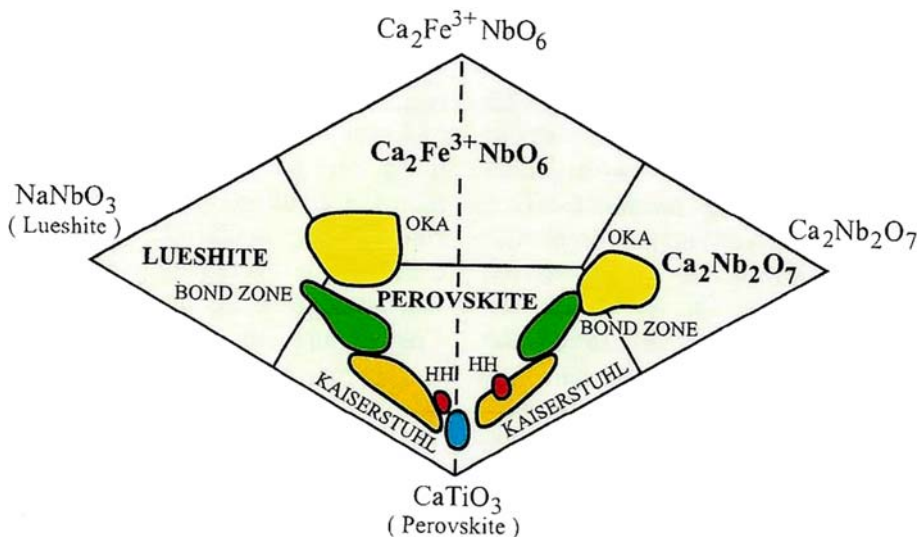
FIG. 18. Compositional variation (mol.%) of Nb-rich perovskites and latrappite from Oka (red, green and yellow fields), Kaiserstuhl (orange field) and Magnet Cove (blue field) carbonatite complexes, depicted in the quaternary system $NaNbO_3$–$CaTiO_3$–$Ca_2Nb_2O_7$–$Ca_2Fe^{3+}NbO_6$ (after Mitchell *et al.*, 1998; Mitchell, 2002).

Mitchell (1998) to exhibit *B*-site mixing. Simple continuous solid solutions between these potential end-member compounds is extremely unlikely, except for examples in which $(Nb + Fe^{3+}) < Ti$ (apfu). Note that most natural *Pbnm* $CaTiO_3$ perovskites exhibit very limited substitution of Ti by Fe^{3+} (1–2 wt.% Fe_2O_3) even in Fe-rich parageneses (Mitchell, 2002). Kimura and Muan (1971*a*,*b*) have shown that under strongly reducing conditions in the system CaO–FeO–TiO_2 there is no appreciable solid solution of Fe in $CaTiO_3$, whereas in air, perovskite can contain up to 83 wt.% Fe substituting for Ti. Chakhmouradian and Mitchell (2001) have found some groundmass perovskite in kimberlites to contain up to 8.3 wt.% Fe_2O_3 which is present as an orthoferrite component (6–13 mol.% $REEFeO_3$).

Mitchell *et al.* (1998), on the basis of Rietveld refinement of the laboratory powder X-ray diffraction pattern, claimed that latrappite from Oka is an orthorhombic *Pbnm*-structured mineral. However, Barnes *et al.* (2009) and Lufaso and Woodward (2004) note that neutron and/or synchrotron diffraction methods are required for determination of the correct crystal structure of many single and double perovskites. Thus, it is highly probable that standard powder laboratory X-ray diffraction methods do not have the required resolution to distinguish between the *Pbnm*, $P2_1/n$ and $Pbn2_1$ space groups.

In their structural study of synthetic binary perovskites with compositions $CaTi_{2-x}Fe_xNb_xO_3$ ($0 \leq x \leq 0.5$), Chakmouradian and Mitchell (1998) found that all had the *Pbnm* structure with complete disorder of Fe^{3+}, Ti^{3+} and Nb^{5+} at the *B*-site. Stachowicz, Welch and Mitchell (unpublished data) have determined the crystal structures of eleven natural Nb-rich (Na, Ca)$_2$(Fe^{3+},Ti^{3+}, Nb^{5+})$_2O_6$ perovskites having $Ca_2Fe^{3+}NbO_6$ (latrappite) contents of 25–62 mol.%, $Na_2Nb_2O_6$ contents of 25–48 mol% and $Ca_2Nb_2O_7$ contents of 8–24 mol.%. There is a clear negative correlation between $Ca_2Nb_2O_7$ and $Ca_2Fe^{3+}NbO_6$ contents. All of these perovskites have the *Pbnm* structure, with Nb^{5+}, Fe^{3+} and Ti^{4+} disordered at the *B*-site. Refinements in space group $P2_1/n$, which allows for ordering at two non-equivalent *B*-sites, indicated almost identical compositions (refined site-scattering values) for these two sites, demonstrating that the disordered *Pbnm* model is correct. No evidence for a 'defect' $Ca_2Nb_2O_7$-type structural component was found, e.g anomalous displacement parameters of oxygen atoms; superlattice reflections violating the *Pbnm* cell. Thus, any $Ca_2Nb_2O_7$ component in these perovskites would appear to be incorporated as a part of the general disorder at the *B*-sites and does not have a distinctive structural signature.

It remains to be shown if latrappites with higher $Ca_2Nb_2O_7$ and Ca_2FeNbO_6 contents can have a structural signature associated with
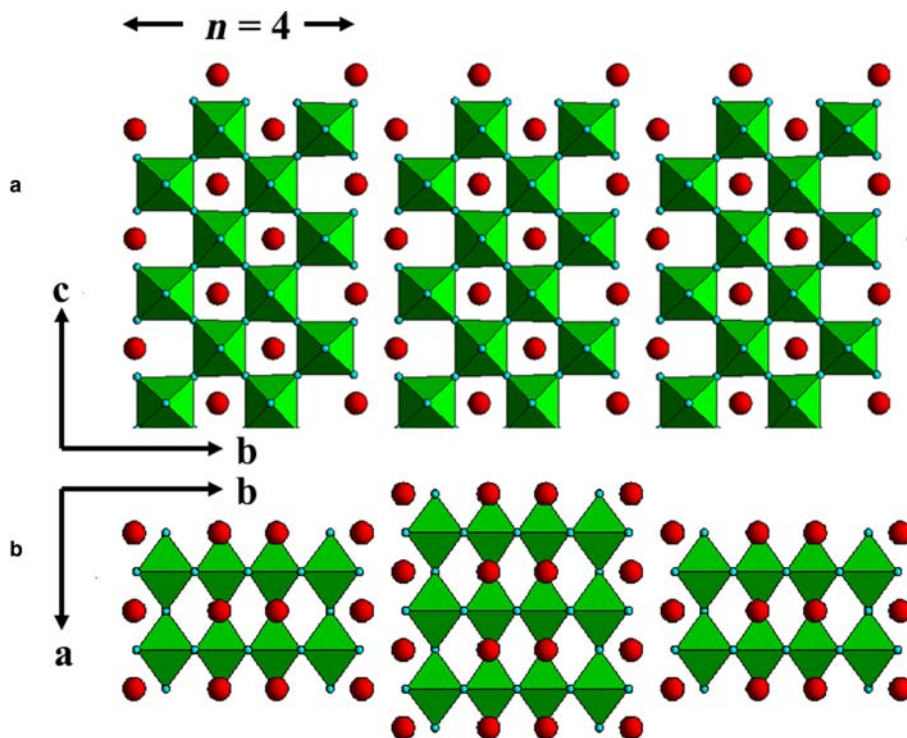
434

FIG. 19. The crystal structure of orthorhombic $Ca_4Nb_4O_{14}$ (or $Ca_2Nb_2O_7$) the $n = 4$ member of the $A_nB_nX_{3n+2}$ homologous series (Scheunemann and Müller-Buschbaum (1974) showing: (*a*) [100] projection; (*b*) [001] projection (after Mitchell, 2002).

vacancies, ordering, or $Ca_2Nb_2O_7$ polysomatic intergrowths (see below). The compositions of the latrappites chosen for structural studies undertaken so far confirm the dominance of the characteristic Ca_2FeNbO_6 component in solid solutions.

The orthorhombic compound $Ca_2Nb_2O_7$ (actually $Ca_4Nb_4O_{14}$) is the $n = 4$ member of the homologous $A_nB_nX_{3n+2}$ series (Levin and Bendersky, 1999). These compounds consist of perovskite-like slabs containing n layers of BO_6 octahedra (Fig. 19) The perovskite slabs are off-set from each other by crystallographic shear with a translation vector of about $(\sqrt{3}/2)a_p$. In effect extra oxygen is added to the vacancies in the BO_6 lattice created by the crystallographic shear. Of relevance to latrappite is that high resolution transmission electron microscopy (HRTEM) studies have revealed that many synthetic $A_nB_nX_{3n+2}$ compounds are actually composed of ordered intergrowths of different members of a homologous series, i.e. a polysomatic series. Portier *et al.* (1974) initially recognized that the

$(NaCa)_nNb_nO_{3n+2}$ or, the $Ca_2Nb_2O_7$–NaNbO$_3$ solid solution series, with $n = 4.5$ were composed of slabs with 4 and 5 layers of octahedra which formed ordered intergrowths in the sequence 5-4-4-5-4-4-5 $(NaCa_{12}Nb_{13}O_{45})$ and 4-5-4-5 $(NaCa_8Nb_9O_{31})$. Other studies (Nanot *et al.*, 1975; Williams *et al.*, 1993; Levin *et al.*, 2000) have reported blocks of 'normal' perovskite interspersed with slabs of layered perovskites. From these studies it is apparent that the homologous series of compounds between $Ca_2Nb_2O_7$ and NaNbO$_3$ (Portier *et al.*,1974) or $Ca_2Nb_2O_7$ and CaTiO$_3$ (Nanot *et al.*, 1975) form a polysomatic series rather than atomic solid solutions. As applied to latrappite it is possible that increasing Nb contents are accommodated by the formation of slabs of layered perovskite between blocks of normal perovskite. Mitchell *et al.* (1998) attempted to obtain evidence for this hypothesis from HRTEM lattice images. However, high-resolution images did not reveal any intergrowths for any of the grains examined. Either these samples did not contain sufficient amounts of the $Ca_2Nb_2O_7$
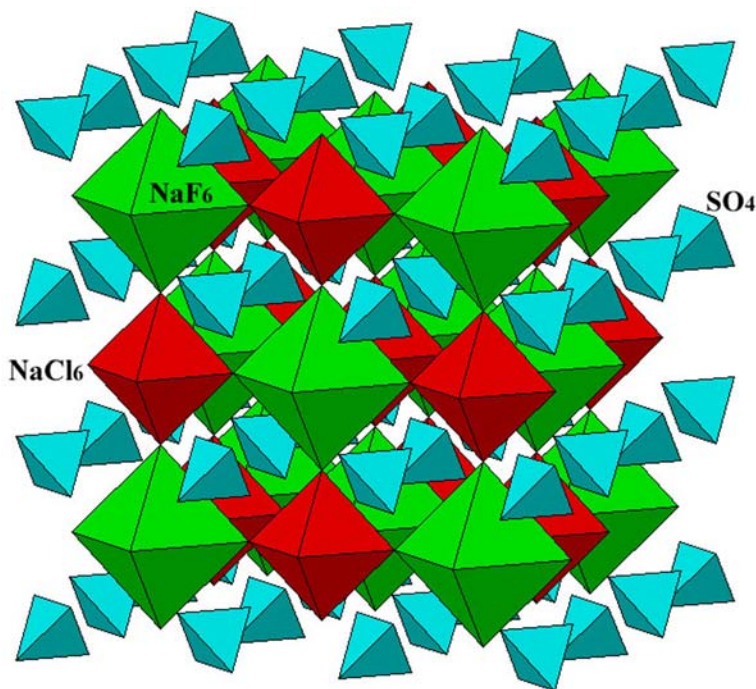
435

Fig. 20. The crystal structure of sulphohalite.

component to permit formation of discrete poly-synthetic intergrowths, or such layers occurred in an orientation that was not visible in this prelim-inary study. In summary, the mechanism by which Fe^{3+} and Nb^{5+} are accommodated as either $Ca_2Fe^{3+}NbO_6$, $Ca_2Nb_2O_7$ or $Ca(Fe^{3+},Nb)O_3$ with or without lattice vacancies remains elusive. Further study of the crystal structure of $Ca_2Fe^{3+}NbO_6$–$Ca_2Nb_2O_7$-rich latrappite by HRTEM and synchrotron X-ray diffraction is desirable to determine whether cation ordering, cation vacan-cies, polysomatic intergrowths, or other compos-itional domains are present or not. The formation of discrete short-range ordered domains with cation vacancies is one possibility.

How is latrappite to be defined if the name is to be retained? The mineral is not merely a Nb-rich *Pbnm* $CaTiO_3$ perovskite and the original definition by Nickel (1964) ignores the Fe^{3+} content. Given the observation that the dominant molecules in very Nb-and Fe^{3+}-rich perovskites appear to be $Ca_2Nb_2O_7$ and $Ca_2Fe^{3+}NbO_6$, we suggest that the potential end-member latrappite be considered as analogous to synthetic 1:1 ordered $Ca_2Fe^{3+}NbO_6$. However, without further crystallographic data, and in order to retain the name latrappite, we

recommend that Ca-rich, Nb- and Fe-rich perovs-kites $[(Ca,Na)_2(Nb,Fe^{3+},Ti)_2O_6]$ whose composi-tions are such that: (1) divalent cations prevail in the *A*-site with Ca dominant; and (2) pentavalent cations prevail in the *B*-site(s) with Nb dominant be termed **latrappite**. Compositions (mol.%) plotting within the $Ca_2Fe^{3+}NbO_6$ and $Ca_2Nb_2O_7$ fields in the quaternary compositional system $Ca_2Nb_2O_7$–$CaTiO_3$–$Ca_2Fe^{3+}NbO_6$–$NaNbO_3$ (Fig.18) can be termed **latrappite**. Note: $Ca_2Nb_2O_7$ is another potential naturally-occurring perovskite supergroup end-member composition for which a name would be desirable.

Double antiperovskite group $B_2XX'A_6$

Sulphohalite subgroup

Sulphohalite, $Na_6FCl(SO_4)_2$, was originally described from the Searles Lake (California) inter-montane evaporate deposits by Hidden and MacKintosh (1888), and its cubic structure deter-mined by Pabst (1934). Sulphohalite has recently been identified by Kaldos *et al*. (2015) in carbonate-rich melt inclusions in jacupirangite from Kerimasi volcano (Tanzania). Krivovichev

436

(2008) has recognized that sulphohalite is an ordered double antiperovskite with the anti-elpasolite structure and the space group $Fm\bar{3}m$. Double antiperovskites have the general formula $B_2X X'A_6$ (Mitchell, 2002, Krivovichev, 2008). In sulphohalite the structure consists of a framework of alternating anion-centred $[FNa_6]$ and $[ClNa_6]$ octahedra with tetrahedral $(SO)_4$ units occupying the cavities in this framework (Fig. 20) We consider that **sulphohalite** is a member of the perovskite supergroup and recommend retention of the name.

Non-stoichiometric perovskites

Here we define 'non-stoichiometric' specifically in relation to the stoichiometry of ABX_3 perovskites in which all sites (cation and anion) are fully occupied, i.e. a non-stoichiometric perovskite has partial occupancy of cation (A,B) and/or anion (X) sites. Such perovskites (Tables 2 and 3; Fig. 7) include: (1) A-site vacant double hydroxides, or hydroxide perovskites, belonging to the söhngeite, schoenfliesite and stottite subgroups; (2) Anion-deficient perovskites of the brownmillerite sub-group (brownmillerite; srebrodolskite, shulamitite); (3) A-site vacant quadruple perovskites (skutterud-ite subgroup); (4) B-site vacant single perovskites (oskarssonite subgroup); (5) B-site vacant inverse single perovskites (cohenite and auricupride sub-groups); (6) B-site vacant double perovskites (diaboleite subgroup); (7) Anion-deficient partly-inverse quadruple perovskites (hematophanite subgroup).

A-site vacant hydroxide perovskites

Natural and synthetic examples of both single and double perovskites are known for hydroxides lacking lacking A-cations and having the general stoichiometry $\square_2(BB')(OH)_6$. The octahedral framework sites can accommodate homovalent and heterovalent cations. The primary distinction made in this classification of hydroxide perovskites is between those with one or two different cations in their end-member formula. Following our hierarchical classification (Table 2; Fig. 7) we refer to these fundamentally different types as 'single' and 'double' hydroxide perovskites.

Paragenesis and current nomenclature

Detailed descriptions of the compositional variation and parageneses of hydroxide perovskite

minerals can be found in Mitchell (2002). The currently IMA-approved nomenclature together with our hierarchical classification of these minerals is given in Table 2. Note that some of the components reported in published analyses may reflect the presence of impurities.

Hydroxide perovskites form as rare secondary minerals resulting from the alteration of primary minerals, especially zinc and tin-bearing minerals, in a very wide range of parageneses. The formation conditions (Eh, pH, f_{O_2} etc) of the hydroxide perovskites have not been determined, although the environment can range from sub-areal supergene to marine sub-aqueous.

Hydroxide perovskite aristotypes

The aristotype of single hydroxide perovskites (Fig. 21), as represented by synthetic $In(OH)_3$ (Mullica *et al*., 1979) and $Sc(OH)_3$ (Schubert and Seitz, 1948) has space group $Im\bar{3}$ (#204) and tilt system ($a^+a^+a^+$). The structure of natural $In(OH)_3$, the mineral dzhalindite, is unknown, but assumed to be $Im\bar{3}$ as powder XRD data indicate a cubic unit cell.

In double hydroxide perovskites (Fig. 22), the ordering of the B and B' cations leads to the loss of I-centring and the aristotype has space group $Pn\bar{3}$ (#201), but with the same tilt system $a^+a^+a^+$. Numerous natural stannate hydroxide perovskites have this space group, including: schoenfliesite $MgSn(OH)_6$; wickmanite $MnSn(OH)_6$; and natanite $FeSn(OH)_6$.

Topological constraints on space groups

The presence of an O–H bond forces the B–O–B' linkages to be non-linear, resulting in highly-tilted octahedra and rendering impossible the aristotypic tilt system $a^0a^0a^0$ (space group $Pm\bar{3}m$) of hydroxide perovskites. Hence, no hydroxide perovskite has a zero tilt. Furthermore, mirror symmetry is only possible for single hydroxide perovskites, such as söhngeite $Ga(OH)_3$ ($P4_2/nmc$, #137; or $P4_2/n$, #86) and $In(OH)_3$ ($Im\bar{3}$, #204), as the mirror planes pass through the oxygen atoms between octahedra. In contrast, while it is theoretically possible for double perovskites to have mirror planes, these must bisect octahedra and the resulting structures have gross distortions due to size mismatch between cations, as seen in the previously reported structures of natanite $FeSn(OH)_6$ ($Pn\bar{3}m$; Strunz and Contag, 1960) and
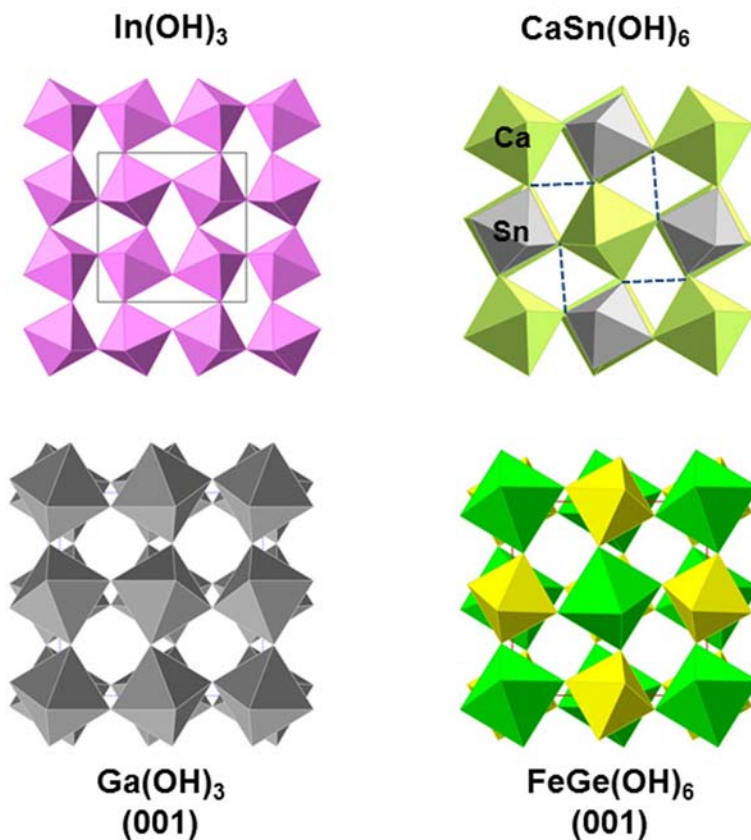
In(OH)₃

CaSn(OH)₆

Ga(OH)₃
(001)

FeGe(OH)₆
(001)

FIG. 21. Examples of framework motifs of single and double hydroxide perovskites. $In(OH)_3$, a single hydroxide perovskite, is cubic $Im\bar{3}$ with a single In site. Burtite $CaSn(OH)_6$, a double perovskite, is cubic $Pn\bar{3}$ with single Ca and Sn sites. The cubic phases have tilts of $a^+a^+a^+$. Söhngeite $Ga(OH)_3$, a single hydroxide perovskite, is tetragonal $P4_2/nmc$ ($a^+a^+c^-$). Four O–(H)···O bridges across the shorter O···O distances (2.8 and 3.0 Å) are shown for the $CaSn(OH)_6$ structure.

$CuSn(OH)_5$ ($P4_2/nnm$, Morganstern-Badarau, 1976) which are clearly incorrect.

Figure 22 shows the hydrogen-bonded arrangement of burtite $CaSn(OH)_6$ ($Pn\bar{3}$; #201) in which an isolated ring of four O–H···O linkages occurs. There are two non-equivalent H atoms, H(1) and H(2), each half-occupied. This isolated ring configuration is characteristic of all cubic hydroxide perovskites. The H(1)···H(1) and H(2)···H(2) distances are ~1 and ~1.4 Å (Basciano *et al.*, 1998). Thus, in the cubic structures ($Pn\bar{3}$ and $Im\bar{3}$) each oxygen atom is both a donor and an acceptor. The two local ring configurations are also shown in Fig. 21. Isolated rings also occur in combination with other O–H···O configurations in some non-cubic space groups. The dual donor-acceptor role of oxygen is a characteristic feature of hydroxide perovskites.

Single hydroxide perovskites

Three natural homovalent, or single, hydroxide perovskites have been found: bernalite [$Fe(OH)_3$] (Birch *et al.*, 1993; Welch *et al.*, 2005); dzhalindite [$In(OH)_3$] (Mullica *et al.*, 1979; Genkin and Mura'eva, 1964); and söhngeite [$Ga(OH)_3$] (Scott, 1971). In addition, a synthetic single hydroxide perovskite, δ-$Al(OD)_3$ (Matsui *et al.*, 2011), has been synthesized which is orthorhombic with space group $P2_12_12_1$ (tilt system $a^-a^-c^+$). Dzhalindite is the only single hydroxide perovskite having a cubic structure (space group $Im\bar{3}$) at ambient conditions.

A definitive structure for bernalite has yet to be reported. Originally, the structure of bernalite was determined in space group $Immm$ (#71; tilt scheme $a^+b^+c^+$) by Birch *et al.* (1993). Subsequently, space

438

group *Pmmn* (#71; tilt scheme $a^+b^+c^-$) was proposed by McCammon *et al.* (1995) and Welch *et al.* (2005), as numerous strong reflections violating *I*-centring were observed.

The original reported structure of söhngeite, $Ga(OH)_3$, from Tsumeb (Scott, 1971) was ortho-rhombic with the non-centrosymmetric space group $Pmn2_1$ (#31; tilt scheme $a^-b^-c^+$). A recent structure determination of söhngeite using single-crystal XRD (Welch and Kleppe, 2016) found that it adopts either space group $P4_2/nmc$ (#137) or $P4_2/n$ (#86) with a very different tilt system ($a^+a^+c^-$), and on heating to 423 K transforms to an $Im\bar{3}$ structure ($a^+a^+a^+$).

Double hydroxide perovskites

All heterovalent double hydroxide perovskites $\square_2BB'(OH)_6$ have ordered frameworks in which different cations alternate on crystallographically non-equivalent *B*-sites e.g. schoenfliesite [MgSn $(OH)_6$]; burtite [CaSn$(OH)_6$]; stottite [FeGe$(OH)_6$]; and mopungite NaSb$(OH)_6$. Complete ordering of heterovalent cations in double hydroxide perovs-kites is required to satisfy bond-valence constraints of bridging O atoms, each of which is bonded to an H atom as OH. Disorder in heterovalent structures is prohibited by under- or over-bonding of these O atoms, e.g. Mg–O–Mg + O–H = 1.67 valence units (vu), Sn–O(H)–Sn + O–H = 2.33 vu, compared with Mg–O–Sn + O–H = 0.33 + 0.67 + 1 = 2 vu. The motifs of burtite and stottite are shown in Fig. 21.

Most double hydroxide perovskites reported to date are stannates and, with the exception of tetrawickmanite MnSn$(OH)_6$ and synthetic CuSn $(OH)_6$, are cubic (reported space groups $Pn\bar{3}$ or $Pn\bar{3}m$). Of the non-stannates, stottite FeGe$(OH)_6$ (Strunz *et al.*, 1958; Strunz and Giglio, 1961; Ross II *et al.*, 1988) and mopungite NaSb$(OH)_6$ (Williams, 1985) are reported as tetragonal with space group $P4_2/n$ (#86). CuSn$(OH)_6$ was reported as having space group $P4_2/nnm$ (Morgenstern-Badarau, 1976), but this is almost certainly incorrect as the mirror planes of this structure bisect octahedra (see above).

Jeanbandyite Fe³⁺Sn(OH)₅O

Kampf (1982) refined unit-cell parameters of type jeanbandyite from Llallagua, Bolivia, from powder X-ray diffraction data as $a = c = 7.648(7)$ Å, recog-nizing that while this cell is metrically cubic, the mineral is optically uniaxial and, therefore, probably
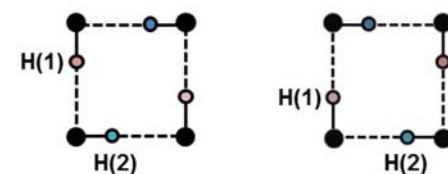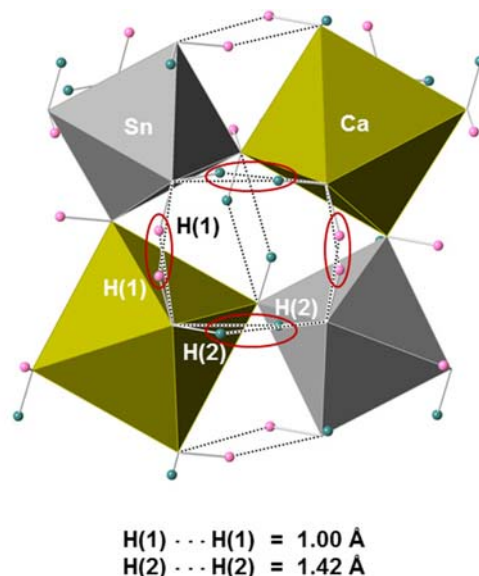

$H(1) \cdots H(1) = 1.00$ Å
$H(2) \cdots H(2) = 1.42$ Å

FIG. 22. The hydrogen-bonding topology of burtite, CaSn$(OH)_6$. The isolated ring comprises four O–H⋯O bridges, having O⋯O distances of 2.8 and 3.0 Å. H⋯H distances are indicated. Isolated four-membered rings are characteristic of all cubic hydroxide perovskites. The lower diagrams illustrate the two local ring configurations of cubic hydroxide perovskites that are averaged in the cubic space groups $Pn\bar{3}$ and $Im\bar{3}$ which require ½ occupancy of each H site in the average structures.

tetragonal. The identification of jeanbandyite as a hydroxide perovskite was based upon the similarity of its unit-cell parameters, powder diffraction pattern and general stoichiometry to stottite-group minerals. The empirical formula of jeanbandyite from the type locality Llallagua, Bolivia, originally reported by Kampf (1982) is $(Fe^{3+}_{0.71}Mn^{2+}_{0.21}Mg_{0.04})$ $(Sn^{4+}_{0.84}Si_{0.03})$ $(OH)_6$, which is not charge-balanced (an excess charge of +0.11), but was preferred over a charge-balanced formula requiring O^{2-} replacing some OH. The +0.11 excess charge was inferred to be due to some minor undetermined amount of Fe^{2+}. Kampf (1982) gave a general formula $(Fe^{3+}_{1-x}\square_x)(Sn_{1-y}\square_y)$

439

$(OH)_6$, in which vacancies are a potentially significant component.

Jeanbandyite was re-examined by Betterton *et al.* (1998) from Hingston Down Quarry, Cornwall (UK), who noted that the empirical formula of Kampf (1982) did not consider the presence of divalent cations and was not charge-balanced. They proposed a revised empirical formula $(Fe^{3+}_{0.46}Fe^{2+}_{0.24}Mn^{2+}_{0.14}Mg_{0.03})(Sn^{4+}_{0.90}Si_{0.05})(OH)_6$, which is charge-balanced. However, this revised formula also implies 13% vacancies at *B*-sites (and 5% vacancies at *B′*-sites).

In view of the uncertainties in the formula of jeanbandyite and the absence of a structure determination, Welch and Kampf (2017) re-examined samples from Llallagua (Kampf, 1982) and Hingston Down (Betterton *et al.*, 1998), and determined the structures of crystals from both localities. All crystals are cubic with space group $Pn\overline{3}$ and have fully-occupied *B*- and *B′*-sites (Fe and Sn, respectively). Welch and Kampf (2017) emphasize that $Pn\overline{3}$ and $P4_2/n$ structures have significantly different octahedral tilt systems ($a^+a^+a^+$ and $a^+a^+c^-$, respectively) that lead to different oxygen arrays which can be distinguished by single-crystal XRD. Bond-valence sums and octahedral volumes of the *B*-sites show clearly that Fe is predominantly in the ferric state. For example, the volume of the $Fe(OH)_6$ octahedron of Hingston jeanbandyite is 11.15 $Å^3$. This value compares with 10.80 $Å^3$ for $Fe^{3+}(OH)_6$ in bernalite $Fe(OH)_3$ (Birch *et al.*, 1993), and 13.13 $Å^3$ for $Fe^{2+}(OH)_6$ in stottite $Fe^{2+}Ge(OH)_6$ (Kleppe *et al.*, 2012). Assuming a linear variation in octahedral volume with composition, then the value observed for Hingston jeanbandyite implies 85% Fe^{3+} and 15% Fe^{2+} at this site. This calculation for Llallagua jeanbandyite gives 78% Fe^{3+} and 22% Fe^{2+}. Bond-valence sums for the *B*-sites of these two crystals are 2.93 vu and 2.82 vu, respectively. Welch and Kampf (2017) confirm that jeanbandyite is a *bona fide* mineral species and revise its end-member formula to $Fe^{3+}Sn(OH)_5O$. As such, jeanbandyite corresponds compositionally to oxidized natanite; it is an example of a stoichiometric partially-protonated hydroxide perovskite. What appears to be an analogous synthetic phase was reported by Nakayama *et al.* (1977) using powder XRD. The reader is referred to Welch and Kampf (2017) for a full discussion of the crystal chemistry of jeanbandyite.

Wunder *et al.* (2011) reported that the synthetic high-pressure '3.65Å-phase', $MgSi(OH)_6$, is also a hydroxide perovskite. Originally, the space group was determined as orthorhombic *Pnam* (#62), but has been shown subsequently to be monoclinic with a space group that is either $P2_1$ (#4) by density-functional theory (Wunder *et al.*, 2012) or $P2_1/n$ (#14) by single-crystal XRD (Welch and Wunder, 2013).

Synthetic hydroxide perovskites

The synthesis of stannate hydroxide perovskites has been investigated extensively by the materials science community in the search for non-spherical hollow nanostructures. Synthesis methods typically involve fast stoichiometric precipitation from alkaline solution (Kramer *et al.*, 2010; Wang *et al.*, 2013) or sonochemical (Cheng *et al.*, 2013) methods at ambient conditions. Numerous synthetic analogues of stannate hydroxide perovskites have been produced by diverse hydrolysis reaction involving metal chlorides and either stannous chloride ($SnCl_4$) with sodium citrate (Wang *et al.*, 2013), or alkali hexa-hydroxide stannates under alkaline conditions (NH_4OH or $NaOH$), e.g.

$$CaCl_2 + K_2Sn(OH)_6.3H_2O$$
$$\rightarrow CaSn(OH)_6 + 2KCl + 6H_2O$$
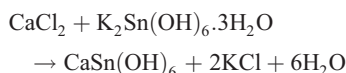
The hydroxide perovskites formed in these reactions are very insoluble in water and precipitate immediately on mixing of the reagents. Rinsed products are usually pure and well-crystallized with no amorphous residue. Studies of synthetic hydroxide perovskites should be particularly useful for understanding the structures and potential solid solutions of natural examples e.g. the schoenfliesite–wickmanite–natanite solid solution series (see below). For example, Neilson *et al.* (2011), in contrast to natural hydroxide perovskites, have shown that precipitation can yield ordered compounds only when the *B* cation is Mn^{2+} or Co^{2+} and not when it is any other transition metal or Zn^{2+}.

Solid solutions

Most natural hydroxide perovskites exhibit very limited solid solution and occur as near end-member compositions. It appears that the framework does not tolerate large differences in atomic radii of divalent cations at the *B*-sites, suggesting that next-nearest-neighbour interactions between homovalent cations are important.

The only examples of significant solid solution found so far are: mushistonite $(Cu, Mn^{2+}, Fe^{2+})Sn(OH)_6$ (Marshukova *et al.*, 1978, 1984); natural and

synthetic $CuSn(OH)_6$–$ZnSn(OH)_6$ hydroxide perovskites (Marshukova *et al.*, 1984; (Mn^{2+}, Fe^{2+}, Mg)$Sn(OH)_6$ in schoenfliesite–wickmanite (Nefedov *et al.*, 1977) and (In, Fe)$(OH)_3$ in dzhalindite (Kiseleva *et al.*, 2008).

The type-locality mushistonite, from the Mushiston tin deposit (Tadzhkistan) is reported by (Marshukova *et al.*, 1978) to exhibit a wide range of composition, i.e. ($Cu_{0.68-0.41}Zn_{0.14-0.41}Fe_{0.23-0.40}$)$Sn_{0.82-1.25}(OH)_{5.69-6.0}$. Natural mushistonite, defined generally as $(Cu,Zn,Fe^{2+})Sn(OH)_6$, has been reported as cubic $Pn\bar{3}m$. However, the synthetic end-member $CuSn(OH)_6$ has a metrically tetragonal unit cell and its structure has been refined in space group $P4_2/nnm$ (Morganstern-Badarau, 1976), corresponding to tilts of $a^0b^+b^+$. However, as noted above, the reported structure is improbable as it requires extremely distorted $Cu(OH)_6$ and $Sn(OH)_6$ octahedra. In addition, a zero tilt is very unlikely on account of the strong hydrogen-bonded bridges and an empty *A*-site. The structure of mushistonite and synthetic $CuSn(OH)_6$ requires re-evaluation and investigation of potential Jahn-Teller effects.

Synthetic vismirnovite $ZnSn(OH)_6$ adopts space group $Pn\bar{3}$ (Cohen-Addad, 1968). For solid solutions between $ZnSn(OH)_6$ and $CuSn(OH)_6$, the cubic ($Pn\bar{3}$) structure extends from vismirnovite $ZnSn(OH)_6$ to $(Cu_{0.4}Zn_{0.6})Sn(OH)_6$. Bulk compositions from $Cu_{50}Zn_{50}$ to $Cu_{80}Zn_{20}$ produce mixtures of tetragonal ($P4_2/n$?) and cubic phases. There is very limited solid solution in the tetragonal phase ($Cu_{90}Zn_{10}$–Cu_{100}). The Raman spectrum of synthetic $CuSn(OH)_6$ contains six peaks and is consistent with space group $P4_2/n$. Vismirnovite from the type locality, the Trudovoe tin deposit

(Kyrgyzstan) has the composition ($Zn_{0.89}Cu_{0.1}Fe_{0.08}$)$Sn_{1.0}(OH)_{6.04}$ (Marshukova *et al.*, 1981) and presumably adopts space group $Pn\bar{3}$.

In a study of hydrothermally-mineralized skarns at Pitkäranta, Nefedov *et al.* (1977) showed that minerals of the schoenfliesite–wickmanite series exhibited a wide range in composition ranging from Mn-rich schoenfliesite (up to 55 atomic % wickmanite) to Fe-rich wickmanite (up to 50 atomic % natanite). The minerals were found to be compositionally heterogeneous on a scale of micrometres and did not represent any regular core-to-rim zoning. Nefedov *et al.* (1977) concluded that there is undoubtedly a continuous solid solution series between schoenfliesite, wickmanite and natanite. Further study is required to verify this hypothesis.

Kiseleva *et al.* (2008) have described optically- and compositionally-zoned dzhalindite from the Bugdaya Au-Mo-W deposit (E. Transbaikalia, Russia). The 30–94 μm oscillatory-zoned cubic crystals (Fig. 23) consist of colourless zones with 0.6–1.1 wt.% Fe and light brown zones with up to 3.6 wt.% Fe. Kiseleva *et al.* (2008) have suggested that the Fe is present as microinclusions of Fe^{3+} compounds and that Fe does not replace In at the lattice site. Further study is required to verify this hypothesis.

Hydrogen-bonding topologies of hydroxide perovskites

The octahedra of hydroxide perovskites are corner-linked and there is no *A*-site cation. Thus, hydrogen-bonded linkages can assume a potentially significant role in controlling the degrees of rotation of octahedra, and prevent zero tilts; they may also drive phase transitions.

Hydrogen positions have been determined using powder neutron diffraction for schoenfliesite, burtite (Basciano *et al.*, 1998) and synthetic $In(OH)_3$ (Mullica *et al.*, 1979). The hydrogen-bonding connectivity of the framework of octahedra as defined by O–H⋯O donor-acceptor bridges, can be inferred. These bridges form across the shorter O⋯O distance (2.5–2.7 Å) in each quartet of octahedra; the other O⋯O distance is far too long (>4 Å) for such bridges to form. Different tilt systems lead to different hydrogen-bonding topologies. Knowing the tilt system permits inference of the hydrogen-bonding connectivity and thereby evaluation of plausible H positions in difference-Fourier maps.
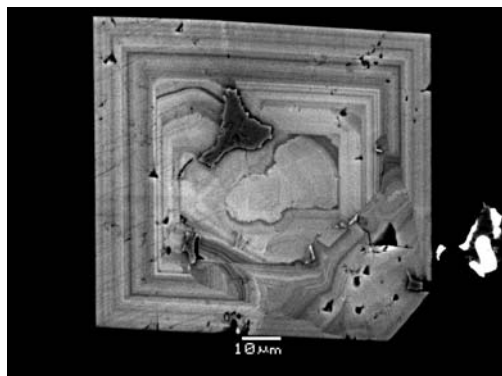

FIG. 23. Back-scattered elctron image of complexly-zoned dzhalindite from the Bugdaya Au-Mo-(W)-porphyry deposit, Eastern Transbaikalia (Russia).

441
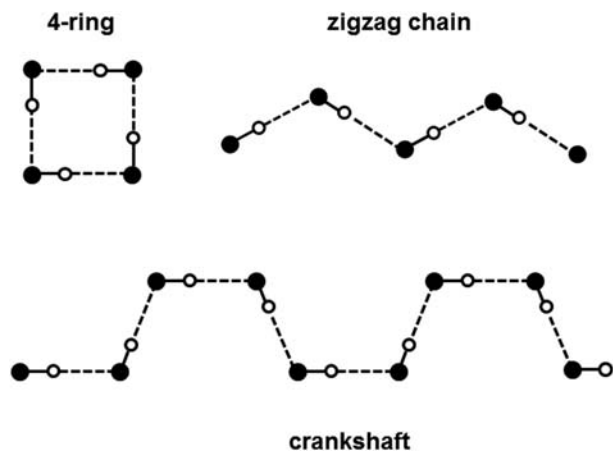
FIG. 24. The three different components of hydrogen-bonding topologies of hydroxide perovskites: isolated ring; crankshaft; and zigzag chain. The inferred local occupancy of hydrogen sites is shown. Hydrogen positions have been located in the cubic phases dzhalindite, schoenfliesite, wickmanite and burtite, all of which have only isolated rings. In these three phases there are two ½-occupied H sites.
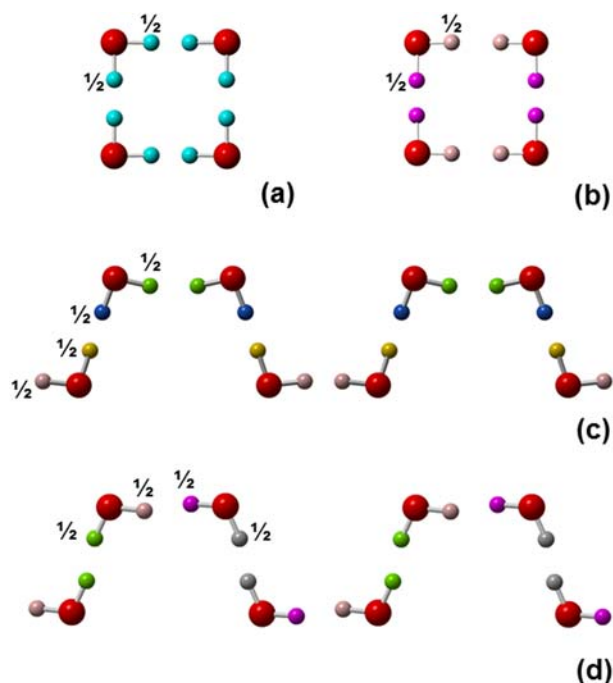
FIG. 25. Hydrogen bonding topologies of hydroxide perovskites determined by single-crystal XRD. Isolated 4-membered rings in (*a*) söhngeite $Ga(OH)_3$ ($P4_2/nmc$) and (*b*) burtite ($Pn\bar{3}$). Crankshafts in (*c*) söhngeite $Ga(OH)_3$ and (*d*) stottite $FeGe(OH)_6$ ($P4_2/n$). All H sites are half-occupied in the averaged structure determined by diffraction methods. The number of non-equivalent OH groups in söhngeite (five) and stottite (six) have been confirmed by Raman spectroscopy. In the ring of söhngeite the pairs of H sites are mirror-related, whereas they are non-equivalent in stottite which being a double-perovskite lacks mirror symmetry.

442

Very recent single-crystal XRD studies of hydroxide perovskites with space groups $Pn\bar{3}$ and $P4_2/n$ have found that [110] merohedral twinning is common (Lafuente *et al.*, 2015; Welch and Kleppe, 2016). Merohedral twinning has been recognized in all $Pn\bar{3}$ and $P4_2/n$ hydroxide perovskites including Mn-schoenfliesite, wickmannite, tetrawickmanite and stottite. Once merohedral twinning has been refined a key aspect of the crystal structure emerges in difference-Fourier maps: the presence of half-occupied H sites, as discussed in detail below. It is, perhaps, surprising that it is possible to assign ½ electron to a plausible half-occupied H site, but the close correspondence between approximate H positions found by single-crystal XRD in wickmannite–schoenfliesite and those determined by neutron diffraction for schoenfliesite, burtite and In(OH)$_3$ leaves little room for doubt.

Once H sites have been located, it is possible to make sense of vibrational (infrared and Raman) spectra in the OH-stretching region which, for non-cubic species, seem to be at variance *prima facie* with the determined space group. The presence of such half-occupied H sites increases the number of OH peaks in spectra beyond that expected for full occupancy. For example, the O–H spectrum of tetrawickmanite (Lafuente *et al.*, 2015) has five resolved peaks, which is incompatible with $P4_2/n$ symmetry if all H sites are full (three non-equivalent OH). The tetrawickmanite structure determined by Lafuente *et al.* (2015) has four half-occupied H sites and a fifth fully-occupied H site in a very different type of location from those of the other four H sites. Analogous features have now been recognized in stottite and synthetic MgSi(OH)$_6$.

Three different components of the hydrogen-bonding connectivities of hydroxide perovskites have been identified: (1) isolated four-membered rings; (2) crankshafts; (3) zigzag chains. Figure 24 shows the local configurations of OH groups associated with each component. Figure 25 shows the hydrogen bonding topologies of söhngeite and stottite determined by single-crystal XRD. In stottite and tetrawickmanite (both $P4_2/n$) pairs of half-occupied H sites lie along the O–(H)–O crankshaft and there is only a single fully-occupied H site in the 4-membered ring, giving five non-equivalent H sites in all. In söhngeite ($P4_2/nmc$) there are again four non-equivalent half-occupied H sites in the crankshaft, but the {100} mirror planes produce four pairs of half-occupied equivalent sites in the four-membered ring.

Tilt systems of hydroxide perovskites

The tilt systems of hydroxide perovskites are shown in Table 2. As with other perovskites, the tilt notation is based upon the orientation of the rotation axes of the cubic aristotype (Glazer, 1972). Natural hydroxide perovskites studied so far have tilt systems $a^+a^+a^+$ ($Pn\bar{3}$ and $Im\bar{3}$), $a^+a^+c^-$ ($P4_2/nmc$, $P4_2/n$, $P2/n$), $a^+b^+c^-$ ($Pmmn$), $a^-a^-b^+$ ($P2_1/n$), $a^-b^-b^+$ ($P2_1$) and $a^+b^-b^-$ ($Pnma$ and $P2_12_12_1$) have been reported for synthetic hydroxide perovskites. Each tilt system is associated with a distinctive hydrogen-bonding connectivity, as described below.

The two cubic space groups of hydroxide perovskites, $Im\bar{3}$ and $Pn\bar{3}$, with the tilt system $a^+a^+a^+$ are the aristotypes of the single and double perovskites, respectively. Both have a unique large vacant cage site located at a centre of symmetry and defined by twelve oxygen atoms at the apices of an icosahedron (Fig. 26). Each pentagonal face of this icosahedron consists of three oxygen and two cation sites. Six O···O distances bounding this cage are O–H···O bridges associated with one of the two non-equivalent H atoms. The hydrogen-bonding connectivity consists only of isolated 4-membered rings.
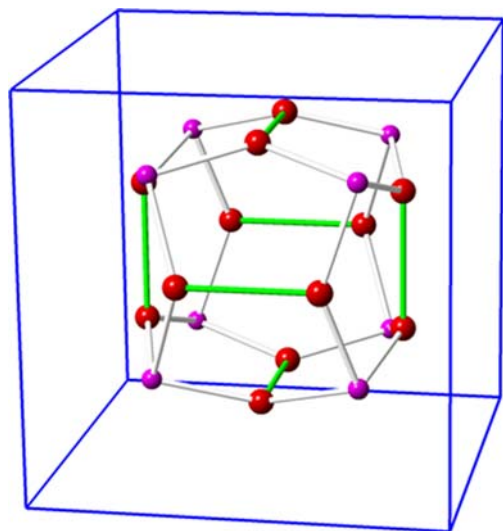

Fig. 26. Cubic hydroxide perovskites have a large empty dodecahedral cage site defined by 12 oxygen and 8 cation sites, as shown here for the single perovskite dzhalindite In(OH)$_3$ ($Im\bar{3}$). There are two dodecahedral cages per unit cell. Six of the O–O edges of the dodecahedron are O–H···O bridges (shown in blue). All other O–O edges (shown in green) are shared with octahedra. Adjacent cages are connected via single octahedra.
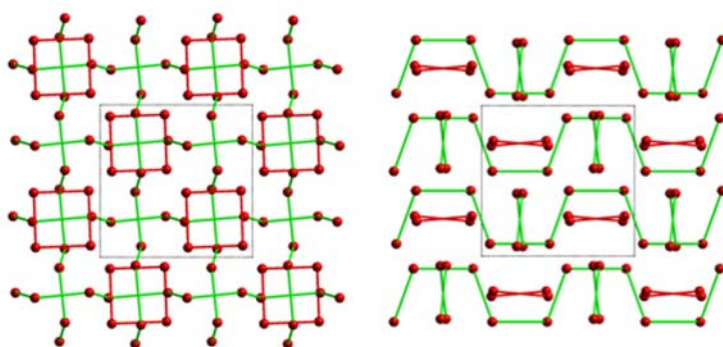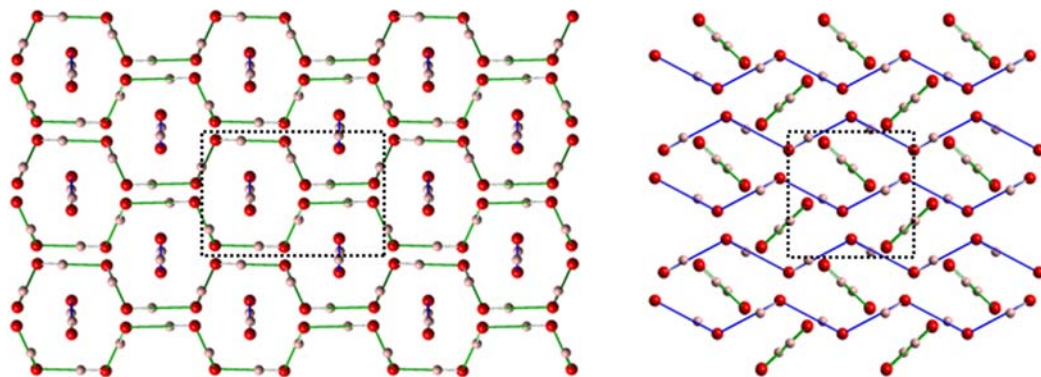
FIG. 27. The hydrogen-bonding topologies of orthorhombic δ-Al(OH)$_3$ and tetragonal FeGe(OH)$_6$. Each line connects the two oxygen atoms of a O–H···O bridge. Isolated 4-membered rings are shown in red, crankshafts in green and zigzag chains in blue. The δ-Al(OH)$_3$ structure has two sets of crankshafts extending ∥[010] oriented interleaved with zigzag chains running ∥[100]. The hydrogen-bonding topology of stottite FeGe(OH)$_6$ consists of two sets of crankshafts running <100> and interposed 4-membered rings within planes ∥(001). There are no hydrogen-bonded connections between chains, crankshafts or rings.

It has been suggested that the icosahedral cage site might host H$_2$O (Birch *et al*., 1993), but there is no clear evidence so far to support this suggestion. For example, no significant residual electron density within the cage site cavity has been found by diffraction methods. However, it is conceivable that H$_2$O could be disordered over several partially-occupied sites within this large cavity.

The second type of non-framework 'cavity' in these cubic structures is much more restricted in volume and is defined by eight cation and eight oxygen sites, with pentagonal bounding faces. A 4-membered ring lies at the centre of this volume.

Hydroxide perovskites with space groups *Pmmn* ($a^+b^+c^-$), *P4$_2$/nmc*, *P4$_2$/n* ($a^+a^+c^-$) and *P2/n* ($a^+b^+c^-$) are characterized by one antiphase tilt and two in-phase tilts. The hydrogen bonding connectivity consists of alternating layers of crankshafts and isolated 4-membered rings. The example of stottite is shown in Fig. 27.

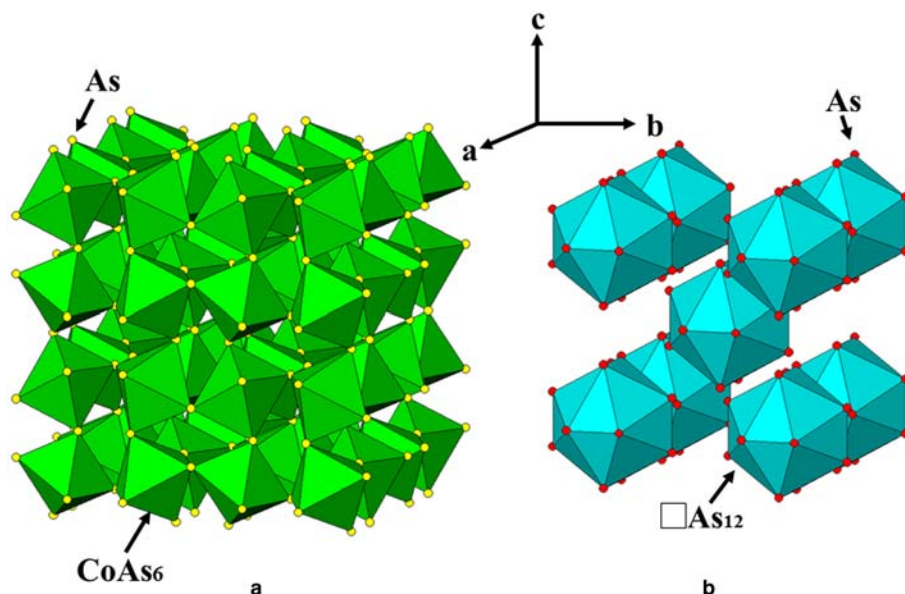Hydroxide perovskites with space groups *Pnma* ($a^+b^-b^-$), *P2$_1$/n* ($a^-a^-c^+$), *P2$_1$2$_1$2$_1$* ($a^-a^-c^+$) and

FIG. 28. The crystal structure of skutterudite ($CoAs_3$) showing: (*a*) The framework of tilted $CoAs_6$ octahedra; (*b*) The icosahedral polyhedra defined by the As anions around the empty *A* sites.

$P2_1$ ($a^-a^-c^+$), are characterized by having two anti-phase and one in-phase tilt. Their hydrogen-bonding connectivity consists of interleaved crank-shafts and zigzag chains. The example of synthetic δ-Al(OH)$_3$ (Matsui *et al*., 2011), space group *Pnma*, is shown in Fig. 27.

Phase transformations of hydroxide perovskites

Compared to oxide and fluoroperovskites, very few investigations of phase transitions of hydroxide perovskites have been undertaken. Possible continuous transitions can, in principle, be postulated using a group theoretical approach. However, account must be taken of the potential effects of strong hydrogen bonding, which might inhibit tilting-related transitions. As such hydroxide perovskites are very suitable structures for evaluating the role of hydrogen bonding in phase transitions. Examination of group-subgroup relations for known hydroxide perovskite space groups suggests that continuous transitions might be rare, due to the avoidance of structures with zero tilts i.e. due to strong hydrogen bonds.

A further constraint on phase transitions relates to the absence of mirror symmetry in double hydroxide perovskites. Only single hydroxide perovskites can have mirror symmetry, as these planes must pass through shared oxygen atoms. As discussed above this is not possible for double hydroxide perovskites as adjacent octahedra are occupied by different cations, and mirror planes bisecting octahedra result in implausible distortions.

In the absence of continuous phase transitions in double hydroxide perovskites involving the creation of mirror symmetry and/or zero tilts, the options seem to be limited. The most obvious possibilities are $P2/n \leftrightarrow P4_2/n \leftrightarrow P4_2/nmc$ in single hydroxide perovskites and $P2/n \leftrightarrow P4_2/n$ in double hydroxide perovskites. Transitions involving loss or gain of centrosymmetry might also be possible i.e., $P2_1/n \rightarrow P2_1$ or $P2_1/n \rightarrow Pn$. Evidence, from Raman spectra, for a pressure induced transition $P2/n \leftrightarrow P4_2/n$ at ~11 GPa in stottite, was reported by Kleppe *et al*. (2012). This transition is reversible but shows clear hysteresis on decompression.

Polymorphism involving structures with different tilt systems can occur in hydroxide perovskites. However, as far as we are aware, the only example of polymorphism in hydroxide perovskites is that of MnSn(OH)$_6$ for which the polymorphs are wickmanite (cubic $Pn\bar{3}$) and tetrawickmanite (tetragonal $P4_2/n$). Following our comments above on space group nomenclature for polymorphs note that tetrawickmanite could also be termed wickmanite-$P4_2/n$. The cubic polymorph has a cell volume (489 Å^3) that is 2% larger than that of tetrawickmanite

445

(480 Å^3); evidently, the change in tilt system permits a marked contraction of the framework. Welch and Kleppe (2016) report a temperature-induced structural transformation in söhngeite Ga(OH)$_3$ from the ambient $P4_2/nmc$ (or $P4_2/n$) structure to cubic $Im\bar{3}$ at ~150°C. This transition has considerable hysteresis and the cubic polymorph is preserved metastably on cooling to room temperature.

Classification of hydroxide perovskites

The hierarchical classification of hydroxide perovskites is given in Table 2 and is based upon composition and symmetry. It highlights the major distinctions and similarities between these phases. In developing this classification we intend to provide a basis for predicting further possible structures, and to allow for the incorporation of future discoveries of new stoichiometries.

The classification of hydroxide perovskites follows that proposed above for ABX_3 and $A_2BB'X_6$ perovskites. Thus, the fundamental distinction is between 'single hydroxide perovskites' and 'double hydroxide perovskites'. This classification of hydroxide perovskites leads to the recognition of three subgroups: the single hydroxides of the söhngeite subgroup; and the double hydroxide perovskites of the cubic schoenfliesite and the tetragonal stottite subgroups. Table 2; Fig. 7).

Finally, it is evident that there are several interesting avenues of research for future study of hydroxide perovskites namely: (1) What are the correct space groups of hydroxide perovskites? (2) What phase transitions occur in hydroxide perovskites? (3) What is the interplay between composition and tilt system? (4) What is the physical significance of the different hydrogen-bonding topologies, e.g. upon compressional behaviour?

A-site vacant quadruple perovskites

Skutterudite subgroup

The skutterudite group (Table 3; Fig. 7) are derivatives of ordered quadruple perovskites $[AA'_3B_4X_{12}]$ characterized by vacant A-sites i.e. $\square\square_3B_4X_{12}$ (B = Fe, Co, Ni, Ru, Rh, Ir, Os; X = As, Sb, P). Many synthetic skutterudite-group compounds have been synthesized but only four minerals have been recognized, namely: skutterudite (CoAs$_{3-x}$; Haidinger, 1845); ferroskutterudite [(Fe,Co)As$_3$; Spiridonov *et al.*, 2007)]; nickelskutterudite (NiAs$_{3-x}$; Spirodov and Gritsenko, 2007);

and kieftite [CoSb$_3$; Dobbe *et al.*, 1994). Other synthetic skutterudites are known with the large A-site filled partially e.g. $A\square_3B_4X_{12}$ (A = La–Yb, U, Th), such as La$\square_3$Fe$_4$P$_{12}$ (Jeitscho and Braun, 1977), but are as yet unknown as minerals.

All skutterudites adopt the space group $Im\bar{3}$ with the tilt system $a^+a^+a^+$. The structure consists of a framework of corner-sharing CoAs$_6$ or CoSb$_6$ octahedra (Fig. 28). The As and Sb anions in the skutterudite subgroup are bonded to form square planar tetramers $[X_4]^{4-}$, making them also good examples of Zintl compounds (Luo *et al.*, 2014). To date B-site ordered derivatives have not been recognized. The structure of the skutterudites is nearly identical to that of the single hydroxide perovskite dzhalindite [In(OH)$_6$], except that in the latter the anion bonds are asymmetrical O–H···O rather than the symmetrical X–X bonds of the skutterudites. Dzhalindite could be also considered as an A-site vacant quadruple perovskite.

B-site vacant perovskites

B-site vacant single perovskites $A\square X_3$

Oskarssonite subgroup

The B-site vacant single fluoride perovskite (Table 3; Fig. 7), oskarssonite (ideally AlF$_3$) has been approved as a valid member of the perovskite supergroup (Table 3; Fig. 7). The mineral is a derivative structure of the cubic ReO$_3$ aristotype formed by tilting of AlF$_6$ octahedra. In common with ReO$_3$ no cations occupy the B site of the octahedron framework.

Although Al-fluorides had been recognized in fumaroles from the Hekla (Oskarsson, 1981) and Mount Erebus (Rosenberg, 1988) volcanoes, a complete structural characterization was not available until material from fumaroles of the Eldfell volcano (Iceland) was undertaken by Jacobsen *et al.* (2014). A mineral with the composition of oskarssonite, together with parascandolaite, has also been found as nano-inclusions in diamonds from Juina by Kaminsky *et al.* (2016). Oskarssonite [Al(F$_{2.62}$(OH)$_{0.49}$)] adopts the rhombohedral space group $R\bar{3}c$ (#167) in common with the synthetic analogue α-AlF$_3$ (Le Bail and Calvayrac, 2006). Oskarssonite is the only known natural perovskite-supergroup mineral with the $a^-a^-a^-$ tilt scheme resulting in an anticlockwise rotation angle (ω) of 10.65° about [111]$_p$ of the AlF$_6$ octahedra (Fig. 29). Oskarssonite transforms to the cubic ReO$_3$ structure above 450°C (Jacobsen *et al.*, 2014).
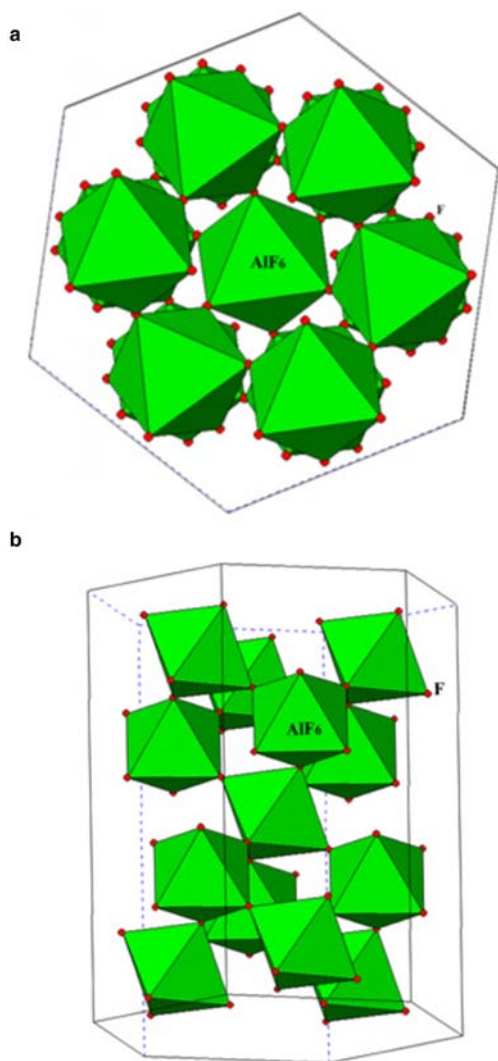
446

a

AlF₆

b

AlF₆

F

F

FIG. 29. Polyhederal representation of the crystal structure of oskarssonite. (*a*) Projection along the c_H axis. (*b*) Projection perpendicular to the c_H axis showing the 6 layers of fluorine atoms (red) in the unit cell.

B-site vacant single antiperovskites $X\square A_3$

Stoichiometric antiperovskites (Table 3; Fig.7) have the composition A_3BX or XBA_3 e.g. K_3OBr; Ca_3NAs (Mitchell, 2002, Krivovichev, 2008). When the *B*-site is vacant, as in $X\square A_3$, derivative synthetic compounds such as $Au\square Cu_3$ (auricupride) and $C\square Fe_3$ are formed (ÒKeefe and Hyde, 1977) Note synthetic auride antiperovkites

containing Au^{-1} anions e.g. $AuOK_3$, have been synthesized by Feldmann and Jansen (1995).

Cohenite Subgroup

Cohenite, $C(Fe,Ni,Co)_3$ is a *B*-site vacant carbide antiperovskite which adopts the space group *Pbnm*. The mineral was initially found in the Magura meteorite (Slovakia) and is a common constituent of other iron meteorites. Other occurrences are in highly reducing environments produced when high temperature basaltic lavas have invaded coal deposits e.g. Qeqertasuaq (Disko) Island, Greenland (Pauly, 1969). Kaminsky *et al.* (2015) have reported the presence of a N-bearing mineral similar to cohenite as nano-inclusions in Juina diamonds.

Auricupride subgroup

Auricupride is a *B*-site vacant intermetallic anti-perovskite ($Au\square Cu_3$) formed in serpentinites by the low-temperature unmixing of Au-Cu alloys. Palladium-bearing varieties were formerly described by the now discredited name rozhoko-vite. Auricupride and the synthetic analogue adopt the space group $Pm\bar{3}m$ (Megaw, 1973), although a tetragonal *P4*/*mmm* polymorph is also known (Bayliss, 1990). Although many intermetallic antiperovskites have been synthesized the only varieties which occur as minerals in a wide variety of serpentinites and platinum-group element ore deposits include: $Pm\bar{3}m$ awaruite ($Fe\square Ni_3$); cheng-deite ($Fe\square Ir_3$); isoferroplatinum ($Fe\square Pt_3$); yixunite ($In\square Pt_3$); and zvyagintsevite ($Pb\square Pt_3$); together with $Fm\bar{3}m$ rustenburgite ($Sn\square Pt_3$); and atokite ($Sn\square Pd_3$). Rustenburgite and atokite form a complete solid solution series. The reduction in symmetry from $Pm\bar{3}m$ in the synthetic analogues to $Fm\bar{3}m$ is considered to result from strain induced during mineral processing (Mihalik *et al.*, 1975).

B-site vacant ordered double perovskites

Diaboleite subgroup

The chloro-hydroxy double perovskite **diaboleite** ($Pb_2Cu\square Cl_2(OH)_4$; *P4mm*) is unusual in that in addition to having vacancies at one octahedral site, its structure exhibits both first order Jahn-Teller and lone-pair effects arising from the presence of Cu and Pb, respectively. Diaboleite was described originally from the iron ore mine located at Higher Pitts Quarry, Mendip Hills, Somerset (UK) by Spencer and Mountain (1923), and has been found subsequently in a variety of parageneses,
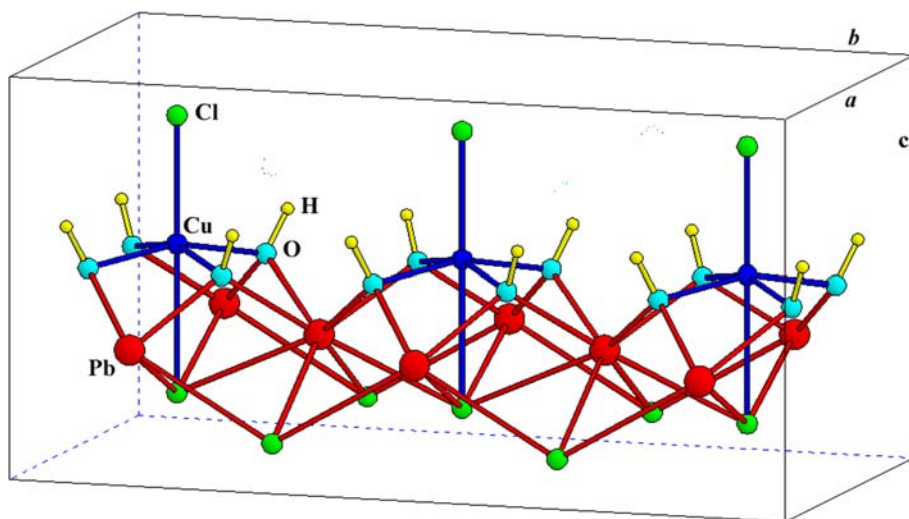
447

FIG. 30. Crystal structure of diaboleite (after Cooper and Hawthorne, 1995) showing the coordination of Cu and Pb.

particularly as a secondary phase in oxidized Ag-Pb veins and chemically-weathered metallurgical slags.

The crystal structure was initially determined by Byström and Wilhelmi (1950) and refined by Rouse (1971) who recognized the mineral is a tetragonal *P4 mm* (#99) defect perovskite. Subsequent work by Cooper and Hawthorne (1995) confirmed the structure as a *B*-site defect perovskite of the type $Pb_2(Cu\square)X_6$ in which half of the octahedra are not occupied by cations. In diaboleite the Pb coordination is highly asymmetric as it is surrounded on one side by four OH^- anions (Pb–OH = 2.46 Å), and on the other by four Cl^- anions (3.22 Å and 3.40 Å) in square antiprismatic coordination (Fig. 30). The lone pair electrons project towards the Cl^- anions. The Cu^{2+} site exhibits strong [4+2] first order Jahn-Teller distortion and is surrounded by four equatorial OH^- anions (Pb–OH = 1.97 Å) and two apical Cl^- anions (Pb–Cl 2.55 Å and 2.95 Å) with Cu^{2+} displaced 0.34 Å from the centre of the polyhedron (Fig. 30). The coordination can be considered as intermediate between octahedral and square pyramidal.

Anion-deficient or defect oxide perovskite subgroups

Anion-deficient, non-stoichiometric perovskites (Table 3; Fig. 7) typically range in composition from ABO_3 to $ABO_{2.5}$, and have the general formula $ABO_{3-\delta}$ ($0 < \delta \le 0.5$). The anion deficiency reflects the replacement of cations by other ions in a lower oxidation state (e.g. Ti^{4+} by Fe^{3+} in $CaTiO_3$; Becerro *et al.*, 1999). The vacancies created can be ordered or random. In the ordered structures the vacancies are arranged in parallel rows along $[101]_p$ of the original cubic cell forming layers on either side of a layer of tilted corner-sharing perovskite BO_6 octahedra. Within the oxygen-deficient layers cations occur as pairs of corner-sharing tetrahedra (Fig. 31). The original perovskite stoichiometry is thus modified to $A_2BTX_5\square$, where T represents a tetrahedral coordinated cation. The compounds with the maximum oxygen vacancy are termed brownmillerites in the materials science literature, after the compound $Ca_2Fe^{3+}AlO_5$, occurring as a mineral and a major component of Portland cement (Colville and Geller, 1971).

Brownmillerite-subgroup

Brownmillerite [(Ca₂(Fe³⁺Al)O₅]
Brownmillerite was recognized, and named (without IMA approval), as a constituent of Portland cement (Hansen *et al.*, 1928; Bogue, 1955) prior to its discovery as a mineral. Natural brownmillerite was recognized subsequently in spurrite- and larnite-bearing metamorphosed argillaceous limestones of the Hatrurim Formation (Israel) and thermally-metamorphosed limestone xenoliths in the lavas of the Ettringer Bellerberg volcano, Eifel District (Germany) by Bentor *et al.*

448

(1963) and Hentschel (1964), respectively. Although, the proposal of Hentschel (1964) to name the material from Bellerberg 'brownmillerite' appeared after the publication of Bentor *et al*. (1963), the latter report did not actually contain any analytical information about the new mineral, and hence, Bellerberg should be considered as the type locality. Compositional data obtained by electron microprobe analysis indicates that the Hatrurim material ranges from Fe-dominant compositions with ~20 mol.% $Ca_2Al_2O_5$ (Sharygin *et al*., 2008) to varieties with Al > Fe (up to 54 mol.% $Ca_2Al_2O_5$: Gross, 1977; Sokol *et al*., 2011). Minor constituents exceeding 0.12 apfu are Mg, Ti and Cr. The crystal structure of neither Hatrurim or Bellerberg samples was determined and, on the basis of the powder XRD patterns, was assumed to be identical to that of synthetic orthorhombic *Ibm*2 (#46) $Ca_2(Fe^{3+}Al)O_5$. Note, however that compositions with < 28 mol.% $Ca_2Al_2O_5$ (e.g. samples M5–31 and H–201 in Table 2 of Sharygin *et al*. (2008) probably adopt space group *Pnma* (see below).

Srebrodolskite ($Ca_2Fe_2^{3+}O_5$)

Srebrodolskite, $Ca_2Fe_2^{3+}O_5$, was initially described from petrified wood 'baked' by burning coal in mines at Kopeisk in the Chelabynsk coal basin, Urals (Chesnokov and Bazhenova, 1985). Note that the mineral and name were approved prior to the IMA decision not to approve technogenic phases as new species. The type material contains 0.08 apfu Mg and 0.03 apfu Mn and is devoid of detectable Al. Subsequently, srebrodolskite has been found in the Clearwater impact crater (Rosa and Martin, 2010), the Bellerberg volcano, the Hatrurim Formation (Sharygin *et al*., 2008), Lakargi Mountain (Galuskin *et al*., 2008), and several other less well-characterized localities.

The crystal structure has not been determined by single-crystal methods for any of these examples but is assumed (Chesnokov and Bazhenova, 1985), on the basis of the powder XRD pattern, to be that of synthetic $Ca_2Fe_2^{3+}O_5$ i.e. *Pnma* (#62: Berggren, 1971). Note that the structural data for synthetic srebrodolskite are also reported in the *Pcmn* (#62: cba) setting (Bertaut *et al*., 1959).

Brownmillerite and srebrodolskite adopt different space groups as the orientation of the TO_4 tetrahedra in the two structure types differ. In brownmillerite, all tetrahedra point in the same direction, to form the sequence $T_{up}OT'_{up}O$ (Fig. 31), whereas in srebrodolskite the sequence is
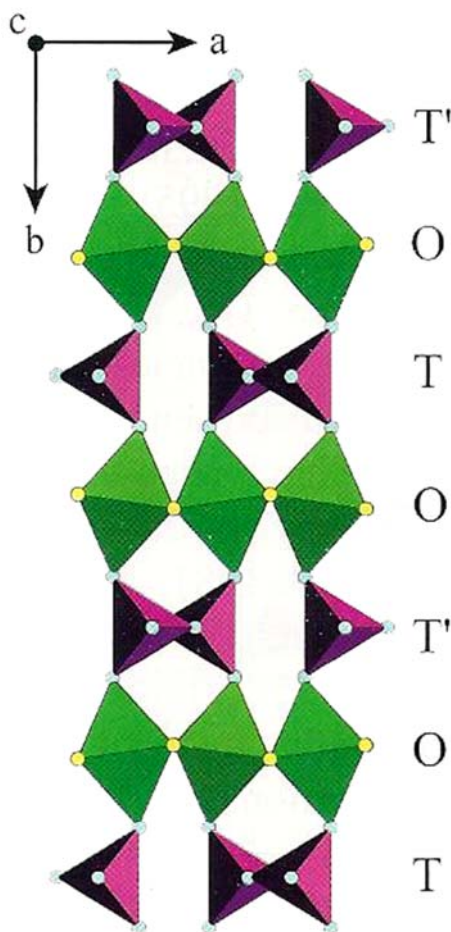
FIG. 31. The crystal structure of *Ibm*2 brownmillerite (Colville and Geller 1971) projected along [001] illustrating the stacking sequence of the octahedral (O) and tetrahedral (T, T′) layers.

$T_{up}OT'_{down}O$. Regardless of this structural difference, studies of synthetic compounds show there is continuous solid solution between brownmillerite and the ferric end-member with the transition from *Ibm*2 to *Pcmn* occurring at $Ca_2Fe_{1.43}^{3+}Al_{0.56}O_5$ (Collville and Geller, 1972; Redhammer *et al*., 2004). The $Ca_2Al_2O_5$ end-member exists only as a quenchable high-pressure phase (P = 2.5 GPa) isostructural with brownmillerite (Kahlenberg *et al*., 2000). At ambient pressure, Al-dominant compositions with as much as 70 mol.% $Ca_2Al_2O_5$ can be prepared (Taylor, 1997).

Pure $Ca_2Fe_2^{3+}O_5$ and compositions in the solid solution series $Ca_2Fe_{2-x}^{3+}Al_xO_5$ with x up to 0.56

449

FIG. 32. The crystal structure of shulamitite (Sharygin *et al*., 2013).

adopt space group *Pnma*, whereas compounds with $x > 0.56$ have *Ibm*2 symmetry (Redhammer *et al*., 2004).Thus, synthetic stoichiometric brownmillerite ($Ca_2Fe^{3+}AlO_5$), and Al-dominant phases adopt space group 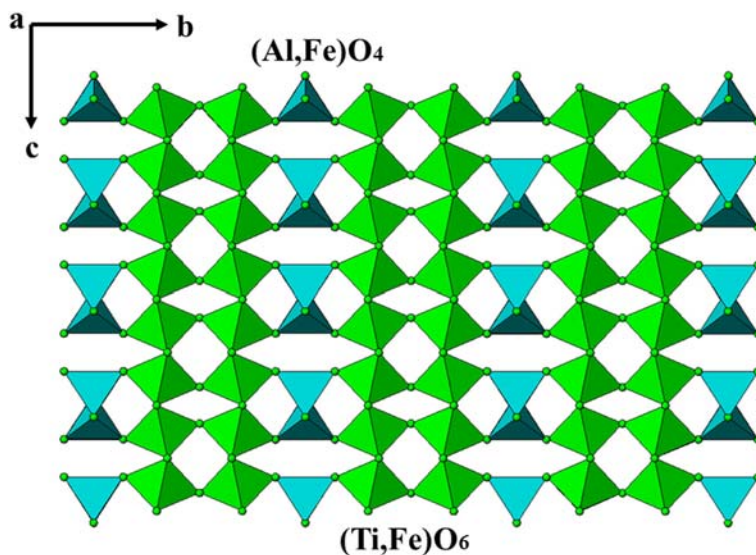*Ibm*2. If naturally-occurring phases conform to the same structural principles as their synthetic counterparts, the name brownmillerite should be applied to all intermediate members of the $Ca_2Al_2O_5$–$Ca_2Fe_2^{3+}O_5$ series which adopt space group *Ibm*2 and those adopting space group *Pnma* should be termed srebrodolskite. However because of preferential partitioning of Al into the *T*-site further structural complexities can arise. Thus, brownmillerites could be defined as minerals/ compounds having a preponderance of Al in the *T*-site, regardless of the Fe/Al ratio. This is because Al is partitioned strongly into the *T* site until about 2/3 of this site is occupied (Redhammer *et al*., 2004). However, any Al exceeding 2/3 *T*-site occupancy is distributed equally between the tetrahedrally and octahedrally coordinated sites (Redhammer *et al*., 2004). Clearly, in addition to brownmillerite *sensu stricto*, where Al is the dominant cation in the *T*-site and Fe^{3+} in the *B* site, compositions with Al as the dominant species in both sites could possibly exist in nature (including high-pressure phases approaching $Ca_2Al_2O_5$ in their composition). These hypothetical phases will represent a mineral species distinct from brownmillerite and hence require a different name. If naturally-occurring brownmillerite-type phases exhibit the same pattern of cation distribution as their synthetic counterparts, at least ~25 wt.% Al_2O_3 is required from Al to be the dominant cation in both the *T*- and *B*-sites. The greatest Al_2O_3 reported to date (23.2 wt.%; Sokol *et al*., 2011) falls short of that value. A possible high-pressure $Ca_2Al_2O_5$ brownmillerite-type phase was reported by Rappenglück *et al*. (2013) as inclusions in Fe-silicides from the Holocene Chiemgau impact strewnfield in southern Germany, but no structural data to support this interpretation were presented.

In, summary, recognizing the complexities of Al distribution in this solid solution series we recommend that brownmillerite and srebrodolskite be retained as valid names and that: (1) **brownmillerites** are minerals in the solid solution series $Ca_2Fe_{2-x}^{3+}Al_xO_5$ with $x > 0.56$ which adopt space group *Ibm*2; (2) **srebrodolskites** are minerals in the solid solution series $Ca_2Fe_{2-x}^{3+}Al_xO_5$ with $x < 0.56$ which adopt space group *Pnma*.

Shulamitite ($Ca_3TiFe^{3+}AlO_8$)

Shulamitite, occurs as a major to accessory mineral in high-temperature metacarbonate larnite rock of the Hatrurim Basin, Israel (Sharygin *et al*., 2013). The mineral can be considered as an intermediate compound between $CaTiO_3$ perovskite and $Ca_2(Fe^{3+},Al)O_5$ bownmillerite and is the natural analogue of synthetic orthorhombic *Pcm*2$_1$ $Ca_3TiFe_2^{3+}O_8$ (Rodrígues-Carvajal *et al*., 1989).

450
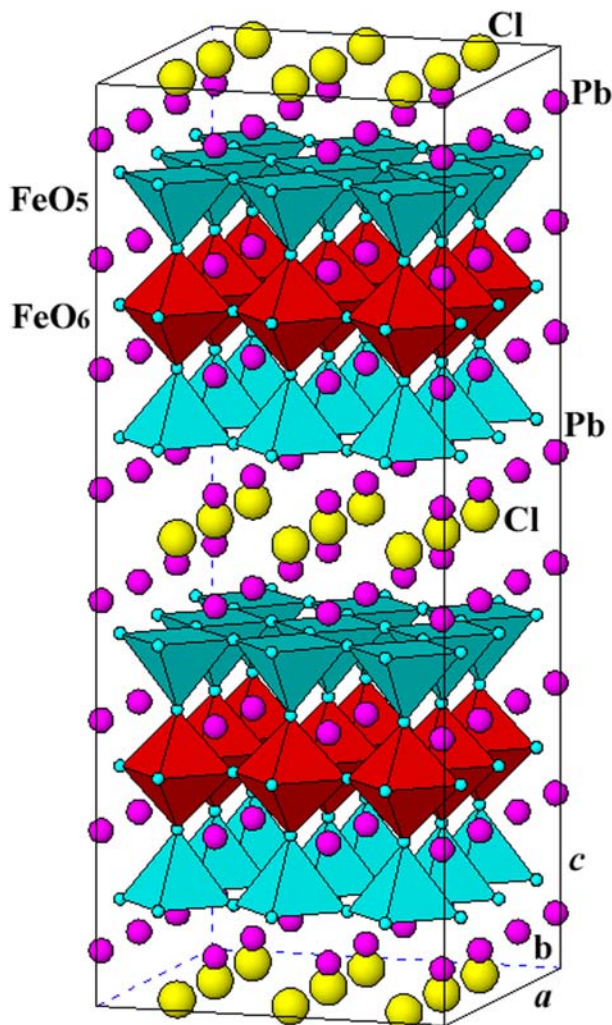
FIG. 33. Polyhedral representation of the crystal structure of hematophanite.

The holotype mineral has the composition $Ca_3TiFe^{3+}(Al_{0.7}Fe^{3+}_{0.3})O_8$. Sharygin *et al.* (2013) recognize other examples for which $Fe^{3+} > Al$ i.e. an unnamed Fe-analogue $[Ca_3(TiFe^{3+})Fe^{3+}O_8]$ of shulamitite assuming the existence of a solid solution between $Ca_3TiFeAlO_8$ and $Ca_3TiFeFeO_8$. Single-crystal structure determination shows that shulamitite adopts the orthorhombic space group *Pmma*, that there is no preferred octahedral site occupancy for Ti or Fe^{3+}, and that the majority of the Al (with some Fe) is in tetrahedral coordination. The crystal structure of shulamitite consists of double layers of tilted $(Ti,Fe)O_6$ octahedra separated by single layers of paired $(Al,Fe)O_4$

tetrahedra. The latter have different orientations between each octahedral double layer (Fig. 32).

Partially vacant *B*-site quadruple perovskites – hematophanite subgroup

Hematophanite was initially recognized from Jakobsberg and Långban, Värmland, Sweden (Johansson, 1928). It is also occurs in slag from Reichelsdorf, Hesse, Germany and at the Kombat Cu-Pb-Ag mine, Namibia.

Rouse (1973) recognized that hematophanite, ideally $Pb_4(Fe^{3+}_3\square)(Cl,OH)(O_8\square_4)$ (or

451

$Pb_4Fe_3^{3+}O_8Cl$), was a derivative of the perovskite structure produced by the stacking of four $PbFeO_3$ perovskite-like cells leading to the hypothetical quadruple perovskite $Pb_4Fe_4O_{12}$. In order to achieve charge balance every fourth Fe^{3+} cation must be replaced by Cl^- (and/or Br^- and OH^-) leading to the introduction of *B*-site vacancies. The *X*-sites that are adjacent to the Cl anion are vacant resulting in partial occupation by oxygen anions.

Thus, the structure of *P4/mmm* hematophanite consists of incomplete perovskite $Pb_4Fe_3O_8$ blocks separated by layers of (Cl,OH) anions. Each perovskite block consists of a corner-sharing FeO_6 octahedral layer that is sandwiched between two FeO_5 square pyramids. Lead atoms occur at sites within this framework (Fig. 33). Batuk *et al.* (2013) have shown hematophanite is actually the $n = 3$ member of a homologous series of layered synthetic perovskites with the general formula $A_{3n+1}B_nO_{3n-1}Cl$.

No other minerals with this structure have been found. We recommend that the name be retained and **hematophanite** be recognised as a *bona fide* member of the perovskite supergroup.

Acknowledgements

References

Abilgaard, H. (1799) Cryolith, Thonerde mit Flussäure. *Allgemeines Journal der Chemie*, **2**, 502–000.

Aguado, F., Rodriguez, F., Hirai, S., Walsh, J.N., Lennie, A. and Redfern, S.A.T. (2008) High-pressure behaviour of KMF_3 perovskite. *High Pressure Research*, **28**, 539–544.

Akber-Knutson, S., Bukowinski, M.S.T. and Matas, J. (2002) On the structure and compressibility of $CaSiO_3$ perovskite. *Geophysical Research Letters*, **29**, 4-1–4-4.

Anthony, J.W., Bideaux, R.A., Bladh, K.W. and Nicholls, M.C. (1997). *Handbook of Mineralogy. Volume III. Halides, Hydroxides, Oxides*. Mineral Data Publishing, Tucson, Arizona, USA.

Arakcheeva, A.V., Lubman, G.U., Pisharovski, D.U., Gekimyants, V.M. and Popov, G.U. (1997) Crystal structure of micro-twinned natural orthorhombic perovskite $CaTiO_3$. *Crystallography Reports*, **42**, 46–54.

Arulesan, S.W., Kayser, P., Kennedy, B.J. and Knight, K. S. (2016*a*) The impact of room temperature polymorphism in K doped $NaTaO_3$ on structural phase transition behaviour. *Journal of Solid State Chemistry*, **238**, 109–122.

Arulesan, S.W., Kayser, P., Kennedy, B.J., Kimpton, J.A. and Knight, K.S. (2016*b*) Phase separation in $NaTaO_3$. Impact of temperature and doping. *Solid State Sciences*, **52**, 149–153.

Atencio, D., Andrade, M.B., Christy, A.G., Gieré, R. and Kartashov, P.M. (2010) The pyrochlore supergroup of minerals: nomenclature. *The Canadian Mineralogist*, **48**, 673–698.

Barnes, P.W., Lufaso, M.W. and Woodward, P.M. (2009) Structure determination of $A_2M^{3+}TaO_6$ and $A_2M^{3+}NbO_6$ ordered perovskites: octahedral tilting and pseudosymmetry. *Acta Crystallographica*, **B62**, 384–396.

Barth, T. (1925) Die Kristallstruktur von Perovskit und verwandten Verbindugen. *Norsk Geologisk Tidskrift*, **8**, 201–216.

Basciano, L.C., Peterson, R.C. and Roeder, P.L. (1998) Description of schoenfliesite, $MgSn(OH)_6$ and roxbyite, $Cu_{1.72}S$, from a 1375 BC shipwreck, and Rietveld neutron-diffraction refinement of synthetic schoenfliesite, wickmanite, $MnSn(OH)_6$ and burtite, $CaSn(OH)_6$. *The Canadian Mineralogist*, **36**, 1203–1210.

Batuk, M., Batuk, D., Tsirlin, A.A., Rozova, M.G., Antipov, E.V., Hadermann, J. and Van Tendeloo, G. (2013) Homologous series of layered perovskites $A_{n+1}B_nO_{3n-1}Cl$: Crystal and magnetic structure of the oxychloride $Pb_4BiFe_4O_{11}Cl$. *Inorganic Chemistry*, **52**, 2208–2218.

Bayliss, P. (1990) Revised unit-cell dimensions, space group, and chemical formula of some metallic minerals. *The Canadian Mineralogist*, **28**, 751–755.

Becerro, A.J., Lauterbach, S., McCammon, C.A., Langhorst, F., Angel, R. and Seifert, F. (1999). Oxygen defect clustering in $CaTiO_3$–$CaFeO_{2.5}$ perovskites: a model for the lower mantle. *European Journal of Mineralogy*, **11**, Supplement 1, p. 27.

Bentor, Y.K., Grass, S. and Heller, L. (1963) High temperature minerals in non-metamorphosed sediments in Israel. *Nature*, **199**, 478–479.

Beran, A., Libowitzky, E. and Armbruster, T.A. (1996) Single crystal infra-red spectroscopic and X-ray diffraction study of untwinned San Benito perovskite

containing OH groups. *The Canadian Mineralogist*, **34**, 803–809.

Berggren, J. (1971) Refinement of the crystal structure of dicalcium ferrite Ca$_2$Fe$_2$O$_5$. *Acta Chemica Scandinavica*, **25**, 3616–3624.

Bertaut, E.F., Blum, P. and Sagnières, P. (1959) Structure du barite bicalcique et de la brownmillerite. *Acta Crystallographica*, **12**, 149–159.

Betterton, J., Green, D.L., Jewson, C., Spratt, J. and Tandy, P. (1998) The composition and structure of jeanbandyite and natanite. *Mineralogical Magazine*, **62**, 707–712.

Birch, W.D., Pring, A., Reller, A. and Schmalle, H.W. (1993) Bernalite, Fe(OH)$_3$, a new mineral from Broken Hill, New South Wales: Description and structure. *American Mineralogist*, **78**, 827–834.

Blackburn, W.H. and Dennen, W.H. (1997) *Encylopedia of Mineral Names.* The Canadian Mineralogist Special Publication **1**. Mineralogical Association of Canada Québec, Canada.

Böggild, O.B. (1912) Krystallform und Zwillingsbildungen des Kryoliths, des Perowskits und des Baracits. *Zeischrift für Kristallographie*, **50**, 439–429.

Bogue, R.H. (1955) *The Chemistry of Portland Cement.* Reinhold, New York.

Bonshtedt-Kupletskaya, E.M. (1946) New observations on minerals of the perovskite group. *Problems in Mineralogy, Geochemistry and Petrography.* Nauka Press, Moscow.

Bowman, H.L. (1908) On the structure of perovskite from the Bergumer Alp, Pfitschtal, Tyrol. *Mineralogical Magazine*, **15**, 156–176.

Britvin, S.A., Kashtanov, M.G., Krzhizhanovskaya, A., Gurinov, O.V., Glumov, S., Strekopytov, S., Kretser, L.Y., Zaitsev, A.N., Chukanov, N.V. and Krivovichev, S.V. (2015) Perovskites with framework-forming xenon. *Angewandte Chemie*, **54**, 14340–14344.

Britvin, S.A., Kashtanov, S.A., Krivovichev, S.V. and Chukanov, N.V. (2016) Xenon in rigid oxide frameworks: Structure, bonding and explosive properties of layered perovskite K$_4$Xe$_3$O$_{12}$. *Journal of the American Chemical Society*, **138**, 13838–13841.

Bruce, D.W., O'Hare, D. and Walton, R.L. (2010) *Functional Oxides.* John Wiley & Sons, London, 304 pp.

Burke, E.A.J. and Kieft, C. (1971) Second occurrence of macedonite, PbTiO$_3$, Långban, Sweden. *Lithos*, **4**, 101–104.

Buttner, R.H. and Maslen, E.N. (1992) Structural parameters and electron difference density in BaTiO$_3$. *Acta Crystallograpica*, **B48**, 764–769.

Byström, A. and Wilhelmi, K.A. (1950) The crystal structure of diaboleite Pb$_2$Cu(OH)$_4$Cl$_2$. *Arkiv Kemi*, **2**, 397–404.

Cao, H., Devreugd, C.P., Ge, W., Li, J., Viehland, D., Luo, H. and Zhao, X. (2009) Monoclinic *Mc* phase in (001) field-cooled BaTiO$_3$ single crystals. *Applied Physics Letters*, **94**, 032901.

Caracas, R. and Wentzcovitch, R.M. (2005) Equation of state and stability of CaSiO$_3$ under pressure. *Geophysical Research Letters*, **32**, L06303.

Carpenter, M.A., Sondergeld, P., Li, B., Liebermann, R.C., Walsh, J.W., Schreuer, J. and Darling, T.W. (2006) Structural evolution, strain and elasticity of perovskites at high pressures and temperatures. *Journal of Mineralogical and Petrological Sciences IMA issue 1*, **101**, 95–109.

Chakhmouradian, A.R. and Mitchell, R.H. (1997) Compositional variation of perovskite-group minerals from carbonatite complexes of the Kola alkaline province, Russia. *The Canadian Mineralogist*, **35**, 1293–1310.

Chakhmouradian, A.R. and Mitchell, R.H. (1998) A structural study of the perovskite series CaTi$_{2-x}$Fe$_x$Nb$_x$O$_3$. *Journal of Solid State Chemistry*, **138**, 272–277.

Chakhmouradian, A.R. and Mitchell, R.H. (2001) Three compositional varieties of perovskite from kimberlites of the Lac de Gras field (Northwest Territories, Canada). *Mineralogical Magazine*, **65**, 133–148.

Chakhmouradian, A.R. and Mitchell, R.H. (2002) New data on pyrochlore- and perovskite-group minerals from the Lovozero alkaline complex, Russia. *European Journal of Mineralogy*, **14**, 821–836.

Chakhmouradian, A.R. and Woodward, P.M. (2014) Celebrating 175 years of perovskite research: a tribute to Roger H. Mitchell. *Physics and Chemistry of Minerals*, **41**, 387–391.

Chakhmouradian, A.R., Yakovenchuk, V., Mitchell, R.H. and Bogdanova, A. (1997) Isolueshite: a new mineral of the perovskite group from the Khibina alkaline complex. *European Journal of Mineralogy*, **9**, 483–490.

Chakhmouradian, A.R., Mitchell, R.H., Pankov, A.V. and Chukanov, N.V. (1999) Loparite and "metaloparite" from the Burpala alkaline complex, Baikal Alkaline Province (Russia). *Mineralogical Magazine*, **63**, 519–534.

Chakhmouradian, A.R., Ross, K., Mitchell, R.H. and Swainson, I. (2001) The crystal chemistry of synthetic potassium-bearing neighborite, Na$_{1-x}$Mg$_x$F$_3$. *Physics and Chemistry of Minerals*, **28**, 277–284.

Chao, E.C.T., Evans, H.T., Skinner, B.J. and Milton, C. (1961) Neighborite, NaMgF$_3$, a new mineral from the Green River Formation, South Ouray, Utah. *American Mineralogist*, **46**, 379–393.

Cheng, P., Yongsheng, N., Yuan, K. and Hong, J. (2013) Fast sonochemical synthesis of CoSn(OH)$_6$ nanocubes, conversion towards shape-preserved SnO$_2$–Co$_3$O$_4$ hybrids and their photodegradation properties. *Materials Letters*, **90**, 19–22.

Cheon, C.L., Joo, H.W., Chae, K.W., Kim, J.S., Lee, S.H., Torii, S. and Kamiyama, T. (2015) Monoclinic ferroelectric NaNbO$_3$ at room temperature: Crystal

structure solved by using super high resolution neutron powder diffraction. *Materials Letters*, **156**, 214–219.

Chesnokov, B.V. and Bazhenova, L.F. (1985) Srebrodolskite, $Ca_2Fe_2O_5$, a new mineral. *Zapiski Vses Mineralogii Obshchestvo*, **114**, 195–199.

Christy, A.G., Mills, S.J. and Kampf, A.R. (2016) A review of the structural architecture of tellurium oxycompounds. *Mineralogical Magazine*, **80**, 415–545.

Cohen-Addad, C. (1968) Étude structurale des hydroxystannates $CaSn(OH)_6$ et $ZnSn(OH)_6$ par diffraction neutronique, absorption infrarouge et resonance magnetique nucleaire. *Bulletin Sociéte de France Mineralogie et Crystallographie*, **91**, 315–324.

Colville, A.A. and Geller, S. (1971) The crystal structure of brownmillerite Ca_2FeAlO_5. *Acta Crystallographica*, **B27**, 2311–2315.

Colville, A.A. and Geller, S. (1972) Crystal structures of $Ca_2Fe_{1.43}Al_{0.57}O_5$ and $Ca_2Fe_{1.28}Al_{0.72}O_5$. *Acta Crystallographica*, **B28**, 3196–3200.

Cooper, M.A. and Hawthorne, F.C. (1995) Diaboleite, $Pb_2Cu(OH)_4Cl_2$, a defect perovskite structure with lone pair behaviour of Pb^{2+}. *The Canadian Mineralogist*, **33**, 1125–129.

Cross, E.B. and Hillebrand, W.F. (1885) Minerals from the neighbourhood of Pikes Peak. *U.S. Geological Survey Bulletin*, **20**, 40–68.

Danø, M. and Sørenson, H. (1959) An examination of some rare minerals from the nepheline syenites of southwest Greenland. *Meddelelser om Grønland*, **162**, 1–35.

Demartin, F., Campostrini, I., Castellano, C. and Russo, M. (2014) Parascandolaite, $KMgF_3$, a new perovskite-type fluoride. *Physics and Chemistry of Minerals*, **41**, 403–407.

Dobbe, R.T.M., Lustenhouwer, W. and Zakrzewski, M.A. (1994) Kieftite, $CoSb_3$, a new member of the skutterudite group from Tunaberg, Sweden. *The Canadian Mineralogist*, **32**, 179–183.

Dunn, P.J., Peacor, D.R., Valley, J.W. and Randell, C.A. (1985) Ganomalite from Franklin, New Jersey, and Jakobsberg, Sweden: new chemical and crystallographic data. *Mineralogical Magazine*, **49**, 579–582.

Fang, C.M. and Ahuja, R. (2006) Structures and stability of ABO_3 orthorhombic perovskites at the Earth's mantle conditions from first-principles theory. *Physics of the Earth and Planetary Interiors*, **157**, 1–7.

Feldman, C. and Jansen, M. (1995) Ternary oxides containing anionic gold. *Zeitschrifte für Anorganische und Allegemeine Chemie*, **621**, 201–206.

Feng, D., Shivaramaiah, R. and Navrotsky, A. (2016) Rare earth perovskite along the join $CaTiO_3$–$Na_{0.5}La_{0.5}TiO_3$ join: Phase transformations, formation enthalpies, and implications for loparite minerals. *American Mineralogist*, **101**, 2051–2016.

Foord, E.E., O'Conner, J.T., Hughes, J.M., Sutley, S.J., Falster, A.V., Soregaroli, A.E., Lichte, F. and Kile, D. E. (1999) Simmonsite, Na_2LiAlF_6, a new mineral from the Zapot amazonite-topaz-zinnwaldite pegmatite, Hawthorne, Nevada, USA. *American Mineralogist*, **84**, 769–772.

Frondel, C. (1948) New data on elpasolite and hagemannite. *American Mineralogist*, **33**, 84–87.

Galasso, F.S. (1990) *Perovskites and High T_c Superconductors*. Gordon & Breach Science Publications, New York.

Galuskin, E.V., Gazeev, V.M., Armbruster, T., Zadov, A. E., Galuskina, I.O., Pertsev, N.N., Dzierzanowski, P., Kadiyski, M., Gurbanov, A.G., Wrzalik, R. and Winiarski, A. (2008) Lakargiite, $CaZrO_3$: A new mineral of the perovskite group from the North Caucasus, Kabardino-Balkaria, Russia. *American Mineralogist*, **93**, 1903–1910.

Galuskin, E.V. Galuskina, I.O., Gazeev, V.M., Dzierzanowski, P., Prusik, K., Pertsev, N.N., Zadov, A.E., Bailau, R. and Gubanov, A.G. (2011) Megawite, $CaSnO_3$: A new perovskite-group mineral from skarns of the Upper Chegem-caldera, Kabardino-Balkaria, Northern Caucasus, Russia. *Mineralogical Magazine*, **75**, 2563–2572.

Galuskin, E.V., Galuskina, I.O., Kusz, J., Armbruster, T., Marzec, K., Dzierzanowski, P. and Murasko, M. (2014) Vapnikite Ca_3UO_6 – a new double perovskite mineral from pyrometamorphic larnite rocks of the Jebel Harum, Palestine Autonomy, Israel. *Mineralogical Magazine*, **78**, 571–581.

Gasparik, T., Wolf, K. and Smith, C.M. (1994) Experimental determinations of phase relations in the $CaSiO_3$ system from 8 to 15 GPa. *American Mineralogist*, **79**, 1219–1222.

Geller, S. (1956) Crystal structure of gadolinium orthoferrite, $GdFeO_3$. *Journal of Chemical Physics*, **24**, 1236–1239.

Genkin, A.D. and Murav'eva, L.V. (1964) Indite and dzhalindite: new indium minerals. *American Mineralogist*, **49**, 439.

Glazer, A.M. (1972) The classification of tilted octahedra in perovskites. *Acta Crystallographica*, **B28**, 3384–3392.

Goldschmidt, V.M. (1926) Geochemische Verteilungsgesetze der Elementer VII. *Skrifter der Norske Videnskaps Akademi Klasse 1. Matematisk Naurvidenskaplig Klasse.* Oslo, Norway.

Gross, S. (1977) The mineralogy of the Hatrurim Formation, Israel. *Geological Survey of Israel Bulletin*, **70**, 1–80.

Gurmeet Kaur and Mitchell, R.H. (2013) Mineralogy of the P2-West "kimberlite", Wajrakarur kimberlite field, Andra Pradesh, India: kimberlite or lamproite? *Mineralogical Magazine*, **77**, 3175–3196.

Haggerty, S.E. and Mariano, A.N. (1983) Srontianloparite and strontio-chevkinite: Two new minerals in rheomorphic fenites from the Paraná Basin

carbonatites. *Contributions to Mineralogy and Petrology*, **84**, 365–381.

Haidinger, W. (1845) *Handbuch der bestimmenden Mineralogie, enthaltend die Terminologie, Systematik, Nomenklatur und Charakteristik der Naturgeschischte des Mineralreiches.* Braumuller & Seidel, Vienna, 550 pp.

Hålenius, U., Hatert, T., Pasero, M. and Mills, S.J. (2016) CNMNC Newsletter No. 30, April 2016, page 413. *Mineralogical Magazine*, **80**, 407–413.

Hansen, W.C., Brownmiller, L.T. and Bogue, R.H. (1928) Studies on the system calcium oxide–alumina–ferric oxide. *Journal of the American Chemical Society*, **50**, 396–406.

Hatert, F., Mills, S.J., Pasero, M. and Williams, P.A. (2013) CNMNC guidelines for the use of suffixes and prefixes in mineral nomenclature, and the preservation of mineral names. *European Journal of Minealogy*, **25**, 113–115.

Hawthorne, F.C. and Ferguson, R.B. (1975) Refinement of the crystal structure of cryolite. *The Canadian Mineralogist*, **13**, 377–382.

Hentschel, G.M. (1964) Myerit, $12Ca_{0.7}Al_2O_3$ und Brown milllerit, $2CaO \cdot (Al,Fe)_2O_3$, zwei neue Minerale in der Lavas des Ettinger Bellerberges. *Neues Jahrbuch für Mineralogie Monatshefte*, **1964**, 22–29.

Hermann, P., Vandenstetten, R. and Hubaux, A. (1960) Sublimés du Nyiragongo (Kivu). *Bulletin des Séances de l'Academie Royal des Sciences d'Outr-mer*, **6**, 961–971.

Hewat, A.W. (1974) Neutron powder profile refinement of ferroelectric and antiferroelectric crystal structures – sodium niobate at 22°C. *Ferroelectrics*, **7**, 83–85.

Hidden, W.E. and MacKintosh, A. (1888) Sulphohalite, a new sodian sulphato-chloride. *American Journal of Science, 3rd Series*, **36**, 463.

Hirose, K. (2014) Deep Earth mineralogy revealed by ultrahigh-pressure experiments. *Mineralogical Magazine*, **78**, 437–446.

Howard, C.J. and Stokes, H.T. (1998) Group theoretical analysis of octahedral tilting in perovskites. *Acta Crystallographica*, **B54**, 782–789.

Howard, C.J. and Stokes, H.T. (2002) Group theoretical analysis of octahedral tilting in perovskites. Erratum. *Acta Crystallographica*, **B58**, 565.

Howard, C.J. and Stokes, H.T. (2004) Octahedral tilting in cation-ordered perovskites – a group-theoretical analysis. *Acta Crystallographica*, **B60**, 674–684.

Howard, C.J. and Stokes, H.T. (2005) Structures and phase transitions in perovskites a group theoretical approach. *Acta Crystallographica*, **A61**, 93–111.

Howard, C.J., Kennedy, B.J. and Woodward, P.M. (2003) Ordered double perovskites – a group theoretical analysis. *Acta Crystallographica*, **B59**, 463–471.

Hu, M., Wenk, H.R. and Sinitsyna, D. (1992) Microstructures in natural perovskites. *American Mineralogist*, **77**, 359–373.

Hutton, J. and Nelmes, R.J. (1981) High resolution studies of cubic perovskite by elastic neutron diffraction. *Acta Crystallographica*, **A37**, 916–920.

Ishizawa, N., Marumo, F., Iwai, S., Kimura, M. and Kawamura, T. (1980) Compounds with perovskite-like slabs III. The structure of a monoclinic modification of $Ca_2Nb_2O_7$. *Acta Crystallographica*, **B36**, 763–766.

Jackson, I. and Rigden, S.M. (1998) Composition and temperature of the Earth's mantle: seismological models interpreted through experimental studies of Earth Materials. Pp. 404–460 in: *The Earth's Mantle: Composition, Structure and Evolution* (I. Jackson, editor). Cambridge University Press, UK.

Jacobsen, M.J., Balić-Žunić, T., Mitolo, D., Katerinopoulou, A., Garavelli, A. and Jakobsson, S. P. (2014) Oskarssonite, AlF_3, a new fumarolic mineral from Eldfell volcano, Heimaey, Iceland. *Mineralogical Magazine*, **78**, 215–222.

Jeitschko, W. and Braun, D.J. (1977) $LaFe_4P_{12}$ filled with $CoAs_3$-type structure and isotypic lanthanoid-transition metal polyphosphides. *Acta Crystallographica*, **B33**, 3401–3406.

Johansson, K. (1928) Hematophanite. *Zeitschrifte fur Kristallographie*, **18**, 87–118.

Johnson, K.E. Tang, C.C., Parker, J.E., Knight, K.S., Lightfoot, P. and Ashbrook, S.E. (2010) The polar phase of $NaNbO_3$: a combined study by powder diffraction, solid state NMR and first principles calculations. *Journal of the American Chemical Society*, **132**, 8732–8746.

Kahlenberg, V., Fischer, R.X. and Shaw, C.S.J. (2000) Rietveld analysis of dicalcium aluminate ($Ca_2Al_2O_5$) – a new high-pressure phase with brownmillerite-type structure. *European Journal of Mineralogy*, **85**, 1061–1065.

Kaldos, R., Guzmics, T., Mitchell, R.H., Dawson, J.B., Milke, R. and Szabo, C. (2015) A melt evolution model for Kerimasi volcano, Tanzania: Evidence from carbonate melt inclusions in jacupirangite. *Lithos*, **238**, 101–119.

Kaminsky, F.V., Zakarchenko, O.D., Davies, R., Griffin, W.L., Khachtryan-Blinova, G.K. and Shiryaev, A.A. (2001) Super-deep diamonds from the Juina area, Mato Grosso State, Brazil. *Contributions to Mineralogy and Petrology*, **140**, 734–753.

Kaminsky, F.V., Wirth, R. and Schreiber, A. (2015) A microinclusion of lower-mantle rock and other minerals and nitrogen lower mantle inclusions in a diamond. *The Canadian Mineralogist*, **53**, 83–104.

Kaminsky, V., Ryabchikov, I.D. and Wirth, R. (2016) A primary natrocarbonatitic association in the Deep Earth. *Mineralogy and Petrology*, **110**, 387–398.

Kampf, A.R. (1982) Jeanbandyite, a new member of the stottite group from Llallagua, Bolivia. *Mineralogical Record*, **13**, 235–239.

Kay, H.F. and Bailey, P.C. (1957) Structure and properties of CaTiO$_3$. *Acta Crystallographica*, **A10**, 219–226.

Kimura, S. and Muan, A. (1971*a*) Phase relationships in the system CaO-iron oxide-TiO$_2$ in air. *American Mineralogist*, **56**, 1333–1346.

Kimura, S. and Muan, A. (1971*b*) Phase relationships in the system CaO–iron oxide–TiO$_2$ under strongly reducing conditions. *American Mineralogist*, **56**, 1347–1358.

Kiseleva, G.D., Kovalenko, V.A., Trubkin, N.V., Borisovsky, S.E. and Mokhov, A.V. (2008) Rare minerals of In, Cd, Mo, and W in gold-base metal veins of the Bugdaya Au-Mo(W)-porphyry deposit, Eastern Transbaikalia, Russia. *Russian Academy of Sciences Fersman Mineralogical Museum New Data on Minerals*, **43**, 13–22.

Kleppe, A.K., Welch, M.D., Crichton, W.A. and Jephcoat, A.P. (2012) Phase transitions in hydroxide perovskites: a Raman study of FeGe(OH)$_6$ stottite to 21 GPa. *Mineralogical Magazine*, **76**, 949–962.

Knight, K.S. and Kennedy, B.J. (2015) Phase coexistence in NaTaO$_3$ at room temperature: a high resolution neutron powder diffraction study. *Solid State Sciences*, **43**, 15–21.

Koděra, P., Takács, Á., Racek, M., Šimko, F., Lupatáková, J., Váczi, T. and Antal, P. (2016) Javorieite. IMA 2016-020 CNMNC Newsletter No. 32, August 2016, page 917. *Mineralogical Magazine*, **80**, 915–922.

Koopmans, H.J.A., van de Velde, G.M.H. and Gellings, P.J. (1983) Powder neutron diffraction study of the perovskites CaTiO$_3$ and CaZrO$_3$. *Acta Crystallographica*, **C39**, 1323–1325.

Knyzazev, A.V. Chernorukov, N.G., Dashkina, Z.S., Bulanov, E.N. and Ladenkov, I.V. (2011) Synthesis, structures, physicochemical properties, and crystal-chemical systematics of M$_2^{II}$A^{II}UO$_6$ (M^{II} = Pb, Ba, Sr; A^{II} = Mg, Ca, Sr, Ba, Mn, Fe, Co, Ni, Cu, Zn, Cs, Pb) compounds. *Russian Journal of Inorganic Chemistry*, **56**, 888–898.

Kramer, J.W., Kelly, B. and Manivannan, V. (2010) Synthesis of MSn(OH)$_6$ (where M = Mg, Ca, Zn, Mn, or Cu) materials at room temperature. *Central European Journal of Chemistry*, **8**, 65–69.

Krenner, J.A. (1883) Die Gronlandischen minerale der kryolithgruppe. *Mathematisk Naturwissenschaften Berichten aus Ungarn*, **1**, 151–172.

Krivovichev, S.V. (2008) Minerals with the antiperovskite structure: a review. *Zeitschrift für Kristallographie*, **223**, 109–115.

Krivovichev, S.V., Chakhmouradian, A.R., Mitchell, R.H., Filatov, S.K. and Chukanov, N.V. (2000) Crystal structure of isolueshite and its synthetic compositional analogue. *European Journal of Mineralogy*, **12**, 597–607.

Kuznetsov, I.G. (1925) Loparite a new rare earth mineral from the Khibina Tundra. *Izvestia Geologicheskogo Komiteta*, **44**, 663–682 [in Russian].

Kwei, G.H., Lawson, A.C., Billings, S.J.L. and Cheong, S.W. (1993) Structures of the ferroelectric phases of barium titanate. *Journal of Physical Chemistry*, **97**, 2368–2377.

Lafuente, B., Yang, H. and Downes, R.T. (2015) Crystal structure of tetrawickmanite Mn^{2+}Sn^{4+}(OH)$_6$. *Acta Crystallographica*, **E71**, 234–237.

Le Bail, A. and Calvayrac, F. (2006) Hypothetical AlF$_3$ crystal structures. *Journal of Solid State Chemistry*, **179**, 3159–3166.

Levin, I. and Bendersky, L.A. (1999) Symmetry classification of the layered perovskite-derived A$_n$B$_n$X$_{3n+2}$ structures. *Acta Crystallographica*, **B55**, 853–866.

Levin, I., Bendersky, L.A. and Vanderah, T.A. (2000) A structural study of the layered perovskite-derived Sr$_n$(NbTi)$_n$O$_{3n+2}$ compounds by TEM. *Philosophical Magazine*, **80**, 411–446.

Lewandowski, J.T., Pickering, I.J. and Jacobson, A.J. (1992) Hydrothermal synthesis of calcium-niobium and tantalum oxides with the pyrochlore structure. *Materials Research Bulletin*, **27**, 981–988.

Liu, L.G. (1976) Orthorhombic perovskite phases observed in olivine, pyroxene and garnet at high pressures and temperatures. *Physics of the Earth and Planetary Interiors*, **11**, 289–298.

Liu, L.G. and Ringwood, A.E. (1975) Synthesis of a perovskite-type polymorph of CaSiO$_3$. *Earth and Planetary Science Letters*, **28**, 209–211.

Lufaso, M.W. and Woodward, P.M. (2004) Jahn-Teller distortions, cation ordering and octahedral tilting in perovskites. *Acta Crystallographica*, **B60**, 10–20.

Lufaso, M.W., Barnes, P.W. and Woodward, P.M. (2006) Structure prediction of ordered perovskites and disordered multiple octahedral cation perovskites using *SPuDs*. *Acta Crystallographica*, **B62**, 397–410.

Lumpkin, G.R. (2014) The role of Th-U minerals in assessing the performance of nuclear waste forms. *Mineralogical Magazine*, **78**, 1071–1095.

Luo, H., Krizan, J.W., Muechler, L., Haldolaarachige, N., Klimczuk, T., Xie, W., Fucillo, M.K., Felser, K. and Cava, R.J. (2014) A large family of filled skutterudites stabilized by electron count. *Nature Communications*, **6**, Article 6489.

Ma, C. (2011) Discovery of meteoritic lakargiite (CaZrO$_3$); a new ultra refractory mineral from the ACFER 094 carbonaceous chondrite. *Meteoritical Society 74th Annual Meeting*, abstract 5169.

Ma, C. and Rossman, G.R. (2008) Barioperovskite, BaTiO$_3$, a new mineral from the Benitoite Mine, California. *American Mineralogist*, **93**, 154–157.

Marshukova, N.K., Sidorenko, G.A. and Chistyakova, N.I. (1978) New data on hydrostannates. *Russian Academy*

of Science Fersman Mineralogical Museum New Data on Minerals of the U.S.S.R., **27**, 89–95.

Marshukova, N.K., Pavlovskii, A.B. and Sidorenko, G.A. and Chistyakova, N.I. (1981) Vismirnovite, ZnSn(OH)$_6$ and natanite FeSn(OH)$_6$, new tin minerals. *Zapiski Vsesoyusnogo Mineralogicheskogo Obshchestva*, **110**, 492–500.

Marshukova, N.K., Pavlovskii, A.B., and Sidorenko, G.A. (1984) Mushistonite (Cu,Zn,Fe)Sn(OH)$_6$ – a new tin mineral. *Zapiski Vsesoyusnogo Mineralogicheskogo Obshchestva*, **113**, 612–617.

Matsui, M., Komatsu, K., Ikeda, E., Sano-Furukawa, A., Gotou, H. and Yagi, T. (2011) The crystal structure of δ-Al(OH)$_3$: Neutron diffraction measurements and *ab initio* calculations. *American Mineralogist*, **96**, 854–859.

McCammon, C.A., Pring, A., Keppler, H. and Sharp, T.A. (1995) A study of bernalite, Fe(OH)$_3$, using Mössbauer spectroscopy, optical spectroscopy, and transmission electron microscopy. *Physics and Chemistry of Minerals*, **22**, 11–20.

McDonald, A.M., Back, M.E., Gault, R.A. and Horváth, L. (2013) Peatite-(Y) and ramikite-(Y), two new Na-Li-Y±Zr phosphate-carbonate minerals from the Poudrette Pegmatite, Mont Saint-Hilaire, Quèbec. *The Canadian Mineralogist*, **51**, 569–596.

McPherson, G.J., Simon, S.B., Davis, A.M., Grossman, L. and Krot, A.N. (2005) Calcium aluminum-rich inclusions: Major unanswered questions. Pp. 225–250, in *Chondrites and the Protoplanetary Disk* (A.N. Krot, A.N. Scott and B. Reipurth, editors). Astronomical Society of the Pacific Conference Papers, **341**.

Megaw, H.D. (1946) Crystal structures of double oxides of the perovskite type. *Proceedings of the Philosophical Society of London*, **58**, 133–152.

Megaw, H.D. (1968) A simple theory of the off-centre displacements of cations in octahedral environments. *Acta Crystallographica*, **B24**, 149–153.

Megaw, H.D. (1973) *Crystal structures: A working approach.* W.B. Saunders Co., Philadelphia, USA.

Menezes Filho, L.A.D., Atencio, D., Andrade, M.B., Downs, R.T., Chaves, M.L.S.C., Romano, A.W., Scholz, R. and Persiano, A.I.C. (2015) Pauloabibite, trigonal NaNbO$_3$, isostructural with ilmenite, from the Jacupiranga carbonatite, Cajati, São Paulo, Brazil. *American Mineralogist*, **100**, 442–446.

Midorikawa, M., Ishibashi, Y. and Takagi, M. (1979) Optical and dilatometric studies of KCaCl$_3$ and RbCaCl$_3$. *Journal of the Physics Society of Japan*, **46**, 1240–1244.

Mihalik, P. Hienstra, S.A. and de Villiers, J.P.R. (1975) Two new platinum group minerals from the Merensky Reef, Bushveld igneous complex. *The Canadian Mineralogist*, **13**, 146–150.

Mitchell, R.H. (1997) Carbonate-carbonate immiscibility, neighborite and potassium iron sulphide in Oldoinyo Lengai natrocarbonatite. *Mineralogical Magazine*, **61**, 779–789.

Mitchell, R.H. (2002) *Perovskites: Modern and Ancient.* Almaz Press, Thunder Bay (www.almazpress.com)

Mitchell, R.H. and Chakhmouradian, A.R. (1996) Compositional variation of loparite from the Lovozero alkaline complex, Russia. *The Canadian Mineralogist*, **34**, 977–990.

Mitchell, R.H. and Chakhmouradian, A.R. (1998) Th-rich loparite from the Khibina complex, Kola Peninsula: Isomorphism and paragenesis. *Mineralogical Magazine*, **62**, 341–353.

Mitchell, R.H. and Liferovich, R.P. (2005) A structural study of the perovskite series Na$_{0.75}$Ln$_{0.25}$Ti$_{0.5}$Nb$_{0.5}$O$_3$. *Journal of Solid State Chemistry*, **178**, 2586–2593.

Mitchell, R.H. and Mariano, A.N. (2016) Primary phases in alumious slags produced by the aluminothermic reduction of pyrochlore. *Mineralogical Magazine*, **80**, 383–397.

Mitchell, R.H. and Vladykin, N.V. (1993) Rare earth element-bearing tausonite and potassium barium titanates from the Little Murun potassic alkaline complex, Yakutia, Russia. *Mineralogical Magazine*, **57**, 651–664.

Mitchell, R.H., Chakhmouradian, A.R. and Yakovenchuk, V.N. (1996) Nioboloparite: a re-investigation and discreditation. *The Canadian Mineralogist*, **34**, 991–999.

Mitchell, R.H., Choi, J.B., Hawthorne, F.C., McCammon, C.A. and Burns, P.C. (1998) Latrappite: a re-investigation. *The Canadian Mineralogist*, **36**, 107–116.

Mitchell, R.H., Chakhmouradian, A.R. and Woodward, P.M. (2000*a*) Crystal chemistry of perovskite-compounds in the tausonite loparite series (Sr$_{1-x}$Na$_x$La$_x$)TiO$_3$. *Physics and Chemistry of Minerals*, **27**, 583–589.

Mitchell, R.H., Burns, P.C. and Chakhmouradian, A.R. (2000*b*) The crystal structures of loparite-(Ce). *The Canadian Mineralogist*, **38**, 145–152.

Mitchell, R.H., Burns, P.C., Chakhmouradian, A.R. and Levin, I. (2002) The crystal structures of lueshite and NaNbO$_3$. *International Mineralogical Association Meeting*, Edinburgh, Scotland, Abstract A9–5.

Mitchell, R.H., Cranswick, L.M.D. and Swainson, I. (2006) Neutron diffraction determination of the cell dimensions and thermal expansion of the fluoroperovskite KMgF$_3$ from 293 to 3.6 K. *Physics and Chemistry of Minerals*, **33**, 587–591.

Mitchell, R.H., Burns, P.C., Knight, K.S., Howard, C.J. and Chakhmouradian, A.R. (2014) Observations on the crystal structures of lueshite. *Physics and Chemistry of Minerals*, **41**, 393–401.

Miyajima, H., Miyawaki, R. and Ito, K. (2002) Matsubaraite, Sr$_4$Ti$_5$(Si$_2$O$_7$)$_2$O$_8$, a new mineral, the Sr-Ti analogue of perrierite from the Itoigawa-Ohmi district, Niigata Prefecture, Japan. *European Journal of Mineralogy*, **14**, 1119–1128.

Morgenstern-Badarau, I. (1976) Effet Jahn-Teller et structure cristalline de l'hydroxyde CuSn(OH)$_6$. *Journal of Solid State Chemistry*, **17**, 399–400.

Mullica, D.F., Beall, G.W. and Milligan, W.O. (1979) The crystal structure of cubic In(OH)$_3$ by X-ray and neutron diffraction methods. *Journal of Inorganic and Nuclear Chemistry*, **41**, 277–282.

Murakami, M., Hirose, K., Kawamura, K., Sata, N. and Ohishi, Y. (2004) Post-perovskite phase transition in MgSiO$_3$. *Science*, **304**, 855–858.

Nakayama, N., Kosuge, K. and Kachi, S. (1977) Magnetic properties of FeSn(OH)$_6$ and its oxidation product FeSnO(OH)$_5$. *Materials Research Bulletin*, **13**, 17–22.

Nanot, M., Queyroux, F., Gilles, J.C., Portier, R. and Fayard, M. (1975) Étude par diffraction X et microscopie electronique de composés inedits de formule A$_n$B$_n$O$_{3n+2}$ dans les systems La$_2$Ti$_2$O$_7$–CaTiO$_3$, Nd$_2$Ti$_2$O$_7$–CaTiO$_3$ et Ca$_2$Nb$_2$O$_7$–CaTiO$_3$. *Materials Research Bulletin*, **10**, 313–318.

Náray-Szabó, S.V. (1943) Der strukturtyp des Perowskites (CaTiO$_3$). *Naturwissenschaften*, **31**, 202–203.

Náray-Szabó, S.V. and Sasvari, K. (1938) Die struktur des Kryoliths Na$_3$AlF$_6$. *Zeitschrift für Kristallographie*, **99**, 27–31.

Nefedov, E.I., Griffin, W.L. and Kristiansen, R. (1977) Minerals of the schoenfliesite wickmanite series from Pitkäranta, Karelia, USSR. *The Canadian Mineralogist*, **15**, 437–445.

Nelmes, R.J. and Kuhs, W.F. (1985) The crystal structure of tetragonal PbTiO3 at room temperature and at 700 K. *Solid State Communications*, **54**, 721–723.

Nickel, E.H. (1964) Latrappite – a proposed new mineral name for the perovskite-type calcium niobate mineral from the Oka area of Québec. *The Canadian Mineralogist*, **8**, 121–122.

Nickel, E.H. and McAdam, R.C. (1963) Niobian perovskite from the Oka, Québec, a new classification for minerals of the perovskite group. *The Canadian Mineralogist*, **7**, 683–697.

Nickel, E.H. and Grice, J. (1998) The IMA Commission on New Minerals and Mineral Names: Procedures and guidelines on mineral nomenclature, 1998. *The Canadian Mineralogist*, **36**, 913–926.

Nielson, J.R., Kurzman, J.A., Seshadri, R. and Morse, D. E. (2011) Ordering double perovskite hydroxides by kinetically controlled aqueous hydrolysis. *Inorganic Chemistry*, **50**, 3003–3009.

Oganov, A.R. and Ono, S. (2004) Theoretical and experimental evidence for a post-perovskite phase of MgSiO$_3$ in Earth's D″ layer. *Nature*, **430**, 445–448.

Oskarsson, N. (1981) The chemistry of Icelandic lava incrustations and the latest stages of degassing. *Journal of Volcanology and Geothermal Research*, **10**, 93–111.

Pabst, A. (1934) The crystal structure of sulphohalite. *Zeitscrift fur Kristallographie*, **89**, 514–517.

Palache, C., Berman, H. and Frondel, F. (1951) *The System of Mineralogy of James Dwight Dana and Edward Salisbury Dana.* Volume II, 7th edition, pp. 91–92. John Wiley and Sons, New York.

Pauly, H. (1969) White cast iron with cohenite schreibersite and sulphides from Tertiary basalts on Disko. *Meddeleser fra Dansk Geologisk Forening*, **19**, 26–28.

Peel, M.D., Thompson, S.P., Daoud-Aladine, A., Ashbrook, S.E. and Lightfoot, P. (2012) New twists on the perovskite theme: Crystal structures of the elusive phases R and S of NaNbO$_3$. *Inorganic Chemistry*, **51**, 6876–6889.

Portier, R., Fayard, M., Carpy, A. and Galy, J. (1974) Étude par microscopie électronique de quelques termes de la serie (Na,Ca)$_n$Nb$_n$O$_{3n+2}$. *Materials Research Bulletin*, **9**, 371–378.

Qi, R.Y. and Corbett, J.D. (1995) Cs$_3$Zr$_6$Br$_{15}$Z (Z = C,B): a stuffed rhombohedral perovskite structure of linked clusters. *Inorganic Chemistry*, **34**, 1657–1662.

Radusinović, D. and Makov, C. (1971) Macedonite – lead titanate: A new mineral. *American Mineralogist*, **56**, 387–394.

Ramsay, W. (1897) Das Nephelinesyenitgebiet auf der Halbinsel Kola II. *Fennia*, **15**, 1–15.

Ramsay, W. and Hackman, V. (1894) Das Nephelinesyenitgebiet auf der Halbinsel Kola I. *Fennia*, **11**, 1–225.

Ranjan, R., Agrawal, A. Senyshyn, A. and Boysen, H. (2006) Phases in the system Na$_{1/2}$Nd$_{1/2}$TiO$_3$– SrTiO$_3$: a powder neutron diffraction study. *Journal of Physics: Condensed Matter*, **18**, 9679–9689.

Rappenglück, M.A., Bauer, F., Hiltl, M., Neumair, A. and Ernstson, K. (2013) Calcium-aluminum-rich inclusions (CAIs) in iron silicide (xifengite, gupeite, hapkeite) matter: evidence of a cosmic origin. *Meteoritics and Planetary Science*, **48** issue s1, abstract #5055.

Redfern, S.A.T. (1996) High-temperature phase transitions in perovskite (CaTiO$_3$). *Journal of Physics of Condensed Matter*, **8**, 8267–8275.

Redhammer, G.J., Tippelt, G., Roth, G. and Amthauer, G. (2004) Structural variations in the brownmillerite series Ca$_2$(Fe$_{2-x}$Al$_x$)O$_5$: Single-crystal X-ray diffraction at 25°C and high-temperature X-ray powder diffraction (25°C ≤ *T* ≤ 1000°C). *American Mineralogist*, **89**, 405–420.

Ringwood, A.E. (1985) Disposal of high level nuclear wastes: Geological perspectives. *Mineralogical Magazine*, **49**, 159–176.

Ringwood, A.E. (1991) Phase transformations and their bearing on the constitution and dynamics of the mantle. *Geochimica et Cosmochimica Acta*, **55**, 2083–2110.

Rodrígues-Carvajal, J., Valett-Regí, M. and González-Calbert, J.M. (1989) Perovskite three-fold super-lattices: a structure determination of the A$_3$M$_3$O$_8$ phase. *Materials Research Bulletin*, **24**, 423–430.

Rosa, D. and Martin, R.F. (2010) A spurrite-, merwinite- and srebrodolskite-bearing skarn assemblage, West Clearwater Lake impact crater, northern Quebec. *The Canadian Mineralogist*, **48**, 1519–1532.

Rose, G. (1839) Beschreibung einiger neuer Mineralien vom Ural. *Pogendorff Annalen der Physik und Chemie*, **48**, 551–572.

Rosenberg, P.E. (1988) Aluminum fluoride hydrates, volcanogenic salts from Mount Erebus, Antarctica. *American Mineralogist*, **73**, 855–860.

Ross II, C.R., Bernstein, L.R. and Waychunas, G.A. (1988) Crystal structure refinement of stottite FeGe $(OH)_6$. *American Mineralogist*, **73**, 657–661.

Ross, K.C., Mitchell, R.H. and Chakhmouradian, A.R. (2003) The crystal structure of synthetic simmonsite, Na_2LiAlF_6. *Journal of Solid State Chemistry*, **172**, 95–101.

Rouse, R.C. (1971) The crystal chemistry of diaboleite. *Zeitschrift für Kristallographie*, **134**, 69–80.

Rouse, R.C. (1973) Hematophanite, a derivative of the perovskite structure. *Mineralogical Magazine*, **39**, 49–53.

Sabelli, C. (1987) Structure refinement of elpasolite from Cetrine Mine, Tuscany, Italy. *Neues Jahrbuch für Mineralogie*, **1987**, 481–487.

Safianikoff, A. (1959) Un nouveau minéral de niobium. *Academe des Seances Royale de l'Outre-mer Bulletin*, **5**, 1251–1255.

Sakowski-Cowley, A.C., Lukaszewicz, K. and Megaw, H.D. (1969) The structure of sodium niobate at room temperature, and the problem of reliability in pseudo-symmetric structure. *Acta Crystallographica*, **25**, 851–865.

Sanematsu, K., Ehma, T., Kon, Y., Manaka, T., Zaw, K., Morita, S. and Seo, Y., (2016) Fractionation of rare-earth elements during magmatic differentiation and weathering of calc-alkaline granites in southern Myanmar. *Mineralogical Magazine*, **80**, 77–102.

Sasaki, S., Prewitt, C.T. and Liebermann, R.C. (1987) The crystal structure of $CaGeO_3$ perovskite and the crystal chemistry of $GdFeO_3$-type perovskites. *American Mineralogist*, **68**, 1189–1198.

Scheunemann, K. and Müller-Buschbaum, H.K. (1974) Zur Kristallstruktur von $Ca_2Nb_2O_7$. *Journal of Inorganic and Nuclear Chemistry*, **36**, 1965–1970.

Schubert, K. and Seitz, A. (1948) Kristallstruktur von Sc $(OH)_3$ und $In(OH)_3$. *Zeitschrifte für Anorganische und Allegemeine Chemie*, **256**, 226–238.

Scott, J,D. (1971) Crystal structure of a new mineral, söhngeite. *American Mineralogist*, **56**, 355.

Seltman, R., Soloviev, S., Shatov, V., Piranjo, F., Naumov, E. and Cerkasov, S. (2010) Metallogeny of Siberia: tectonic, geologic and metallogenic settings of selected significant deposits. *Australian Journal of Earth Sciences*, **57**, 655–706.

Shan, Y.J., Nakamura, T., Inaguma, Y. and Itoh, M. (1998) Preparation and dielectric properties of the novel perovskite-type oxides $(Ln_{/2}Na_{1/2})TiO_3$ (Ln = Dy, Ho, Er, Tm, Yb, Lu). *Solid State Ionics*, **108**, 123–128.

Sharygin, V.V., Sokol, E.V. and Vapnik, Y. (2008) Minerals of the pseudobinary perovskite-brownmillerite series from combustion metamorphic larnite-rocks of the Hatrurim Formation (Israel). *Russian Geology and Geophysics*, **49**, 709–726.

Sharygin, V.V., Lazic, B., Armbruster, T.M., Murashko, M.N., Wirth, R., Galuskina, I.O., Galuskin, E.V., Vapnik, Y., Britvin, S.N. and Logvinova, A.M. (2013) Shulamitite $Ca_3TiFe^{3+}AlO_8$ – a new perovskite-related mineral from the Hatrurim Basin, Israel. *European Journal of Mineralogy*, **25**, 97–111.

Shcheka, S.S. and Keppler, H. (2012) The origin of the terrestrial noble gas signature. *Nature*, **490**, 531–535.

Sleight, A.W. (1963) *A study of the incidence of the ordered perovskite structure*. PhD Thesis, University of Connecticut, USA.

Sokol, E.V., Gaskova, O.L., Kokh, S.N., Kozmenko, O.A., Seryotkin, Y.S., Vapnik, Y. and Murashko, M.N. (2011) Chromatite and its Cr^{3+}- and Cr^{6+}-bearing precursor minerals from the Nabi Musa Mottled Zone Complex. Judean Desert. *American Mineralogist*, **96**, 659–674

Spencer, L.J. and Mountain, E.D. (1923) Diaboleite. *Mineralogical Magazine*, **20**, 76–80.

Smith, C.B., Allsopp, H.L., Gravie, O.G., Kramers, J.D., Jackson, F.S. and Clement, C.R.C. (1989) Note on the U-Pb perovskite method for dating kimberlites: Examples from the Wesselton and De Beers mines, South Africa and Somerset Island, Canada. *Chemical Geology*, **79**, 137–145.

Spiridonov, E.M. and Gritsenko, Y.D. (2007) Ferroskutterudite, nickelskutterudite and skutterudite from the Norilsk Ore Field. *Russian Academy of Science Fersman Mineralogical Museum, New data on Minerals*, **42**, 16–27.

Spiridonov, E.M., Gritsenko, Y.D. and Kulikova, I.M. (2007) Ferroskutterudite $(Fe,Co)As_3$: A new mineral species from the dolomite-calcite veins of the Norilsk Ore Field. *Doklady Akademi Nauk Earth Sciences Section*, **417**, 242–244.

Stachel, T., Harris, J.W., Brey, G.P. and Joswig, W. (2000) Kankan diamonds (Guinea) II: lower mantle inclusion parageneses. *Contributions to Mineralogy and Petrology*, **140**, 16–27.

Stokes, H.T., Kisi, E.H., Hatch, D.M. and Howard, C.J. (2002) Group theoretical analysis of octahedral tilting in ferroelectric perovskites. *Acta Crystallographica*, **B58**, 934–936.

Strunz, H. and Contag, B. (1960) Hexahydroxystannate [Fe, Mn, Co, Mg, Ca,]$Sn(OH)_6$ und deren Kristallstruktur. *Acta Crystallographica*, **13**, 601–603.

Strunz, H. and Giglio, M. (1961) Die Kristallstructur von Sottit Fe[Ge(OH)$_6$]. *Acta Crystallographica*, **14**, 205–208.

Strunz, H., Söhnge, G. and Geier, B.H. (1958) Stottit, ein neues Germanium-Mineral und seine Paragenese in Tsumeb. *Neues Jahrbuch für Mineralogie Monatshefte*, **1958**, 85–96.

Sugahara, M., Yoshiasa, A., Yoneda, A., Hashimoto, T., Sakai, S., Okube, M., Nakatsuka, A. and Ohtaka, O. (2008) Single-crystal X-ray diffraction study of CaIrO$_3$. *American Mineralogist*, **93**, 1148–1152.

Sun, P.H., Nakamura, T., Shan, Y.J., Inaguma, Y. and Itoh, M. (1997) High temperature quantum paraelectricity in perovskite-type titanates Ln$_{1/2}$Na$_{1/2}$TiO$_3$. (Ln = La, Pr, Nd, Sm, Eu, Gd, and Tb). *Ferroelectrics*, **200**, 93–107.

Tanaka, T. and Okumura, K. (1977) Ultrafine barium titanate particles in the Allende meteorite. *Geochemical Journal*, **11**, 137–145.

Tarrida, M., Larguem, H. and Madon, M. (2009) Structural investigations of (Ca,Sr)ZrO$_3$ and Ca(Sn, Zr)O$_3$ perovskite compounds. *Physics and Chemistry of Minerals*, **36**, 403–413.

Taylor, H.F.W. (1977) *Cement Chemistry.* Thomas Telford, London, 459 pp.

Tikhnenkov, I.P. and Kazakova, M.E. (1957) Niboloparite – a new mineral of the perovskite group. *Zapiski Vsesoyusnogo Mineralogicheskogo Obshchestva*, **86**, 641–644.

Tschauner, O., Ma, C., Beckett, J.R., Prescher, C., Prakapenka, V.B. and Rossman, G.R. (2014) Discovery of bridgmanite, the most abundant mineral in the Earth, in a shocked meteorite. *Science*, **346**, 1100–1102.

Tsuchiya, T., Tsuchiya, J., Umemoto, K. and Wentzcovitch, R.M. (2004) Phase transitions of MgSiO$_3$ perovskite in the earth's lower mantle. *Earth and Planetary Science Letters*, **224**, 241–248.

Tsuda, K., Yasuhara, A. and Tanaka, M. (2013) Two-dimensional mapping of polarizations of rhombohedral nanostructures in the tetragonal phase of BaTiO$_3$ by the combined use of scanning transmission electron microscopy and convergent-beam electron diffraction methods. *Applied Physics Letters*, **103**, 082908.

Vorobyev, E.I., Konev, A.A., Malyshonok, Y.V., Afonina, G.F. and Sapozhnikov, A.N. (1984) Tausonite SrTiO$_3$. A new mineral of the perovskite group. *Zapiski Vsesoyusnogo Mineralogicheskogo Obshchestva*, **113**, 86–89.

Vousden, P. (1953) The structure of the ferroelectric sodium niobate at room temperature. *Acta Crystallographica*, **4**, 545–551.

Wang, Z.Y., Wang, Z.C., Wu, Z.Y. and Lou, X.W.D. (2013) Mesoporous single crystal CoSn(OH)$_6$ hollow structures with multilevel interiors. *Nature Scientific Reports*, **3**, srep 01391.

Welch, M.D. and Kampf, A.R. (2017) Stoichiometric partially-protonated states in hydroxide perovskites: the jeanbandyite enigma revisited. *Mineralogical Magazine*, **81**, 297–303.

Welch, M.D. and Kleppe, A.K. (2016) Polymorphism of the hydroxide perovskite Ga(OH)$_3$ and possible proton-driven transformational behaviour. *Physics and Chemistry of Minerals*, **43**, 515–536.

Welch, M.D. and Wunder, B. (2013) A single crystal X-ray diffraction study of the 3.65Å-phase MgSi (OH)$_6$, a high-pressure hydroxide perovskite. *Physics and Chemistry of Minerals*, **39**, 693–697.

Welch, M.D., Crichton, W.A. and Ross, N.L. (2005) Compression of the perovskite-related mineral bernalite Fe(OH)$_3$ to 9 GPa and a re-appraisal of its structure. *Mineralogical Magazine*, **69**, 309–315.

Williams, S.A. (1985) Mopungite, a new mineral from Nevada. *Mineralogical Record*, **16**, 73–74.

Williams, T., Lichtenberg, F., Widmer, D., Bednorz, G.and Reller, A. (1993) Layered perovskitic structures in pure and doped LaTiO$_{3.5-x}$ and SrNbO$_{3.5-x}$. *Journal of Solid State Chemistry*, **103**, 375–386.

Woodhead, J.D., Phillips, D., Hergt, J.M. and Paton, C. (2009) African kimberlites revisited: In situ Sr-isotope analysis of groundmass perovskite. *Lithos*, **112**, 311–317.

Woodward, P. (1997) Octahedral tilting in perovskites. I. Geometrical considerations. *Acta Crystallographica*, **B53**, 32–43.

Wu, F., Yang, Y.H., Mitchell, R.H., Li, Q.L., Yang, J.H. and Zhang, Y.B. (2010) In situ U-Pb age determination and Nd isotopic analysis of perovskites from kimberlites in southern Africa and Somerset Island, Canada. *Lithos*, **155**, 205–222.

Wunder, B., Wirth, R. and Koch-Müller, M. (2011) The 3.65 Å phase in the system MgO–SiO$_2$–H$_2$O: Synthesis, structure and composition. *American Mineralogist*, **96**, 1207–1214.

Wunder, B., Jhan, S., Koch-Müller, M. and Speziale, S. (2012) The 3.65 Å phase, MgSi(OH)$_6$: structural insights from DFT-calculations and T-dependent IR spectroscopy. *American Mineralogist*, **97**, 1043–1048.

Yakovenchuk, V., Ivanyuk, G., Pakhpmovsky, Y. and Men'shikov, Y. (2005) *Khibiny.* Laplandia Minerals, Apatity, Russia, 468 pp.

Yanamaka, T., Hirai, N. and Komatsu, Y. (2002) Structural changes of Ca$_{1-x}$Sr$_x$TiO$_3$ perovskite with composition and pressure. *The American Mineralogist*, **87**, 1183–1189.

Zhao, Y. (1998) Crystal chemistry and phase transitions of perovskites in P-T-X space: Data for (K$_x$Na$_{1-x}$)F$_3$. *Journal of Solid State Chemistry*, **141**, 121–132.

Zhao, Y., Weidner, D.J., Leinenweber, K., Liu, X., Li, B., Meng, Y., Pacalo, E.G., Vaughan, M.T., Wang, Y. and Yaganeh-Haeri, A. (1994) Perovskite at high P-T conditions: In situ synchrotron X-ray diffraction study of NaMgF$_3$ perovskite. *Journal of Geophysical Research*, **99 B2**, 2871–2885.

Zurevinski, S.E., Heaman, L.M. and Creaser, R.A. (2011) The origin of Triassic/Jurassic kimberlite magmatism, Canada: Two mantle sources revealed from the Sr-Nd isotopic composition of groundmass perovskite. *G3: Geochemistry Geophysics Geosystems*, **12**, https://doi.org/10.1029/2011GC003659

ADDENDUM

Popova *et al.* (2017) have recently described a non-centrosymmetric variety of loparite from the Khibiny complex with space group *Imma*2 [$a = 5.51292(2)$; $b = 5.5129(2)$; $c = 7.7874(5)$ Å]. This loparite adopts this space group and the tilt scheme $a^0b^-b^-$ as result of being richer in the $Na_{0.5}Ce_{0.5}TiO_3$ component than the *Pbnm* loparite described by Mitchell *et al.* (2000*b*) from the same locality.

Popova, E.A., Lushnikov, S..G., Yakovenchuk, V.N. and Krivovichev, S.V. (2017). The crystal structure of loparite; a new acentric variety. *Mineralogy and Petrology*, DOI 10.1007/s00710-017-0498-y.